Detecting torsional motion of kinesin motor proteins using birefringent microspheres and high-resolution optical tweezers.

Dissertation

der Mathematisch-Naturwissenschaftlichen Fakultät

der Eberhard Karls Universität Tübingen

zur Erlangung des Grades eines

Doktors der Naturwissenschaften

(Dr. rer. nat.)

vorgelegt von

Avin J. Ramaiya

aus Mumbai, Indien

Tübingen
2016

Gedruckt mit Genehmigung der Mathematisch-Naturwissenschaftlichen Fakultät der
Eberhard Karls Universität Tübingen.

Tag der mündlichen Qualifikation: 5. Mai 2017

Dekan:	Prof. Dr. Wolfgang Rosenstiel
1. Berichterstatter:	Prof. Dr Erik Schäffer
2. Berichterstatter:	Prof. Dr. Ana J. García-Sáez

Detecting torsional motion of kinesin motor proteins using birefringent microspheres and high-resolution optical tweezers.

Abstract

The kinesins motor proteins transport cellular cargo such as vesicles, organelles and chromosomes inside cells. They walk along microtubule tracks and are using adenosine-triphosphate-(ATP)[60] as an energy source. The kinesin motor proteins move cellular cargo such as vesicles, organelles and chromosomes on microtubule tracks. They are best known for their role in cell division and in axonal transport in neurons. A defect in kinesin function leads to diseases, typically involving defective transport of cell components or pathogens, or defects in cell division. Kinesin-1 is a dimeric molecular machine transporting vesicular cargo while[18,70,164] while stepping[158] in a hand-over-hand manner[8,78,144,179] along microtubules. The mechanics of kinesin motor motion has been studied extensively in the last decades. Because of the identical subunits[88], the motor has been proposed to rotate during stepping[69]. For each step the motor is expected to rotate by 180-degree and a torque transferred from the motor head, through the stalk, onto the motor bound cargo should then be visible as angular steps for every translational step. Yet, experiments mostly done at low ATP concentrations only revealed occasional motor stalk reversals and an asymmetry of consecutive steps, so-called limping, which was attributed to loads perpendicular to the microtubule axis[8,46,59,66,71,175]. The stepping rate of kinesin motors is slower at low ATP concentrations and faster at higher ATP concentrations. At high, physiological ATP concentration, rotations have not been detected because of long response times of rotational probes.

Recent work on intermediate states during stepping indicate continuous rotations[73,113], however, direct evidence for such rotational motion is lacking. Here, I used high-resolution optical tweezers combined with a sensitive optical micro-protractor and torsion balance employing highly birefringent, liquid crystalline probes to directly and simultaneously measure the translocation, rotation, and generation of force and torque of single kinesin-1 motors. Birefringent microspheres were chosen as optically anisotropic probes and the synthesis standardized, so as to control the size and birefringence. Spherical particles also simplify rotation calibration and measurement. I developed a fast and efficient protocol to couple birefringent microspheres to bio-molecules making them versatile probes for single molecule biological experiments. Due to their pico-Newton force range, sub-pN positional resolution and adaptability for torque measurement, I used optical tweezers for single-molecule experiments with kinesin motors. I modified a stable optical tweezers setup to resolve individual translational and rotational steps of kinesin. Surprisingly, we found that motors translocating along microtubules at saturating ATP concentrations rotated unidirectionally producing significant torques on the probes. Accounting for the rotational work, makes kinesin a highly efficient machine. Because motors also limped, these results imply that the motor's gait follows a rotary asymmetric hand-over-hand mechanism. Our method is generally applicable to study rotational motion of molecular machines and our findings implicate further complexities for kinesin-driven cellular processes.

The results are consistent with a unidirectional rotation of kinesin motors in contrast to the current asymmetric hand-over-hand model which resembles a human gait. Sustained uni-directional rotation implies that, the motor head during stepping is not free to rotate. Thus, the head should be directly guided from one binding site to the next, for example by electrostatic interactions[55]. We also observed that kinesin is capable of storing multiple twists within its stalk. Our method of rotation detection can allow us to determine the compliance of individual motifs within the kinesin stalk. The rate at which the stalk stores torque compared to torque relaxation, can lead to interesting insights about the nature of intra-molecular friction. The detection and measurement of rotation using optical tweezers opens an additional dimension to the study of single bio-molecules.

German translation:

Detektion der Rotationsbewegung von Kinesin Motorproteinen mittels doppelbrechender Mikrokugeln und hoch aufgelöster Optischer Pinzetten.

Die Kinesin Motorproteine transportieren zelluläre Fracht, wie z.B. Vesikel, Organellen und Chromosomen. Sie bestehen aus einem Dimer, laufen auf Mikrotubuli Filamenten, und nutzen adenosinetriphosphate-(ATP) als Energiequelle[60]. Sie spielen eine wichtige Rolle bei der Zellteilung und im dem axonemalen Transport in Neuronen. Kinesin-1 transportiert vesikuläre Fracht[18,70,164], indem es entlang der Mikrotubuli[158] "hand-over-hand" Schritte[8,78,144,179] vollführt. In den letzten Jahrzenten wurde der Mechanismus der Kinesin Motor Fortbewegung intensiv untersucht. Aufgrund der identischen Unterheinheiten[88] wurde vorgeschlagen, dass der Motor während des Laufens rotiert[69]. Es wurde erwartet, dass der Motor bei jedem Schritt um 180°rotiert und dadurch ein Drehmoment vom Motorkopf, über den Stiel, auf die Motor-gebundene Fracht überträgt. Diese Rotation sollte dann als Rotationsschritt für jeden einzelnen Translationsschritt beobachtbar sein. Jedoch zeigten Experimente, hauptsächlich durchgeführt bei geringen ATP Konzentrationen, nur gelegentliche Stielumkehrungen ("stalk reversals") und eine Asymmetrie aufeinander folgende Schritte, so genanntes Hinken ("limping"), was Belastungen perpendikulär zur Mikrotubulus Achse zugeschrieben wurde[8,46,59,66,71,175].

Kürzliche Arbeit über Zwischenzustände während des Laufens weist auf eine kontinuierliche Rotation hin[73,113], jedoch fehlt der direkte Nachweis für eine solche Rotationsbewegung. In dieser Arbeit benutze ich eine hoch auflösende Optische Pinzette kombiniert mit einem sensitiven optischen Mikro-Winkelmesser und einer Torsionswaage unter der Nutzung von stark doppelbrechenden, anisotropen Proben, um direkt und simultan Translokation, Rotation und Kraft- und Drehmomenterzeugung einzelner Kinesin-1 Motoren zu messen. Doppelbrechende Mikrokugeln wurden als optisch anisotrope Proben ausgewählt und die Synthese selbiger standardisiert, um die Größe und optische Anisotropie kontrollieren zu können. Kugelförmige Partikel erleichtern außerdem Rotationskalibration und -messung. Ich entwickelte ein schnelles und effiziente Protokoll um doppelbrechende Mikrokugeln an Biomoleküle zu koppeln, wodurch sie als Proben für biologische Einzelmolekülexperimente verwendbar wurden. Wegen ihres Pikonewton Kraft Messbereiches, ihrer sub-pN Positionsauflösung und ihrer Anpassungsfähigkeit bei Drehmomentmessungen, habe ich eine Optische Pinzette für Einzelmolekülexperimente mit Kinesinmotoren verwendet. Ich habe eine Optische Pinzette modifiziert um einzelne Translations- und Rotationsschritte eines Kinesins beobachten zu können. Überraschenderweise haben wir herausgefunden, dass Motoren, die entlang von Mikrotubuli bei sättigender ATP Konzentration translozieren, einseitig signifikantes Drehmoment auf die Probe übertragen. Bezogen auf die Rotationsarbeit ist Kinesin eine hoch effiziente Maschine. Aufgrund der Tatsache, dass Motoren hinken, implizieren diese Ergebnisse, dass der Gangart des Motors eine asymmetrische"hand-over-hand" Rotation zugrundeliegt. Unsere Methode ist allgemein anwendbar, um Rotationsbewegungen molekularer Maschinen zu untersuchen und unsere Erkentnisse implizieren weitere Komplexität der Kinesin-getriebenen zellulären Prozesse.

Die Ergebnisse sind konsistent mit einer einseitigen Rotation von Kinesinmotoren, und sprechen gegen das derzeitig anerkannte asymmetrische "hand-over-hand" Modell, das dem menschlichen Gang gleicht. Fortwährende einseitige Rotation impliziert, dass der Motorkopf während des Laufens nicht frei rotiert. Demnach sollte der Kopf direkt von einer Bindestelle zur nächsten geleitet werden, zum Beispiel durch elektrostatische Interaktionen[55]. Wir beobachteten auch dass der Stiel von Kinesin mehrere Verwindungen aufnehmen kann. Unsere Methode der Rotationsdetektion erlaubt uns die Compliance individueller Motive innerhalb des Kinesinstiels zu bestimmen. Die Rate mit der der Stiel Drehmoment speichert, im Vergleich zur Relaxation des Drehmoments, kann zu interessanten Erkentnissen über die Art intramolekularer Reibung führen. Der Nachweis und die Vermessung der Rotation mittels der Optischen Pinzette stellen eine weitere Dimension bereit einzelne Biomoleküle zu untersuchen.

Contents

List of figures

To Ma and Pa

0

Introduction

Motor proteins are microscopic machines which consume ATP as fuel, to perform mechanical work[161]. Three types of cytoplasmic motors are known: myosins, which move on actin filaments, and, dyneins and kinesins, which use microtubules as tracks (Figure 1). The protein structure of these two groups varies significantly, although each of these proteins hydrolyzes ATP, converting chemical energy to work. The ATP hydrolysis domain, which brings about the conversion is much smaller compared to the whole protein but a structural change at this point produces a chain reaction within multiple domains in the protein bringing about the stepping motion. An individual motor protein consists of a motor domain, structural or stalk domain, some flexible linkers, and a cargo binding domain. Variations in these domains at an amino acid level enabling these proteins to perform different functions inside cells. The group as a whole is called the motor protein super-family[146].

The kinesin and the myosin family has been extensively studied. Crystallography and other structural

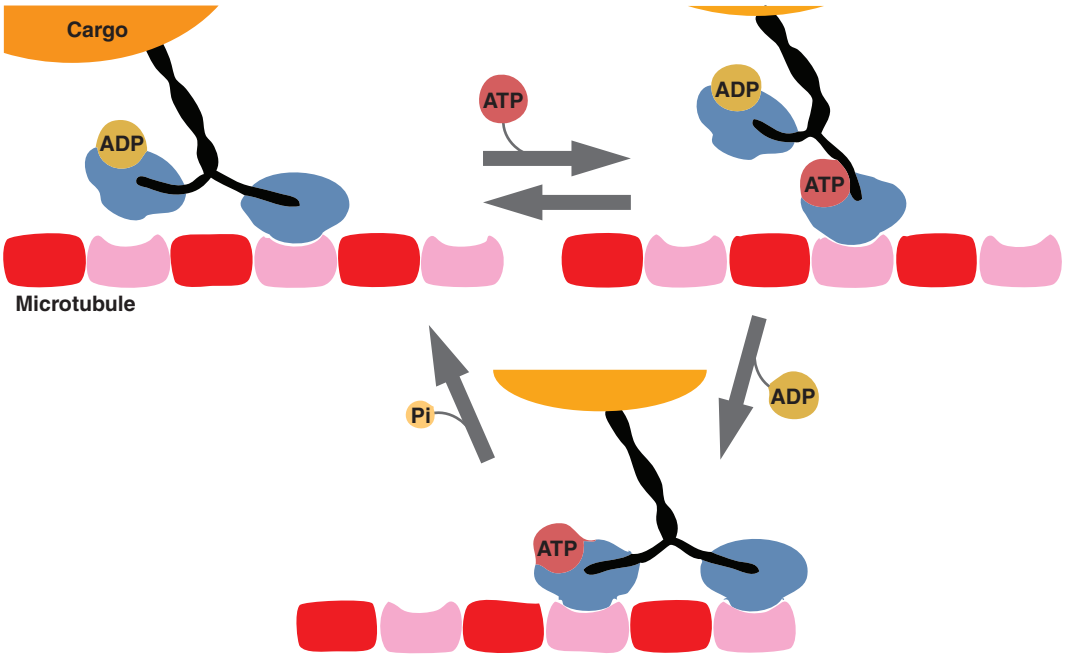

Figure 1: ATP dependent transport of cellular cargo by kinesin on microtubules.
Kinesins carry cellular cargo over microtubules in a stepping manner. Hydrolysis of one ATP powers the individual step. The ATP hydrolysis domain and the microtubule binding domain is a part of the so called 'motor head'. The motor head binds to the tubulin dimers in an alternating hand-over-hand manner.

studies reveal that key amino acid residues in these families are similar[161]. Within an individual super-family, motors may function as monomers, dimers, trimers or tetramers. These motors require microtubules or actin as tracks to walk on. Some motors are extremely processive, i.e. they move over longer distances without detaching, while others are not so. Two super-families of microtubule-based motor proteins have been discovered, kinesins and dyneins. Genetic and protein screening has fueled an explosive discovery of new microtubule-based motor proteins. More than 90 kinesin sequences are presently entered into the sequence data base[114,115,119]. The kinesin motors are found in all eukaryotes. The yeast Saccharomyces cerevisiae genome encodes one dynein and six kinesin genes[171]. Interest in motor proteins derives from their dynamic role in many essential cell biological process. An absence of functional molecular motors is cause of certain diseases[45,109]. Microtubule-based motility is vital for cell survival. Segregation of chromosomes during cell division[182], transport of intracellular membrane organelles[67], localization of cytoplasmic mRNA[112], asymmetric localization of morphogens[99] in early embryos, transport of pigment granules[21] are well-known processes that require kinesin transport. In this thesis, I am interested in kinesins, which employ microtubules as tracks and their processivity varies within the family.

To achieve intracellular transport, molecular motors exert force on intra-cellular cargo due to their stepping motion on microtubular tracks. The stepping has been shown to be due to conformational changes in the protein structure which is a result of ATP hydrolysis [2](Figure 1). The conventional microtubule-motor has the remarkable ability to take multiple steps along a microtubule before dissociating. The observation that single kinesin molecules can transport microtubules or microspheres was first shown by Howard et al. [70] and byBlock et al. [18] respectively. Single kinesin molecules moving along microtubules have been observed by tracking a single fluorescent dye molecule attached to kinesin by Vale [161]. Processivity has also been detected by ATPase measurements, which show that a kinesin molecule undergoes multiple rounds of ATP hydrolysis per encounter with a microtubule,[54,60,106] undertaking hundreds of successive 8-nm steps, hydrolyzing one ATP molecule per step.

It is possible to probe these systems at the single-motor level with high resolution, due to advances in single molecule biophysical techniques. A number of microscopy techniques have been developed to assay discrete displacements or steps produced by single kinesin motor proteins. In 1994, Svoboda & Block [157] showed that dimeric kinesin moves with 8-nm incremental steps along a microtubule as measured with optical tweezers, with a high-resolution motion detector. The dimension of these steps corresponds to the distance between sequential tubulin dimers along a microtubule protofilament [34,85]. These findings indicate that the kinesin motor undergoes a stepping motion from one binding site to the next along a microtubule. The currently favored model for kinesin stepping movement is the "hand-over-hand" mechanism (Figure 2). In this mechanism, the heads of kinesin move forward in an alternating way, exchanging leading, and trailing roles at each step. It was observed by Asbury et al. [8] that alternating steps of kinesin vary in time they require to take the next step, the dwell time. This variation is called "limping" of kinesin motors and is attributed to the asymmetric nature of hand-over-hand mechanism. In an asymmetric hand-over-hand mechanism, the individual heads of kinesin move in an alternating left and right manner, similar to the motion of our legs while walking. Another model of kinesin motion is the "symmetric hand-over-hand" mechanism(Figure 2). Because kinesin exists as a homo-dimer, it is expected that both the heads of kinesin function in the same way or symmetrically. The symmetric hand-over-hand mechanism, like the asymmetric mechanism, suggests an alternating motion of kinesin heads over microtubules, with the exception that the heads continue to travel in one of the direction left or right. Kinesin motors are homo-dimers [88] attached at the so-called stalk through a coiled-coil structure. It is proposed that the stepping translation of kinesins must be accompanied by rotation [69] of the stalk.

If kinesin were a nearly rigid molecule, 180°reorientations of the stalk would be anticipated whenever the two heads exchange positions during stepping. Experiments at low ATP concentrations however, reveal only occasional motor stalk reversals and an asymmetry of consecutive steps attributed to loads perpendicular to the microtubule axis[8,46,59,66,71,175]. Recent work on intermediate states during stepping indicates continuous rotations[73,113], however, direct evidence is lacking.

I decided to probe this question further and apply an interdisciplinary approach to understand the torsional motion of kinesin. To observe any rotation while a single kinesin steps, I employed optical tweezers and modified them to detect torque with the help of birefringent microspheres.

Optical tweezers are an ideal tool to study the forces and distances inherent in molecular motor processes. These devices are based on the premise that photons carry momentum, hence, if the direction of a photon is altered, by scattering or by refraction, a force is exerted on the scattering or on the refractive interface. This force is negligible on macroscopic objects as compared to smaller objects, like microspheres, the effect of this force is significant. As the name suggests optical tweezers can effectively orient a dielectric microscopic object in a three-dimensional plane. Since their invention, optical tweezers have been used to study many biological systems, e. g., myosin motor proteins[12], DNA polymerase[108], the elasticity of DNA[170], the unfolding of proteins[183], membrane tube formation[86], and the polymerization of microtubules[30]. Forces up to 1 nano-Newton with sub-pico Newton resolution and displacement down to a few angstroms can be measured with this technique[75,142]. The versatility of optical tweezers allows them to be combined with multiple microscopic tools, facilitating simultaneous characterization of diverse molecular activity. Constructing stable traps with the capability of high resolution detection and repeatable precision is demanding. Such devices require temperature control and unique housing to avoid thermal, electric and acoustic fluctuations. The scope of single molecule motility assays with optical tweezers is also limited by the probes employed for the experiment.

To detect rotational motion, we employed highly birefringent, liquid crystalline probes to directly and simultaneously measure the translocation, rotation, and force and torque production of single kinesin-1 motors. birefringent microspheres have an advantage that they have an isotropic shape of a sphere, making displacement, force and size calibration easier compared to other anisotropic probes like polymer nano-rods and quartz crystals[41,151]. The anisotropy required to detect rotation arises from the specific alignment of the mesogens in the liquid crystalline material. A birefringent microsphere changes the polarization of incident light relative to the angle of the director axis of the particle with respect to the angle

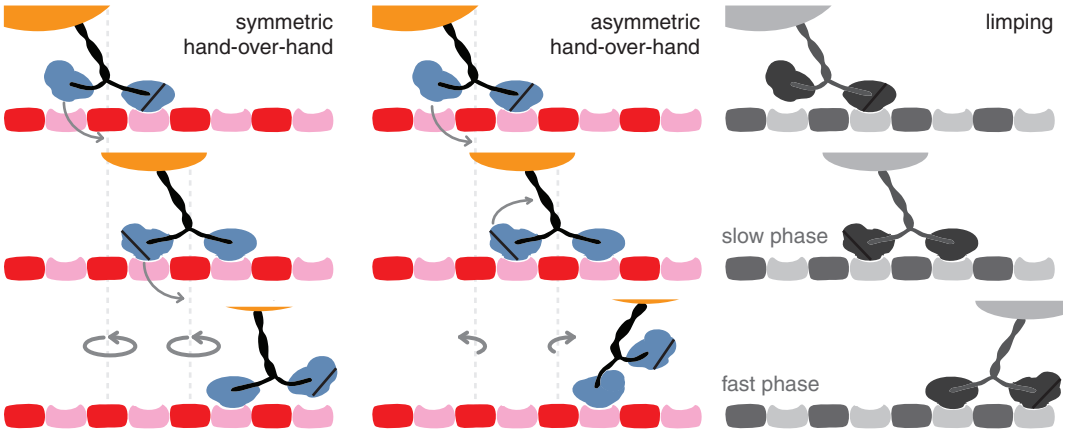

Figure 2: Proposed models of the stepping mechanism of kinesin
Kinesins carry cellular cargo over microtubules in a stepping manner. Hydrolysis of one ATP powers the individual step. The ATP hydrolysis domain and the microtubule binding domain is a part of the so called 'motor head'. The motor head binds to the tubulin dimers in a alternating hand-over-hand manner.

of the light polarization. The birefringent microspheres align with the linear polarization of the incident laser beam and any rotational fluctuations can be detected with a very high angular and temporal resolution using a quadrant photo-diode. Interestingly, I was able to observe these microspheres rotate with a very high frequency upon interaction with circularly polarized light. The birefringent microspheres were calibrated and characterized for detecting steps of kinesin and angular motion around the axis parallel to the propagation of light also called yaw. In this process, I was also able to, for the first time to my knowledge, observe the phenomenon of pitch and roll of these microspheres.

Using a combination of the methods above, we were able to observe interesting features of the rotation-stepping mechanism of kinesin. At saturating ATP concentrations, I found that motors rotated unidirectionally producing significant torques on the probes. Observing the individual steps, we were able to infer that the motor is capable of 180° rotation per step. Our method is generally applicable to study rotary motion of molecular machines and our findings have implications for cargo transport and other motor activities such as microtubule bundling during mitosis.

This thesis describes the various approaches and associated results to understand how molecular kinesin motors work.

The first chapter in this thesis discusses the necessity of having anisotropic probes for detecting rotational motion at the microscopic scale. The chapter further elucidates the various innovative probes used by previous researchers and their respective applicability for detecting microscopic torques. I then go on to present the novel probes synthesized by me for detecting kinesin rotation, and the challenges to

couple these to biological molecules.

The second chapter introduces the characteristics of optical tweezers, which make them ideal for my experiments. I then go on to show the methods required to modify an optical tweezers to the so called, optical–micro-protractor, a device which allows precise and sensitive measurement of microscopic angular motion. The chapter also enlists the various protocols of calibrating such a device for detecting microscopic torques.

The last chapter presents results for the single molecule motility assays of kinesin motor protein. I describe kinesin motion on microtubules and the specific problem of the torsional stiffness of kinesin as a facilitator of transferring and storing torque. I also present single-molecule motion of kinesin comprised of both translation and rotation of birefringent microspheres, using our micro-protractor.

Finally, I discuss possible experiments to understand the role of individual domains of kinesin in stepping and torsion, with the system I established. I also comment on the role of birefringent microspheres as efficient probes for optical tweezers.

"We demand rigidly defined areas of doubt and uncertainty!"

Douglas Adams

1

Liquid crystalline birefringent microspheres

Microspheres as probes, are indispensable tools for observing and manipulating biological molecules. Microspheres range in sizes from 0.1 μm to 100 μm and available as fluorescent, magnetic or birefringent. These versatile probes have found application in the fields of drug delivery[39], microrheology[84,118,155], fluorescence imaging[104], cell sorting[17] and force transduction and measurement in magnetic and optical tweezers (Chapter 2)[20,52,74,168].

Owing to their monodispersity and physical and chemical characteristics, dielectric silica or polystyrene microspheres are often used as optical-trapping probes. The optical properties of these materials together with the size determine the trapping efficiency, specifically the displacement sensitivity and the trap stiffness. However, using only a single, homogeneous, isotropic, unstructured material limits the range of trapping properties and thereby the applications of optical tweezers. Novel microspheres may have prop-

erties which are lacking in polystyrene and silica microspheres. These custom-made microspheres either enable the generation of high-forces, a higher force/time resolution [75] or the possibility to apply and measure torques [16,50,92,131].

Over the years, applying and measuring microscopic torque was of interest to answer questions in biology and physics. Optical and magnetic tweezers are often the tools of choice when small molecules, weak forces and torques are to be measured. As probes, polystyrene microspheres lack the inherent anisotropy required to observe microscopic rotation. Other materials like vaterite [7,84,103,118,166,174] and quartz [41,92,130,139] are optically anisotropic and employed for rotation assays in optical tweezers. The limitations with these crystals is that their synthesis and surface coupling to bio-compatible molecules is often not possible. Vogel et al. [166] have shown a successful synthesis and surface modification of vaterite particles but to the best of my knowledge, complete biological assays using these microspheres are still lacking.

In this chapter, the application of liquid crystal microspheres as probes for inducing and measuring microscopic torque is discussed. The chapter starts with an introduction to liquid crystals, followed by their chemical properties, synthesis, polymerization and finally surface modification and protein coupling. The optical properties are discussed in the subsequent chapter. The probes employed for trapping are interchangeably referred to as microspheres or simply particles in this thesis.

1.1 Liquid crystals and liquid crystalline phases

1.1.1 States of matter and liquid crystals

Matter is most often classified as being in a solid, liquid, and gas phase depending on the amount of kinetic energy and the molecular structure. A mesophase exists between solids and liquids, also known as the liquid crystals.

In 1888, Reinitzer [137], while conducting experiments on cholesteryl benzoate, discovered a strange phenomenon. Reinitzer was trying to figure out the correct formula and molecular weight of cholesterol but he realized that cholesteryl benzoate when heated, melts at 145 °C to form a milky liquid, and at 179 °C the milky liquid becomes clear. When the substance is cooled, the reverse processes occur: The clear liquid turns milky at 179 °C , and the milky liquid solidifies at 145 °C . Eventually Lehmann [97] realized that the cloudy liquid was a new state of matter and coined the term “liquid crystal”. Liquid-crystals, much like their name suggests, are mesophases which possess similarities to liquids as well as to solid crystals [94].

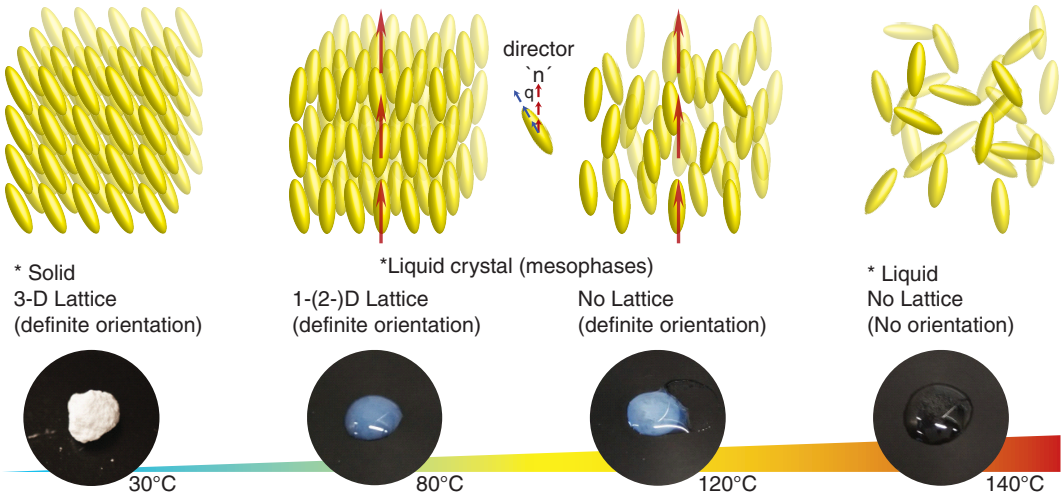

Figure 1.1: Temperature dependent phases of liquid crystals and the director axis.
Liquid crystals like most solids exhibit different phases with an increase in temperature. Each ellipsoid represents one mesogen molecule. The vertical red arrow indicates the direction of the director axis 'n' of the liquid crystal (adapted from Andrienko [6]). The pictures at the bottom show the state of mesogen RM257 at temperatures of 30 °C, 80 °C, 120 °C and 140 °C. It is interesting to see, two milky mesophases at 80 °C and 120 °C and the transparent liquid at 140 °C (clearing temperature of RM257 is 127 °C).

In this liquid-crystalline phase, the molecules of a liquid crystal, or "mesogens" have a partial orientational order and partial translational order as seen in Figure 1.1. Liquid crystals have weak inter-molecular forces which hold the molecules together. These forces are easily affected by changes in temperature, pressure, and electromagnetic fields and can be visualized from the orientation of individual mesogen or by observing the interaction of bulk liquid crystal with electric, magnetic or electromagnetic fields [32]. A liquid crystalline phase can be attained by changing temperature as discussed above or through mechanisms co-dependent or independent of the temperature as discussed below.

1.1.2 Lyotropic, Thermotropic and Amphotropic phases

Depending on the mechanism of formation of the mesophasic state, liquid crystals can be categorized as lyotropic, thermotropic and amphotropic. The mesogenic molecules which self-assemble at a specific concentration in a solvent are called lyotropic liquid crystals and are ubiquitous in everyday life (e.g. Television screens, soaps, some clays etc.) and in biological systems, forming bilayers, micelles, and vesicles. Thermotropic liquid crystal phases occur in specific temperature ranges. The typical method to obtain thermotropic liquid crystal phase is to heat up a certain solid or cool down a certain liquid. Usually as temperature decreases, the material increases its degree of order and may go through different liquid crystalline phases before it turns to a crystal. Amphotropic liquid crystals exhibit both lyotropic and

thermotropic properties. Through the rest of this thesis only thermotropic liquid crystals are discussed.

A thermotropic liquid crystal exhibits a variety of temperature dependent phases. Several degrees of orientational and positional order can exist due to different arrangements of the molecules at different temperatures. In this way, several liquid crystal phases were identified for the first time by Friedel [48] and classified as either nematic or smectic. Each of these phases shows a unique alignment of individual mesogens with respect to their neighbors.

1.1.3 Nematic and Smectic phases

The simplest of the phases is the nematic phase. The word nematic originates from the Greek word νήμα (nema), meaning "thread". Thread-like topological defects are often observed in nematic liquid crystals, hence "nema". In a nematic phase, the mesogens or the rod-shaped molecules have no positional order, but they self-align with their long axis roughly being parallel to have long-range directional order [93]. Nematic liquid crystals exhibit an average orientational order only along the long axis of the molecules (director, n), while their centers of mass are distributed isotropically (Figure 1.1). The nematic phase is also the one observed at the highest temperature. Cooling a nematic phase leads to another level of ordering in the form of a layered structure, representative of a one-dimensional positional order called the smectic phase. A particular type of mesogen, when subjected to increasing temperatures, may exhibit various smectic phases followed by the nematic phase and finally the isotropic phase [33]. The classification of different mesophases as described here is valid for rod-like molecules, also known as calamitic liquid crystals. Over time, different geometric molecular shapes have also been shown to display mesomorphic behavior. Chandrasekhar discovered the discotic liquid crystal phase [29] and more recently banana-shaped molecules [125] and metallomesogens [150] have received considerable interest. Discotic liquid crystals involve flat, disk-like molecules and exist in a nematic or smectic phase.

In this study, liquid crystal microsphere synthesis was carried out by first synthesizing calamitic liquid crystals and then locking them in the nematic phase.

1.1.4 Orientational order and optical anisotropy in nematic liquid crystals

The order parameter is a means to describe the amount of orientational order that a liquid crystal possesses. It is defined by averaging the function $\frac{1}{2}(3cos^2\vartheta - 1)$ for all the liquid crystal molecules, where ϑ is the angle between the director 'n' and the molecule axis [33]. The order parameter can range from 0 to 1,

but often ranges from 0.3 to 0.9; 0 refers to no order (complete disorder, like an isotropic liquid), and 1 refers to complete order (like a solid)[33,105].

As shown in Figure 1.1, an individual mesogen in a liquid crystal is not parallel to the director.Only on average, a group has a parallel alignment[93]. This alignment occurs due to attractive van der Waals forces, and due to conservation of packing energy. The correlations in the positions between the centers of gravity of neighboring nematic mesogens (order parameter) are similar to those existing in a conventional liquid, because nematic liquid crystals flow like liquids. The order of nematic liquid crystals is observable in its macroscopic tensor properties: for instance, a nematic birefringent microspheres is uniaxial, with the optical axis along n. The ordering of individual molecules in a liquid crystalline phase is extensive and extends up to the entire domain size (few micrometers). This ordering is usually not observed as a macroscopic effect like for the macroscopic crystal shape as seen for solid liquid crystals. However, the final shape can be imposed using boundaries or via an applied electric field, to enforce a single ordered domain in a macroscopic liquid crystal. The ordering in a liquid crystal might extend along only one dimension, with the material being essentially disordered in the other two direction[33,42]

Since the objective of this thesis is to synthesize birefringent microspheres, it is imperative to understand the properties of liquid crystals suspended in a medium.

1.1.5 Liquid crystals in confined Geometries

When a liquid crystal is confined by a surface, the alignment of individual mesogens is defined by competing intra- and inter-molecular forces (also called "surface anchoring"). A colloidal liquid crystal differs from conventional liquid crystal formations in that, its structure and shape is governed only by the intra-molecular forces and the temperature. One example of a confined liquid crystal that has attracted particular interest from physicists is the nematic droplet. Independent of the method used, phase separation[43,140], encapsulation[27,44], or permination[35,36], these systems have one underlying theme: a symmetry breaking non-planar confinement imposed by the surrounding matrix.

In 1904, Otto Lehmann reported the confinement of liquid crystals[172]. Lehmann was able to suspend large droplets of nematic liquid crystal in a viscous isotropic medium while observing these droplets with a polarizing microscope, he was able to comment on the relation of the director configuration with that of the material composing the liquid crystal. Spherical nematic droplets gained interest only towards the end of the last century, when it was discovered that sub-micrometer and micrometer droplets could easily

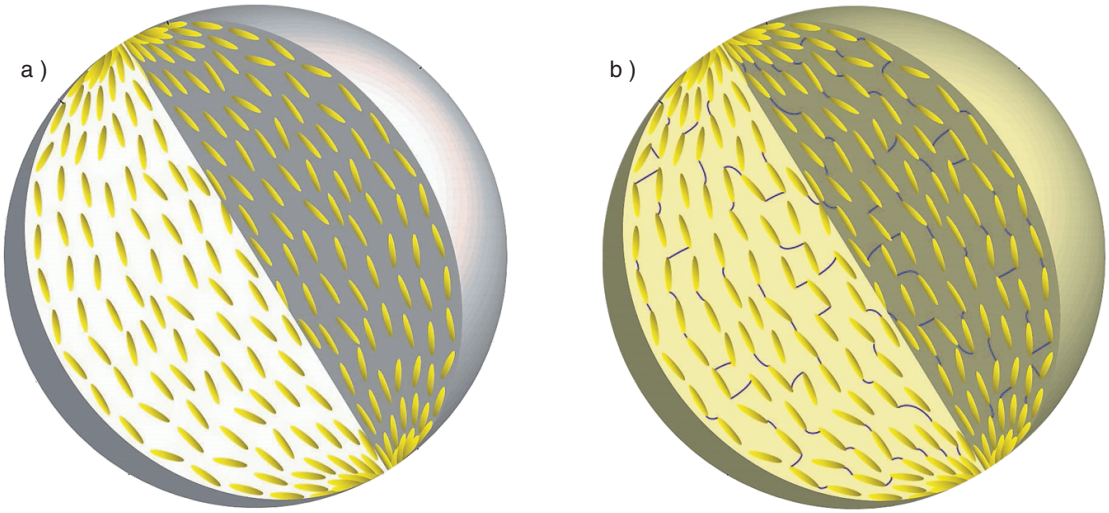

Figure 1.2: An illustration of non-polymeric and polymeric birefringent microspheres.
a) non-polymeric and b) polymeric birefringent microspheres. The ellipsoids represent the individual mesogen and the blue lines connecting these mesogens in b) represents polymerization. The (-Ac) indicates exposed Acrylate groups. The concentration of ellipsoids at the ante-poles represent boojums and the lines of ellipsoid indicates director axis 'n'.

be dispersed in a rigid polymer binder by either phase separation [43,140] or emulsification [44].

Our system consists of solid droplets of the nematic liquid precursor (RM257) in the nematic liquid crystalline phase (polymerized or non-polymerized, Figure 1.2) dispersed in a liquid (aqueous solution).

1.1.6 Colloidal birefringent microspheres

Microspheres capable of rotating under the influence of light have found application in interesting fields such as micro-rheometers [155], optical switches [27] and as microfluidic stirrers and valves. Many commercially available non-birefringent colloidal (like CuO) particles have the ability to absorb light, thus substantial optical forces can be exerted on them. It is possible to exert torsional forces on these (absorptive) particles as shown by Friese et al. [49] with elliptically polarized laser beams and by He et al. [64], Simpson et al. [154] using beams with helical phase structure . A drawback of this technique is the inability to rotate particles at a higher rate and the biological incompatibility due to material toxicity. An absorptive system may overheat depending on the power of incident light. Heating can be avoided by using transparent optically anisotropic (birefringent) particles.

In 1936, Beth [14] showed that torque can be imparted on a quartz wave-plate due to a change in polarization of transmitted light. The wave-plate used by Beth for his experiments was $\approx 10.7cm$ in diameter. Measuring and imparting torque at the microscopic scale requires that a given amount of light should

be able to rotate the director of the particle sufficiently, so as to create a measurable change, detectable in a cross-polarized setup. Early experiments with microscopic birefringent particles were carried out with crushed fragments of a crystal of 'Iceland spar' calcite[50].

Recently, more convenient and reproducible sources for particles which could be rotated have been employed. These particles can be classified into three groups[140]: (i) fluoropolymer latex particles, (ii) inorganic particles, and (iii) particles made by emulsification of liquid crystals.

The fluoropolymer particles made with PTFE[40] have a very high director order (crystallinity of 70-80 %) with a birefringence of $\Delta n \approx 0.04$. However, these particles are not spherical (rod-shaped) and their diameters are small (≈150 nm), making them difficult to handle.

Quartz ($\Delta n \approx 0.009$), calcite ($\Delta n \approx 0.15$) and vaterite ($\Delta n \approx 0.1$) particles represent the group of inorganic birefringent materials. The particles too have a high director order, and correspondingly high birefringence. However, there are drawbacks when it comes to applicability. They are poly-crystalline, their shape or size is difficult to control, they dissolve in acid and buffers and their surfaces are difficult to modify. Many inorganic particles exhibit birefringence due to their particular shape. When particles with one refractive index and an anisotropic shapes, such as rods, are suspended in a medium with a different refractive index, they exhibit "form birefringence". Bio-molecules like collagen and microtubules exhibit form birefringence due to their filamentous nature. A notable exception to this case are the spherical vaterite particles. These particles can be grown in a controllable manner, to as large as a few microns and a surface modification protocol is already established by Vogel et al.[166]. Though, spherical vaterite particles smaller than a few micrometers have not been synthesized. Vaterite has been a favorite candidate for surface modification. Kim & Lee[81] used fluo-silicic acid to enhance acid resistance of calcium carbonate crystals18 while, Zhang et al.[181] modified the surface of Calcium carbonate crystals using wax grafting maleic anhydride (MA-g-PEW) coupling agent, Walsh et al.[167] coated vaterite micro-sponges with PVC polymer to stabilize the particles against short term dissolution. Fuchigami et al.[51] produced hemispherical hollow silica micro-capsules by applying a silica coating onto hollow vaterite particles. Nieminen et al.[123] mentioned silica coating of vaterite microspheres for tailoring their optical properties. Vogel et al.[166] used mixed layer coatings of silica and organo-silica to stabilize and functionalize vaterite microspheres and make them applicable for biological experiments. Other techniques that have been attempted involve spin or spray coating, plasma treatment, micro-encapsulation, mechanical/chemical treatment, sputtering, physical vapor deposition, ionic beam, and chemical vapor

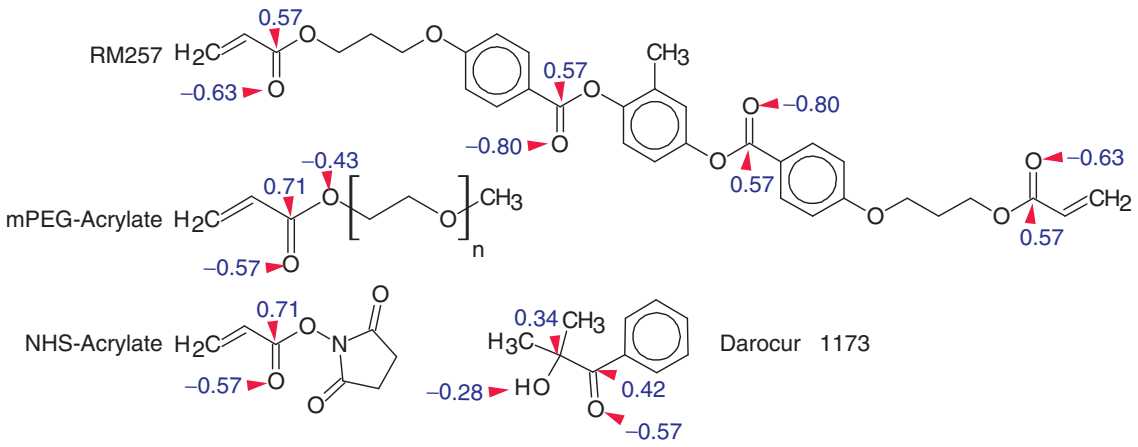

Figure 1.3: Chemical structure of molecules involved in synthesis of surface modified birefringent microspheres. Chemical structure of molecules involved in synthesis of surface modified birefringent microspheres. RM257 is a symmetric di-acrylate capable of polymerization and acrylate coupling with mPEG-acrylate and NHS-Acrylate. Darocur 1173 is the photo-initiator catalyst which activates the acrylate groups. The numbers in blue and the red arrows indicate the charge on the respective atoms. The charges were computed by Jmol (http://www.jmol.org/).

deposition[178].

The third class of optically anisotropic colloids is liquid crystal emulsions. The optical properties of these ordered materials have potential for use as birefringent colloidal or as viewing correction films[165], since they have a high birefringence $\Delta n \approx 0.25$ at 589 nm[24] for 4-biphenylyl 4-(6-acryloyloxy-hexyloxy)benzoate. The optical properties can be stabilized over a wide operating temperature range, by capturing the nematic order by photo-polymerization. One way to prepare these particles is by dispersing the liquid crystal into a co-flowing, surfactant-laden continuous phase via a narrow orifice. The particle size is a function of the diameter of the orifice, the velocity of the continuous phase, the extrusion rate, and the viscosity and interfacial tension of the two phases. Highly mono-disperse birefringent particles as small as 2 μm can be prepared by this method[160]. To synthesize small (200 nm to 2 μm) birefringent microspheres, I employed a precipitation method using nematic liquid-crystal mesogen RM257.

The following section will elaborate on the protocol modified from Sandomirski et al.[140]. The protocol involves the precipitation of RM257 diacrylate mesogen as polymerized or un-polymerized microspheres in an aqueous medium, in the presence or absence of photo-initiator Darocur 1173 (Figure 1.3) respectively. As shown in Figure 1.3 the molecules NHS-acrylate and mPEG-acrylate are used for protein coupling and surface passivation respectively.

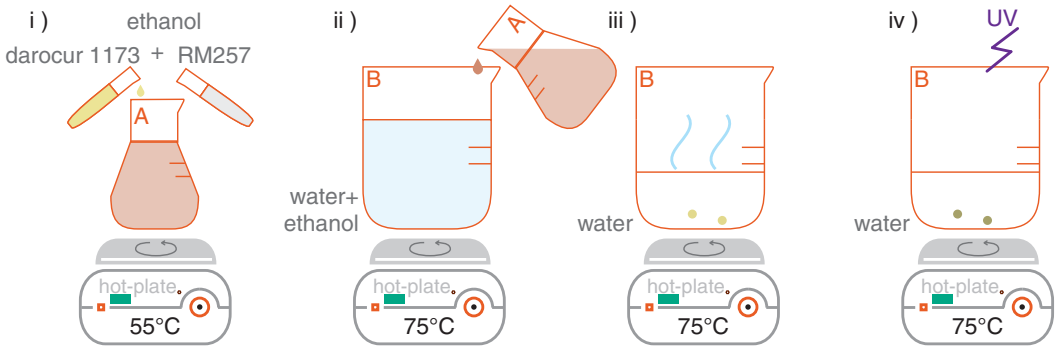

Figure 1.4: Graphical representation of the protocol for synthesis of birefringent microspheres.
(i) Heat Ethanol to 55 °C, dissolve RM257 and/or photo-initiator Darocur 1173 in it, 'Solution-A'. (ii) Heat water or ethanol/water mixture on a separate heating plate to 75 °C, add solution-A in a drop wise manner while constantly stirring the solution, 'Solution-B'. (iii) Evaporate solution-B till all the added ethanol evaporates. (Cool at RT). (iv) To make polymerized microspheres, maintain solution-B at 75 °C and irradiate with UV.

1.2 Synthesis of birefringent RM257 microspheres

The fabrication procedure starts by dissolving the nematic liquid crystal precursor in an organic solvent at elevated temperatures. Subsequently, evaporation of the solvent causes a precipitation of spherical particles into the aqueous solution (Figure 1.4)[140]. The microsphere size and polydispersity can be controlled by varying the amount of liquid crystal precursor, volume of the organic solvent, and evaporation rate. At room temperature, the microspheres are solid. Addition of a photo-initiator to the reaction mix before precipitation enables the cross-linking of the mesogen. In this manner, a fixed orientation can be locked, which makes the microspheres more robust at higher temperatures and increases their shelf-life. The birefringence of polymerized microspheres is lower than that of non-polymerized ones[140]. However, polymerized microspheres remain suspended for a longer time and can be suspended in ethanol for centrifugation. The microspheres can be functionalized using silica chemistry once a silica coating has been added or by acrylate chemistry.

1.2.1 Chemical properties of liquid crystal precursor, RM257

The achiral diacrylate, RM257 (Merck)[27] is also known as 4-(3-Acryloyloxypropyloxy)-benzoesure-2-methyl-1, 4-phenylester. The systematic name is 2-Methylbenzene-1, 4-diyl bis4-[3-(acryloyloxy) propoxy] benzoate. The molecular weight is 588.60 and the bulk index of refraction is 1.564. At room temperature RM257 exists as a white amorphous solid. RM257 is crystalline up to 65 °C, nematic up to 127 °C, and isotropic above 127 °C (Figure 1.1).

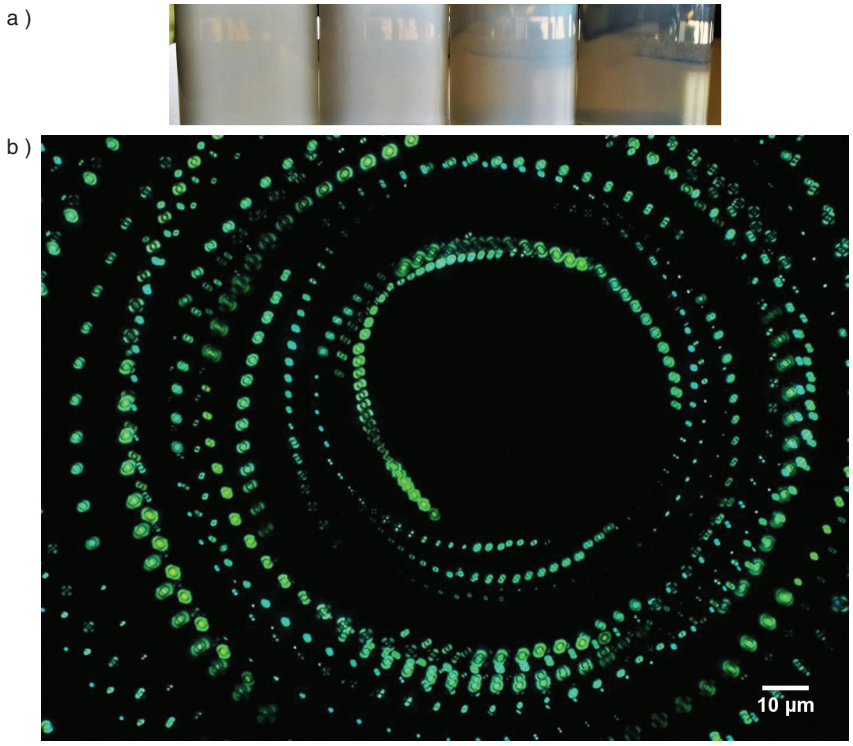

Figure 1.5: Isogyres of birefringent microspheres observed in a polarization microscope.
a) Birefringent beads of different sizes diffract different amount of light. The vials from the left to right have an average bead size of 1.2 µm , 1 µm , 0.8 µm and 0.4 µm respectively. b) The synthesized RM257 microspheres are tested for birefringence from the Maltese-cross patterns (isogyres) observable with a polarizing microscope. The image was taken by rotating the microspheres-sample on a Zeiss Axio Imager-A2m polarization microscope.

RM257 is a unique mesogen, in that it has terminal acrylate groups which can be used for polymerization with other RM257 or acrylate groups from other compounds. UV-curing in the presence of photo-initiator Darocur 1173 activates the terminal acrylate groups catalyzing polymerization.

Photo-initiator

The photo-initiator mixed with the RM257 is Darocur 1173 (Ciba Specialty Chemicals Inc.). Darocur 1173 is a versatile, highly efficient liquid photo-initiator which is used to initiate the polymerization of chemically unsaturated prepolymers like the achiral diacrylate RM257. The systematic name of Darocur 1173 is 2-Hydroxy-2-methyl-1-phenyl-propan-1-one and its molecular weight is 164.2.

1.2.2 Procedure for synthesis of birefringent microspheres

The procedure for synthesizing birefringent microsphere relies on the insolubility of the RM257 liquid-crystal precursor and its nematic nature at temperatures above 70 °C . Briefly, I weigh RM257 powder

and dissolve it in preheated organic solvent like ethanol. Darocur 1173 is added at this step if polymerized microspheres are desired. The solution is stirred at 55 °C till RM257 is completely dissolved. This solution is then transferred in a drop-wise manner to another preheated solution of ethanol and water. This temperature should be greater than 70 °C , the nematic temperature of RM257. The ratio of ethanol to water can be varied from 0 to 1 to get smaller or larger particles respectively. The ethanol water solution is stirred at 75 °C till the entire amount of ethanol evaporates completely (Figure 1.4). The rate of evaporation can be controlled by covering the beaker with an aluminum foil with holes cut out. The diameter of these holes can then be adjusted to adjust the evaporation rate. The birefringent microspheres are observed as turbid white suspension. The turbidity of the solution is also a rough way to estimate the size of microspheres (Figure 1.5 a). The birefringent microspheres when observed in a polarizing microscope show a characteristic interference pattern (isogyres) (Figure 1.5 b). The isogyres for a uniaxial liquid-crystal like RM257 changes intensity as the polarization of light is rotated from 0 to 90 degrees. The interference pattern has the maximum intensity when the fast axis of light is parallel to the director axis of the birefringent microspheres and looks like a "dumb-bell", at an angle perpendicular to the fast axis, the intensity is minimum, the interference pattern observed as a "maltese-cross". The individual mesogens are aligned in an averagely parallel manner towards the center of the microsphere. The surface-tension forces the mesogens to curve around the microsphere as shown in Figure 1.2a. The two termini along the axis of the birefringent microspheres are called "boojums", these are usually the points of surface defects in these microspheres.

The suspension can be irradiated with ultra violet light(UV) light for 30 to 60 minutes to polymerize these microspheres. The UV intensity, the distance of UV source to the suspension and the time of incidence decides the rate of polymerization. The polymerized microsphere suspension can be observed as light yellow in color. The orientation of mesogens is locked due to end-to-end acrylate polymerization of the individual mesogens (Figure 1.2b). The polymerized birefringent microspheres are more stable than the un-polymerized ones with respect to the shelf-life and, tolerance to centrifugation and washing. The microsphere synthesis protocol is described in greater detail in appendix A.2.3.

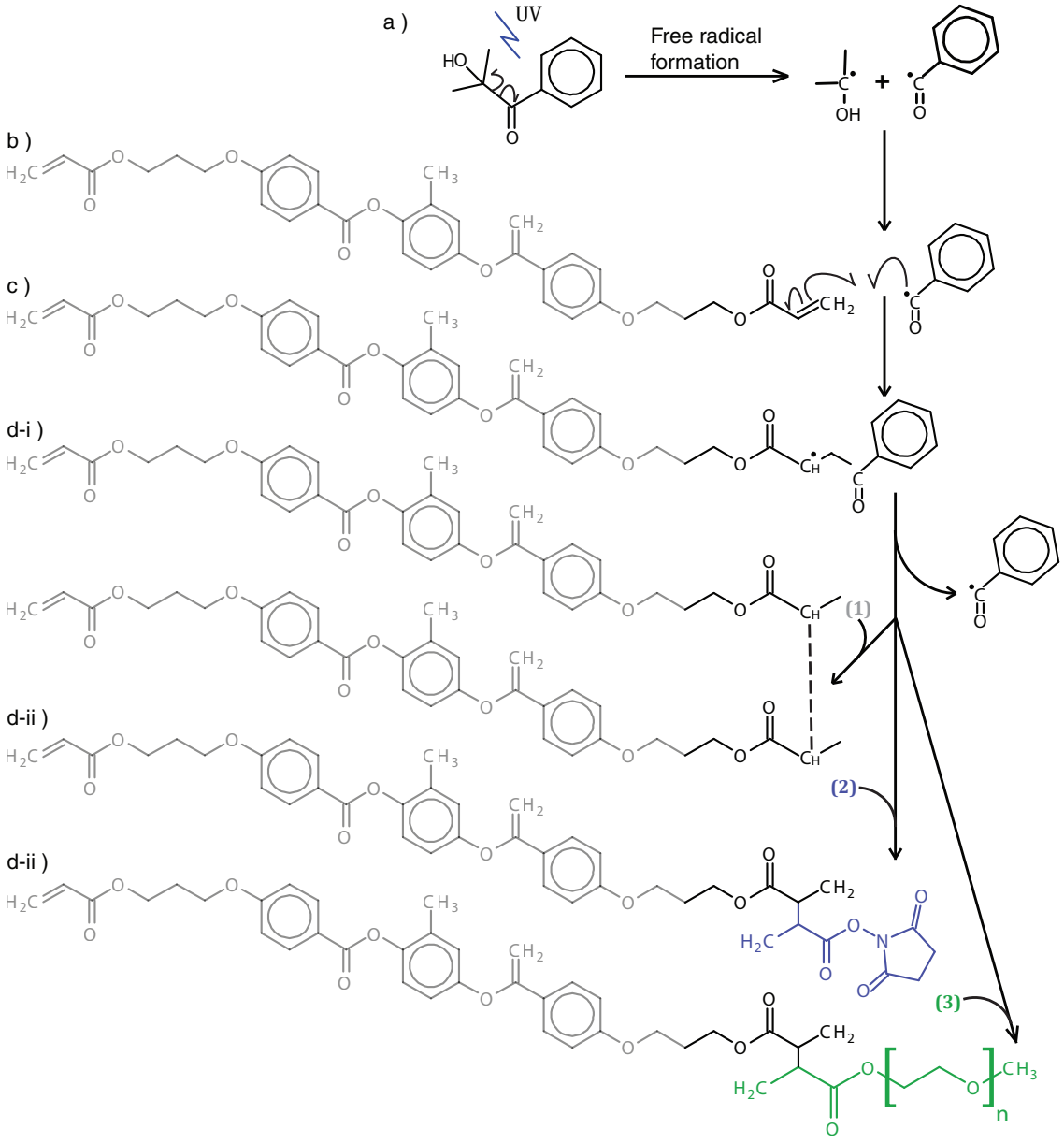

Figure 1.6: Reaction mechanism of acrylate polymerization.
The terminal acrylate groups on RM257, mPEG-Acrylate and NHS-Acrylate are activated by photo-initiator, Darocur 1173. Since the RM257 is polymerized post crystallization into the liquid crystal state, end-to-end linear polymerization is encouraged. A non-polymeric and a polymeric microspheres are assumed to expose free acrylate groups on the surface which then can couple with the acrylate groups of mPEG and NHS, in case the surface of the microspheres is to be modified for protein coupling.

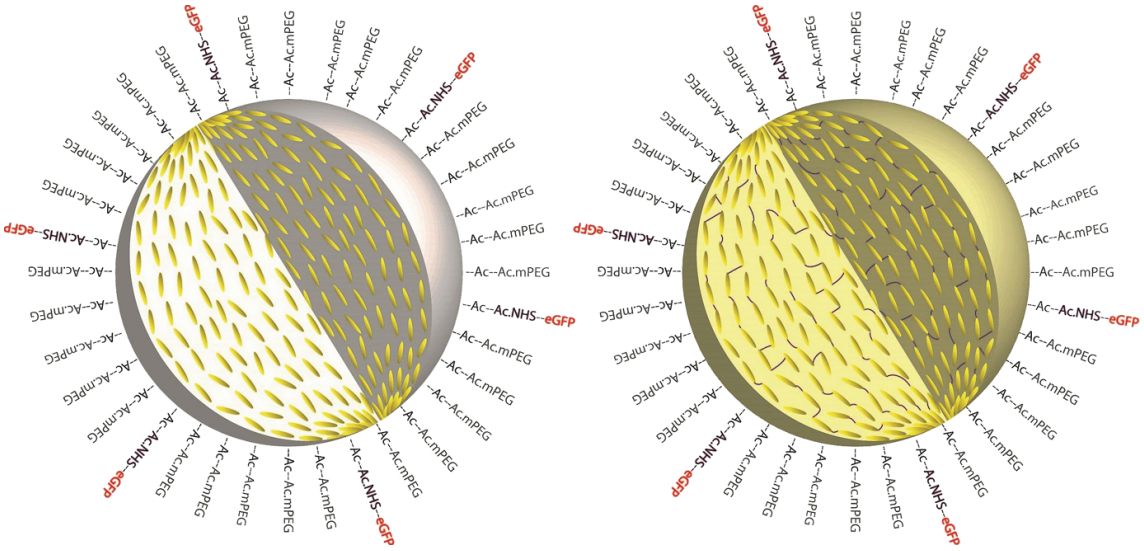

Figure 1.7: Activation of birefringent particles to couple biological molecules.
Birefringent microspheres have acrylate groups on their surface. These groups afford an efficient and easy mechanism to couple molecules with similar acrylate groups through photo polymerization. This protocol can be used to synthesize non-polymeric (a) and polymeric (b) protein coupled birefringent microspheres.

1.3 Surface modification of birefringent microspheres

The use of colloidal microspheres can be exploited fully by coupling functional molecules to their surface. Surface modification can make fragile colloidal particles stable, improve optical properties[75] and, allow biological experiments. Colloidal liquid crystals can be silica coated to keep them emulsified and to make them more robust. Bio-molecules like motor proteins, covalently attached to the birefringent microsphere surface are a stable system for invitro single molecule experiments. Decorating these microsphere surfaces with poly ethylene glycol brush prevents non-specific binding of these microspheres to the glass walls of the sample chamber, and to other proteins.

In this thesis two approaches were attempted: The silica coating of RM257 particles and the surface modification and functionalization via acrylate coupling.

1.3.1 Surface chemistry of RM257 birefringent particles

The reaction scheme for surface modification of RM257 microspheres is shown in Figure 1.6. Of particular interest are methoxy-polyethylene glycol (mPEG) and N-hydroxysuccinimide (NHS-ester) moieties which passivate the microsphere surface and present specific active areas to allow binding of single protein molecules (like kinesin) respectively. PEGs are long (ethyleneoxide-) chained hydrocarbons which

form an inert layer on microsphere surface. Methoxy-PEG forms a dense brush around the NHS-protein, to block unspecific binding of protein to the microspheres surface. The PEGylation of the surface also blocks the microspheres from unspecific sticking to the surface of sample chamber. NHS esters are reactive groups formed by carbodiimide-activation of carboxylate molecules. NHS ester-activated crosslinkers and labeling compounds react with primary amines in physiologic to slightly alkaline conditions (pH 7.2 to 9) to yield stable amide bonds. The reaction releases N-hydroxysuccinimide (NHS). The individual PEGs and NHS ester are acrylate functionalized to facilitate acrylate polymerization to exposed acrylate groups on the microsphere surface. The terminal acrylate groups of participating molecules (see Figure 1.6) and NHS ester molecules passively couple to amine groups on proteins. NHS ester-activated crosslinkers and labeling compounds react with primary amines in physiological and alkaline conditions (pH 7.2 to 9) to yield stable amide bonds[65].

Note that, hydrolysis of the NHS ester competes with the primary amine reaction. The rate of NHS hydrolysis increases with an increase in buffer pH and temperature, thus decreasing crosslinking efficiency. The half-life of hydrolysis for NHS-ester compounds is 4 to 5 hours at pH 7.0 and 0 °C. This half-life decreases to 10 minutes at pH 8.6 and 4 °C. The extent of NHS-ester hydrolysis in aqueous solutions free of primary amines can be measured at 260 to 280 nm, because the NHS byproduct absorbs in that range. NHS-ester crosslinking reactions are most commonly performed in phosphate, carbonate-bicarbonate, HEPES or borate buffers at pH 7.2 to 8.5 for 0.5 to 4 hours at 4 °C. Primary amine buffers such as Tris (TBS) are not compatible, because they compete for reaction[65].

The surface modification of birefringent microspheres requires a working understanding of the molecules involved in the reaction. The charge distribution of individual molecular domains with respect to the medium they are suspended in, decides the functional groups available on the microsphere surface.

Visualizing the partial charge of the atoms in a molecule is a good approach to understand its interactions. Typically, an atom with the greater partial charge, is more susceptible to associate with other atoms where the partial charge is opposite in magnitude. The partial charge of molecules involved in our experiments, namely RM257, Darocur 1173, NHS-Acrylate and mPEG-Acrylate (methoxy-PEG) is calculated using Jmol (Figure 1.3). The reactive mesogen RM257 has four negatively charged ester groups which are known to have strong interactions with positively charged ions. Like wise the hydroxyl group and the ketone group on Darocur 1173 is strongly negative. Imparting a general negative charge to RM257 microspheres. The molecules NHS-Acrylate and mPEG-acrylate are positive and about neutral, respec-

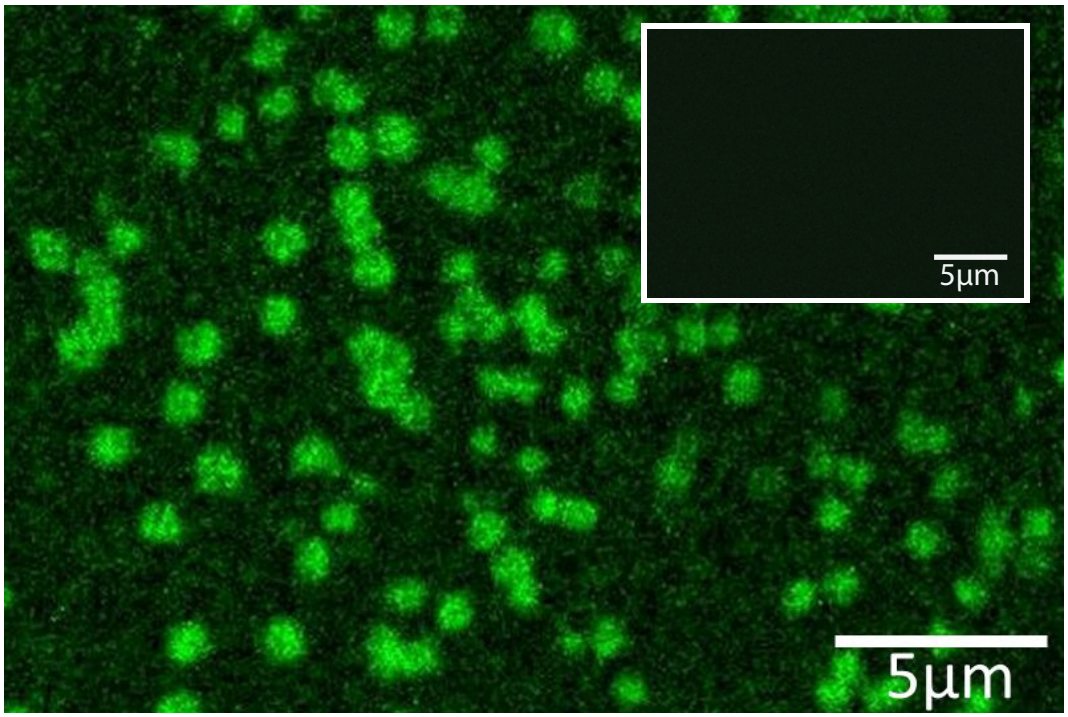

Figure 1.8: RM257 birefringent microspheres coated with GFP and imaged under an epi-fluorescence microscope. Birefringent microspheres coated with saturating concentrations of GFP and imaged under an epi-fluorescence microscope. The fluorescence indicates the presence of GFP on the microspheres and serves as proof of principle for protein coupling. A control experiment with no surface modification showed no fluorescence at all (inset).

tively. I assumed that colloidal RM257 microspheres attract molecules of NHS-Acrylate strongly and mPEG-acrylate weakly. Once in close proximity and in the presence of photo-initiator Darocur 1173, the terminal acrylate groups could be activated by UV irradiation followed by polymerization reaction. The reaction scheme also assumes that the relatively short irradiation time (20 seconds) is short enough to avoid any polymerization beyond the surface of the microspheres. Non-polymerized microspheres are preferred over polymerized ones, since polymerizing birefringent microspheres reduces their birefringence[140]. The microsphere synthesis is modified to retain trapped photo-initiator in unpolymerized birefringent microspheres (Appendix A.2.3). The trapped photo-initiator then acts as a catalyst for coupling acrylate-functional molecules to the microsphere surface. Figure 1.8 shows birefringent microspheres coupled to green fluorescent protein(GFP) via NHS acrylate coupling. A similar coupling was employed in Chapter 3 to couple anti-GFP antibody to the microsphere which further binds to the GFP on the tail domain of the kinesin motor protein.

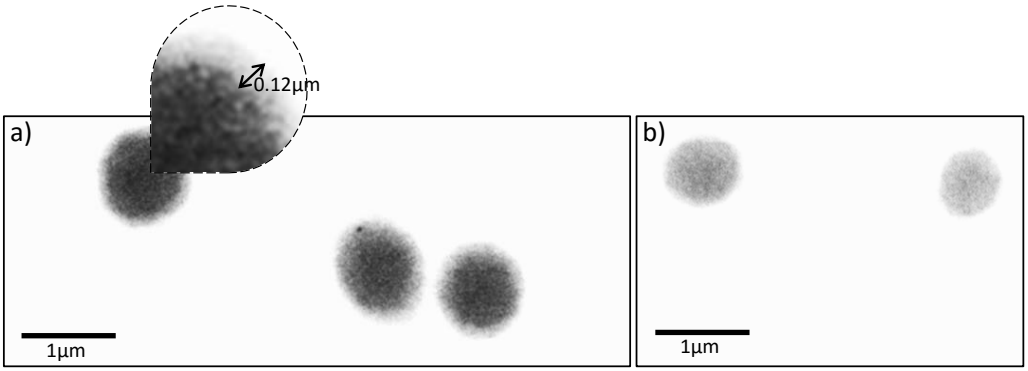

Figure 1.9: An electron micrograph (TEM) of Silica coated and non-coated birefringent microspheres.
Silica coating is a robust method of creating a shell on birefringent microspheres. a) Under an electron microscope the silica shells appear brighter against the dark birefringent core. b) The birefringent particles without shell did survive the electron microscopy and seem to retain a spherical shape.

1.4 Silica coating of birefringent microspheres

Silica coating of microspheres[134] enhances the stability and allows the application of standard surface modification reactions. The silica shell is produced via a conventional base-catalyzed, sol-gel reaction via the hydrolysis and condensation of tetraethyl orthosilicate (TEOS) in ethanol according to the Stöber et al.[156] method modified by using RM257 microspheres as negatively-charged cores and using the surfactant Cetrimonium bromide (CTAB) as a template for mesopores which are formed through the self-assembly of CTAB. This protocol was first established by Suman De in our lab for silica coating of nanodiamonds and modified further to suit RM257 microspheres.

The coating method was originally based on the formation of polydisperse, mesoporous silica microspheres[57] of type MCM-41[89]. The pores with a diameter of about 3–4 nm result from worm-like micelles (with a persistence length of about 15 nm) that CTAB forms at concentrations well above its critical micelle concentration (CMC ≈1 mM; we use about 10 mM)[28,152] in particular in the presence of negatively charged molecules. The surfactant and ethanol[102] are also crucial for a monodisperse[180] coating on negatively charged, nanometer-sized cores[82]. Ethanol (i) segregates to the micelles and swells them and (ii) slows-down the hydrolysis and condensation reaction of TEOS promoting the growth of spherical particles via a reaction-limited monomer-cluster growth, also called Eden growth, in combination with Ostwald ripening (pp. 199–201 in[143]). The shell thickness is determined by the amount of both, CTAB and TEOS[134].

Figure 1.9a shows a silica coated birefringent microsphere as observed with TEM electron micrograph.

The microspheres are visible as a densely colored birefringent core and a mild colored silica shell. In the case of birefringent microspheres we desired thin silica shell to reduce any depolarizing effects. I was able to produce a shell thickness as small as 0.12 μm .

1.5 Discussion and conclusion

We have generated different sized, polymerized and non-polymerized, birefringent microspheres using a precipitation approach. We could polymerize these particles while preserving their shape, to form polymer-stabilized microspheres of nematic liquid crystals. We were further able to coat these particles with a silica shell and with bio-compatible molecules so as to use these particles in biological systems. These results pave the way for the use of birefringent microspheres for the micromanipulation of single biological molecules such as DNA or motor proteins in an optical trap capable of exerting and measuring torques.

This was the tricky bit. The really tricky bit, trickiness cubed.

Hugh Laurie

2

Optical tweezers, Force and Torque

In 1619, Kepler[80], an alumni of the University of Tübingen, proposed that Comet tails point away from the direction of the sun due to solar radiation-pressure. In 1873, Maxwell[111] supplied the relevant theoretical evidence, followed by Nichols & Hull[122] and Lebedew[95]'s experimental detection of radiation pressure on macroscopic objects in 1901. But it was only in the late twentieth century when the momentum of light was transferred into an application by Ashkin[9] for an optical trap. One concept which usually escapes notice is that light beams also carry a spin angular momentum as shown by Poynting[133] in 1909. The landmark experiment by Beth[14] further paved the way for expanding optical tweezers as tools for measuring and exerting torque. This chapter discusses how to design, calibrate and measure forces and angles using optical tweezers.

2.1 Principles of optical tweezers

2.1.1 The application of momentum of light in optical tweezers

Light can be thought of either as particles, or as waves. Like all wave phenomena, light has mechanical properties. In 1905, John Poynting developed the theory of radiation pressure and momentum density and, in 1921, Albert Einstein showed that Planck's black body law and the motion of molecules in a radiation field could be explained as the single photon carrying energy $\varepsilon = hc/\lambda$ and linear momentum $p = h/\lambda$, where h is Planck's constant, c is the speed of light, and λ is the wavelength. From Newton's laws, the amount of force generated by an optical trap can be calculated by considering linear momentum transferred from the light to the trapped microsphere. The rate of change of linear momentum (equal to the force) represented by $F = dp/dt = (1/c)d\varepsilon/dt$ or $F = \wp/c$, where $\wp = d\varepsilon/dt$ is the optical power.

With the development of lasers in 1960 by Theodore H. Maiman, light induced force has been applied for various purposes, from optical trapping and manipulating live cells, bacteria, and viruses[10,11] to the cooling and trapping of neutral atoms[31,132]. Optical traps or optical tweezers have developed into a very powerful tool and are widely employed in biophysics, colloid research, micro-rheology and physics[157]. Optical tweezers are popular tools for biologist owing to their non-invasive mode of functioning in living cells, as compared to other force transducers like the atomic force microscope[121]. The scope of optical tweezers is fully exploited by the use of dielectric microspheres which act as probes to observe and manipulate molecules too small to be trapped directly. Independent of the optical trap itself, the characteristics of microspheres, their shape, size and their refractive index sets bound to the resolution, applicability and the strength of the optical tweezers. In practice, forces up to a few nanonewton with sub-piconewton resolution and sub-nanometer displacements are feasible[53,75,142].

Trapping of microspheres using an optical trap can be explained by a ray optics treatment, through an electron dipole approximation, or via the time-dependent or time-harmonic Maxwell equations using appropriate boundary conditions. The mode of explanation depends on the size of the microsphere with respect to the wavelength of the light employed for trapping.

2.1.2 Ray optics: a theory to explain trapping in optical tweezers

For a microsphere, sized greater than the wavelength of light, the trapping phenomenon can be explained using ray optics. An optically trapped dielectric object is subject to two types of optical forces: scattering

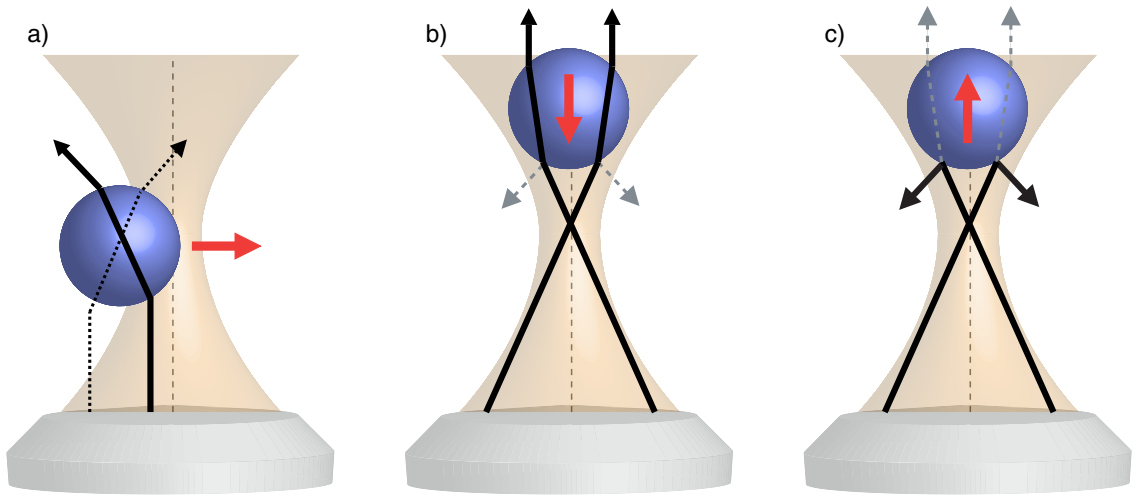

Figure 2.1: A ray optics explanation of trapping by optical tweezers.
The figures shows a laser focus optical trap in beige, a dielectric sphere in blue. The black arrows represent the direction of force due to incident light, the gray arrows represent the direction of force due to momentum conservation and the red arrow shows the vector sum of the forces on the sphere. A dielectric sphere laterally away from the laser focus a) experiences a force, in the direction of the focus, due to stronger gradient forces. While a stably trapped sphere experiences equal amount of upward and downward axial force due to the light refracted (b) and reflected (c) from the sphere.

forces, which push objects along the direction of propagation of the light or away from the beam focus, and gradient forces, which pull objects along the spatial gradient of light intensity[31]. An object is stably trapped when optical gradient forces exceed the scattering force. A simplistic view of the scattering and gradient forces could be understood from looking at the individual rays interacting with a spherical dielectric microsphere in an optical trap. As we know, light rays carry momentum and a light ray interacting with a microsphere could reflect, refract or transmit straight through the microsphere. Each of this case would follow the Newton's third law where, for every change in momentum of light there would be an equal and opposite momentum transferred on the microsphere. A reflected ray of light will push the microsphere away from itself while a refracted ray of light will exit the microsphere with its direction changed thus pushing the microsphere in equal and opposite direction (towards the focus). For a microsphere trapped at the beam focus, the individual rays of light refract symmetrically through the microsphere, resulting in no net lateral force. The scattering or reflecting rays impart a small net force on the microsphere, pushing it slightly away from the trap focus (axially). A microsphere displaced from the beam focus, tends to return to it because more intense beams impart a larger momentum change towards the center of the trap than less intense beams. The net momentum change, or force, returns the microsphere to the trap center (Figure 2.1).

Optical tweezers achieve large spatial gradients by passing a near-infrared laser beam through a high-numerical aperture microscope objective to create a sharp focus[121] so that the gradient forces exceed the scattering force, resulting in a stable trap. The explanation for microspheres significantly smaller than the wavelength of incident light can be referred from works of Harada & Asakura [63] and Nieminen et al. [124].

2.1.3 Optical tweezers employed for rotation detection of birefringent microspheres

A variant of optical tweezers is the ability to impart and detect rotation with microscopic birefringent particles (see Chapter 1). Tweezers modified for torque detection can measure instantaneous lateral, angular displacement, and the proportional torque applied to birefringent microspheres, trapped in a focused beam of suitably polarized light. The torque imparted to the microspheres via a polarized laser beam or an external source (e.g. motor proteins) is measured by detecting the change in angular momentum of the transmitted/reflected beam. The angular calibration of these traps is performed by measuring the rotational Brownian motion of the trapped microsphere and its power spectral density. Such traps are also called optical torque wrench (OTW) by La Porta & Wang [92]. The ability to impart and detect torque has been shown by several other groups via various mechanisms [50,127,129]. Most of these techniques rely on the ability of light to transfer angular momentum and hence optical torque to an anisotropic microsphere.

2.1.4 Principles of angular momentum of light and transfer of optical torque

Light not only carries energy and linear momentum but also spin angular momentum and orbital angular momentum. The linear momentum of light as discussed above could localize a microsphere close to the focus of an incident light beam in three dimensions; similarly the angular momentum of the light can transfer angular momentum to a suitable microsphere, thus rotating the microsphere about its own axis or about the axis of the incident wavefront. In 1936, Beth [14] showed that it is possible to transfer angular momentum of circularly polarized light to a quartz plate. This momentum transfer was observed by the deflection of a quartz wave plate hung from a fine quartz fiber, while a suitably polarized light was sent through this plate. This mechanism of momentum transfer involving the polarization of incident light is called spin angular momentum [128] transfer mechanism. Another mechanism of transfer of angular momentum is due to the shape of the light wavefront and this is referred to as the orbital angular momentum (OAM) [3] transfer mechanism. Both of these mechanisms have been successfully employed with

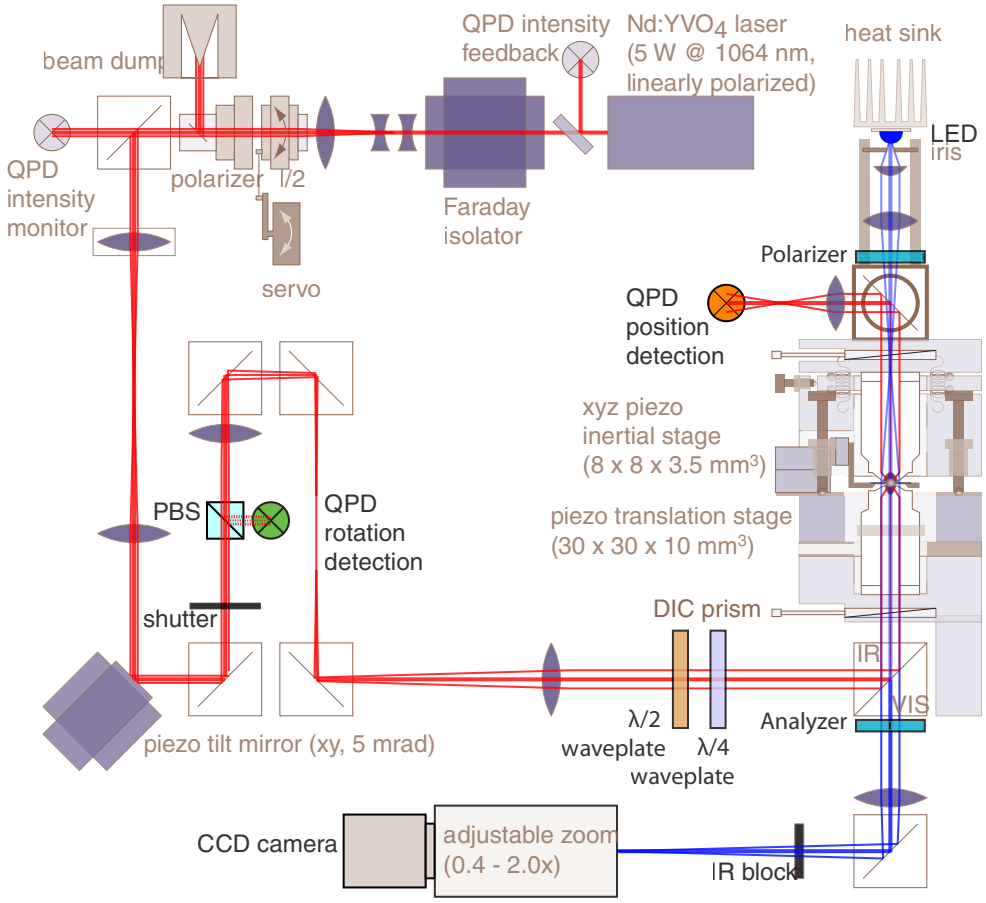

Figure 2.2: A graphical layout of the optical tweezers setup[107].
The rotation detection elements are highlighted and labeled in black. The $\lambda/4$ plate is inserted only when circularly or elliptically polarized light (red) is desired. The rotation detection QPD (green) is used to record the total intensity of the back-reflected signal (dashed red). The light detected by the rotation detection QPD is reflected from the microsphere and directed towards the QPD via a polarization beam splitter cube. The DIC prisms are removed to achieve crossed polarized imaging with visible light (blue).

optical tweezers to understand diverse phenomenon ranging from measuring effects of single molecules on DNA coiling to making micro-rheological measurements[4,49,98,141,154].

The setup employed for inducing and measuring optical torque, the associated modifications and the methods of calibrating an optical trap, are discussed in the following section.

2.2 The optical tweezers setup

All the experiments mentioned in this thesis were performed on an ultra-stable optical tweezers setup, developed in the lab by Mahamdeh & Schäffer[107] (Figure 2.2). Home built setups can be modified for a particular experiment, are more stable than commercially available setups, and cost efficient. The setup

is comprised of a laser box, the microscope body, the tower, and an illumination and detection unit. The laser box is populated by the laser head, alignment, and beam sizing optics, laser positioners and an intensity controller. The optics are specially coated to reduce reflections of the 1064 nm laser and mounted on anodized aluminum rails and mounts from Linos (Qioptiq, Göttingen, Germany). The laser intensity is controlled with a polarizing beam splitter cube in conjunction with a halfwave plate. The servo induced rotation of the halfwave plate allows for variable intensity to be transmitted from the polarizing cube. The XY translation of the laser is achieved with a silver mirror mounted on a piezoelectric stage. The entire laser box is encased in a thick vibration and thermal isolation housing.

The microscope body and the condenser tower are machined anodized aluminum pieces chosen for thermal and vibration stability. The microscope body is the three-legged base of the microscope. The trapping objective (infinity corrected CFIS Fluor 100x/0.7–1.3 oil objectives, Nikon, Japan) is screwed into the microscope body for more stability and it is thermally stabilized by a temperature feedback[107]. The sample can be positioned relative to the objective in a fine (P-733, Physik Instrumente, Germany) and a long-ranged, coarse manner (MS30, Mechonics Ag, Germany). A sub-ångstrom resolution from the stages enable accurate displacements and calibration of the trap. The light from the laser box is reflected into the objective with a dichroic mirror, which reflects 1064 nm light while passing visible through. The condenser stands on top of the microscope body on three fine adjustment screws (9S127N-25, Standa, Lithuania). The height is set such that the trapping objective and an identical condenser objective are confocal with respect to the trapping laser. The condenser objective is aligned relative the trapping objective using linear positioners (Smaract 1730,Smaract, Oldenburg, Germany). The position of the trapped microsphere is detected on a quadrant photo diode (QPD, QP154-Q-HVSD, Pacific Sensor) optimized for 1064 nm. The QPD is mounted on the condenser tower in the plane conjugate to the back focal plane. The QPD itself is mounted on a movable stage. Displacement of the trapped microsphere within the focus leads to a change in the laser interference pattern in the back focal plane which are recorded as difference and intensity changes on the QPD. For small displacements from the focus center (≈200 nm depending on the microsphere size) the signals from the QPD are proportional to the displacement. The sample is illuminated by an LED, Luxeon Rebel 'royal blue' 447.5 nm,LED-Tech, Germany), mounted on the condenser. Nomarski prisms inserted in a crossed polarized setup leads to a differential interference contract (DIC) for high resolution imaging of microtubules. The sample is then imaged on a monochrome camera (LM130m, Lumenera, Canada). The measurements were performed in a single-

beam optical tweezers. The setup and calibration procedures for translation and force measurements are described in detail in [107,142] and schematically depicted in Extended Data Figure 2.2. This setup has near-Å resolution in surface-coupled assays, is equipped with a millikelvin precision temperature control, and a lateral-force feedback using piezo tilt mirrors [26]. Here, we added a half- and quarter-wave plate before the trapping objective to adjust the laser polarization state. In addition, we introduced a polarizing beam splitter (PBS) to couple out the back-scattered laser light onto a photodiode (Model: QP45-Q TO, First Sensor AG, Berlin, Germany operated at 50 V reverse bias). For circular polarization, the back-scattered light reverses its polarization direction and after passing the quarter-wave plate is linearly polarized with a polarization direction perpendicular to the incoming light. Thus, the photodiode after the PBS detects all back-scattered light.

2.2.1 Optical tweezers modifications for inducing and detecting rotation

For rotation detection, we modified the optical tweezers. A servo rotor is mounted with a half-wave retardation plate ($\lambda/2$) followed by a removable static quarter-wave retardation plate($\lambda/4$). Without a $\lambda/4$, the angle of plane polarized light could be rotated with a precision of 0.5 degree. The $\lambda/4$ allows to change the ellipticity of the incident light. The rotation detection is enabled on the reflection path of the incident light using a polarizing beam splitter cube. This cube diverts the reflected light onto a QPD (QP45-HVSD, Pacific Sensor). The QPD is aligned to receive a maximum intensity of light upon reflection, ensuring that the laser hits at the center of the QPD. To use the QPD signals for quantitative measurements, they need to be calibrated.

2.3 Calibrating optical tweezers for detecting translation and rotation

Like any measuring device, optical tweezers need a calibrated reference to be able to accurately deduce displacements and force. Via Hooke's law, over the years many methods have been developed to calibrate the tweezers, like measuring the Brownian motion (equipartition theorem), inducing drag through flow (Stokes' drag) and our a sinusoidal calibration method [135] developed in our laboratory. Earlier methods employed CCD-video cameras for undertaking either of these methods. The lack of high temporal and spatial resolution in these cameras compared to quadrant photo diodes results in inaccurate or less sensitive calibration of the trap. The back-focal method of detection employs a position detection QPD

conjugated to the back focal plane of the condenser to monitor the alteration of the light field due to a trapped microsphere. From the detector signal the displacement of the microsphere with respect to the trap center and the corresponding forces acting on the microsphere are determined. Calibration methods involving Brownian motion [13,25,120] and flow dependent drag [91,153] require the knowledge of the drag coefficient of the trapped object. The calculation of drag coefficient leads to an assumption of the diameter and shape of the microsphere, the viscosity of the medium and the distance to a surface. The method developed by Tolić-Nørrelykke et al. [159] combines both these methods to provide for an assumption independent and highly sensitive calibration method.

2.3.1 Lateral calibration of optical tweezers using sinusoidal oscillations

The trapping force of a microsphere in a harmonic trap potential is described by Hooke's law $F_{trap} = \kappa\, \delta x$, where κ is the trap stiffness and δx is the relative displacement of the microsphere from the laser focus. Thus knowing the displacement of the microsphere δx from the laser focus yields the force being exerted on the microsphere. The displacement measured from the QPD is in volts and a proportionality factor the displacement sensitivity β, is required to convert volts to nanometers. Trapped microspheres experience multiple forces acting on them. These forces are the thermal force, the viscous force and the force from the light beam itself. An accurate calibration of the trap requires an accurate estimation of each of these forces [142,159]. The viscous force $F_{vis} = \gamma \dot{x}$ damps the motion of the microsphere and introduces a factor called the drag coefficient. The drag coefficient γ can be estimated by measuring the shape, the size, the distance of the microsphere from the surface and the viscosity of the medium. $\dot{x}$ is the velocity of the particle in the liquid. A microsphere in a parabolic potential, the optical trap, undergoing brownian motion under the influence of thermal forces can be tracked precisely with a QPD. The power spectrum of this motion fits to a Lorentzian-like function [159]. The corner frequency f_c of the power spectrum allows for the calculation of trap stiffness κ, where $\kappa = 2\pi\gamma f_c$. The value of drag coefficient γ is unknown and can be measured with a drag force method. In this method, a microsphere is trapped at a certain height from the surface in a flow-cell sample chamber. The flow-cell is then translated with a small amplitude at a known frequency using a piezo stage. Several power spectra are then recorded, averaged and fit to a Lorentzian and the corresponding values of the corner frequency f_c and the plateau height P_o are extracted. A unique feature which arises out of the sinusoidal sample motion is a sharp peak at the frequency of translation. The amplitude of the peak is lower than the amplitude of translation. This de-

crease is an estimate of the drag coefficient on the microsphere, encompassing the effect of its size, shape, height from the surface and viscosity of the medium. Figure 2.4(blue) shows a sample calibration power spectrum with the translation peak.

The combination of the Lorentzian fit and the drag coefficient provides an accurate measurement of trap stiffness and displacement sensitivity. Repeating the same measurement at different heights from the surface, fitting the drag coefficient to the Faxen's law[62,142] subsequently gives the diameter d of a spherical microsphere. This can be explained as follows. The trap stiffness κ and the displacement sensitivity β of a given spherical microsphere depends on the distance l of the microsphere from the surface of the flow cell. Additionally, the drag coefficient γ is known from the sinusoidal peak. By fitting the dependence of the drag coefficient on the height, the position of the surface is estimated precisely. The drag measured deep in the flow cell away from any surface is equivalent to the Stokes drag $\gamma_0 = 3\pi\eta d$. The viscosity of the medium is calculated from the known temperature. Together the calibration allows for a precise calculation of the microsphere diameter d. The raw data is automatically analyzed by a global fitting routine, written in Matlab (Natick, Massachusetts, USA) by Volker Bormuth, Tobias Jachowski and Steve Simmert. Data acquisition and fitting is enabled by a custom written LabVIEW (National Instruments, Austin, USA) program.

2.3.2 High resolution rotation detection and calibration

Rotation of microscopic microspheres has been a topic of great importance to the micro-manipulation community. Conventional systems that are used to rotate microspheres are magnetic tweezers[100], optical tweezers[50,58,92], rotation of attached micropipettes[96,101] and even acoustic fields[149]. These techniques are employed to tackle problems in both physics[110,118,130] and biology[41,176].

Rotation by optical tweezers has been limited to less than 1000 Hz with maximum torque applicable on such systems to about 1 nN nm[130]. Some such microspheres are cylindrical structures of quartz[41,130], crushed calcite[92], vaterite[166] and liquid crystal microspheres[77]. The forthcoming sections elaborate the observation of fast rotation (very high maximum torque) of RM257 liquid crystal microspheres due to their high birefringence and their calibration under elliptically polarized light.

2.3.3 Instrumentation for rotation calibration in reflection mode

The optical tweezers used for my experiment is a home built inverted microscope system described in detail in Section 2.2[107], has a maximum laser power of 1.4 W at the sample plane at 1064 nm wavelength. A polarizing beam splitter is placed just before the input microscope objective. A quarter waveplate and a half waveplate are inserted between the polarizing beam splitter and the objective to control the degree of ellipticity of the beam and the long axis of polarization. When a microsphere is trapped at the sample plane, a part of the input light is scattered in the forward direction and another part is back-scattered. The forward scattered portion is made incident on QPD to estimate the translational motion along the three directions. The light in the back-scattered direction with a polarization perpendicular to the incoming one is detected through the second port of the polarizing beam splitter onto a QPD also called the rotation detection QPD. The amplitude of the detected light signal depends on the orientation of the particle. Similarly it also depends on the orientation of the polarized incident light with respect to the microsphere.

The trapping objective temperature was 29.200 °C . Time traces were recorded with 40 kHz with an alias-free analog-to-digital converter. Traces were smoothed with a running median filter with a bandwidth of 200 Hz. The force-clamp was operated with an update rate of 500 Hz. In the torsion balance mode, we could resolve angular steps as low as 0.05 degree (0.9 mrad) at a bandwidth of 100 Hz.

For linear polarization under ideal circumstances, the backscattered light intensity that reaches the photodiode is proportional to the incident intensity as $\sin^2(2 * \vartheta)$ where ϑ is now the angle between the microsphere's extraordinary axis and the laser polarization direction. However, the the dichroic mirror in the real system introduces retardance into the system. Thus, when $\vartheta = \alpha = 20$ degrees, and having a retardance of φ =20 degrees, the backscattered intensity has a non-extremum value. The slope of the backscattered intensity curve is also non-zero as depicted in (Figure 2.5 b). When we estimate the rotational Brownian motion, we find the slope of the backscattered intensity at $\alpha = \vartheta = 20$ degrees. The angular dependence results in a 4-fold rotational symmetry. To calibrate the rotational signal for the case of linear polarization, we first calibrated the parameters for the translation and force measurements[142]. In this manner, the lateral displacement sensitivity, trap stiffness, and, importantly, the microsphere's translational drag coefficient is measured. From the latter, we calculate the microsphere radius, which we use as an input for the rotational calibration. We record a power spectrum of the rotational Brown-

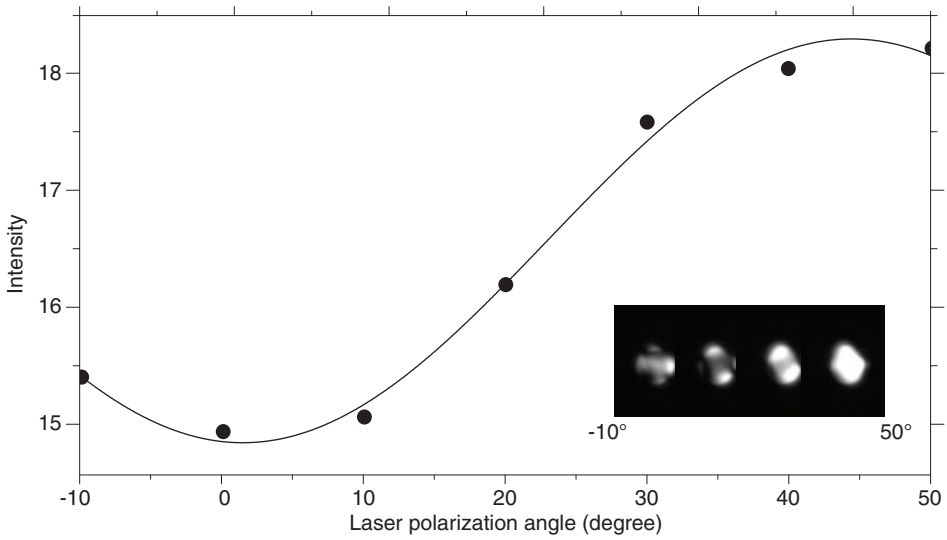

Figure 2.3: Intensity variation of a birefringent microsphere as a function of its angular orientation.
The average intensity I of a region of interest around the microsphere (circles) is plotted versus the orientation angle ϑ of the microsphere. The intensity I was proportional to $\sin^2(2\vartheta)$ (solid line)[110].

ian motion (Figure 3.10) and determine the angular sensitivity, which is related to the torsional stiffness of the trap, as described in[131] using the known microsphere radius and, thus, the known rotational drag coefficient.

2.3.4 Probes for rotation calibration

We use a nematic liquid crystal (LC) precursor RM257 (Merck, Germany) as described in chapter 1, to synthesize birefringent microscopic microspheres, which has a bulk ordinary and extraordinary refractive index of $n_o = 1.508$ and $n_e = 1.687$, respectively, resulting in a very high bulk birefringence of Δ n = 0.179*comparedtoquartz, whichhas*"$\Delta n = 0.009$[140].

RM257 microspheres are suspended in double distilled water and placed inside a sample chamber. The sample chamber is made of two cover slips of 100 µm thickness with a set of double sticking or parafilm spacers. Such a sample is then placed under the microscope.

2.3.5 Rotation calibration with crossed polarized visible light illumination

The birefringent microspheres when rotated under a crossed polarized illumination show diffraction patterns or isogyres (Figure 1.5). The rotation pattern of these isogyres modulates from minimum intensity to maximum intensity when rotated with known angles(Figure 2.3). In order to quantitate this rotation we suspend these particles in a flow cell with water and trap them in the linearly polarized optical

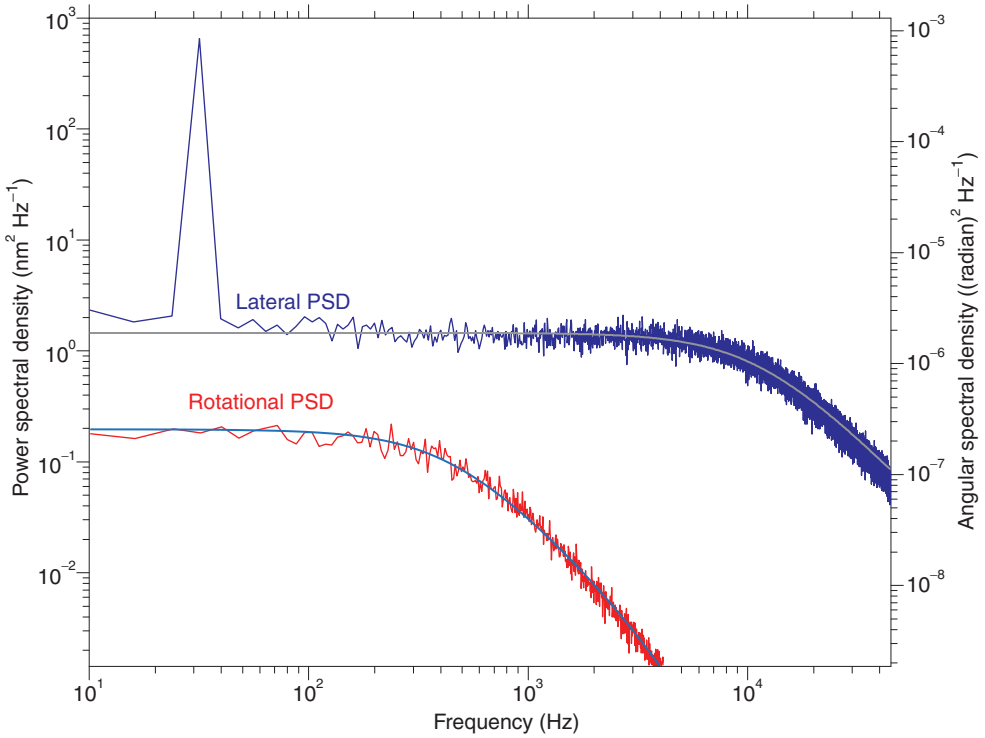

Figure 2.4: Calibration of angular sensitivity and torsional stiffness
A birefringent microsphere (blue) is oscillated with a sinusoidal frequency of 32 Hz. The spectra are recorded for the lateral axis in the forward QPD, and the rotation spectrum is recorded in the back-reflection QPD. The forward QPD shows a peak at 32 Hz in the direction of oscillation (blue). The power of this peak allows for an estimation of displacement sensitivity β. The rotation spectra (red) is fitted to a Lorentzian with parameters P_o for the plateau and f_c for the corner frequency. The power spectral density of the angle as a function of frequency for a microsphere of 710 nm diameter trapped in an optical trap with a laser power of 12 mW. The corresponding angular sensitivity is 190 rad V^{-1} and the torsional stiffness is about 2500 pN nm rad^{-1}.

trap. The particles are illuminated with a blue LED and the DIC prisms are removed to create a crossed polarized extinction. With polarizer set to extinction only blue light that has its polarization rotated is imaged on the CCD camera. An infrared filter blocks the laser allowing a background free imaging of the blue light transmitted through the birefringent microspheres. The linear laser polarization is then rotated through -10°to 50°with known intervals of 10°and a visible image is recorded at every interval. The birefringent microsphere images are then processed with a region of interest in FIJI[145] and the average intensity I at every frame is plotted against the orientation angle ϑ of the extra ordinary axis of the microsphere with respect to polarization direction of the visible light. As expected, the intensity I fits to a $\sin^2(2\vartheta)$ function[110].

2.3.6 Rotation calibration of optical tweezers in reflection mode

Much like the linear calibration, rotation calibration can be accomplished by obtaining a complete set of three parameters, the angular sensitivity β_{rot} (rad/V), the torsional stiffness κ_{rot} (pN·nm/rad), or equivalently, the maximum torque τ_o (pN·nm), and the angular drag coefficient γ_{rot} (pN·nm·s). For the optical torque wrench, a thorough analysis of different ways to calibrate torque is described by Pedaci et al. [131].Unlike for lateral calibration of an optical trap, rotation calibration methods are not widely reported. Of the three [47,58,131] reports described in the literature, the summary provided by Pedaci et al. [131] is the most rigorous.

Our method of calibration combines the parameters acquired from the linear calibration, specifically the radius from the drag coefficient γ with those from the rotation detection to calculate the three parameters mentioned above. The rotational drag coefficient γ damps the rotational motion of a birefringent microsphere. Since γ is independent of the light intensity or polarization and rather a property of the microsphere and the medium surrounding it, measuring the lateral drag coefficient γ using the sinusoidal method [159] mentioned above is sufficient to calculate the rotational drag coefficient. According to Stokes law, the lateral drag coefficient $\gamma = 6\pi\eta r$. Similarly, the rotational drag coefficient is $\gamma_r = 8\pi\eta r^3$. The drag coefficient of the particle is estimated from the power under the 32 Hz peak, in the lateral power spectral density (blue) in Figure 2.4. The calculation for displacement sensitivity β and the drag coefficient γ are performed with an automatic routine in MATLAB. The torsional stiffness κ_{rot} is calculated according to $\tau_o = \pi\gamma_r f_c$. f_c is the corner frequency estimated from fitting the rotational power spectrum (red) in Figure 2.4 to a lorentzian.

Calibration for translation and force measurements

The lateral-force feedback is provided by piezo tilt mirrors [26]. A half- and quarter-wave plate before the trapping objective adjust the laser polarization state. The back scattered light is carried to the back-scattered QPD through a polarizing beam splitter (PBS), this photodiode detects all back-scattered light. The amplitude of the detected light depends on the orientation of the particle and is proportional to $\sin(2\vartheta)$, where ϑ is rotation angle of the microsphere. For linear polarization, the back-scattered light intensity that reaches the photodiode is proportional to $(r_e - r_o)^2 \sin^2(2\vartheta)$, where ϑ is the angle between the microsphere's extraordinary axis and the laser polarization direction. r_e and r_o are the reflection co-

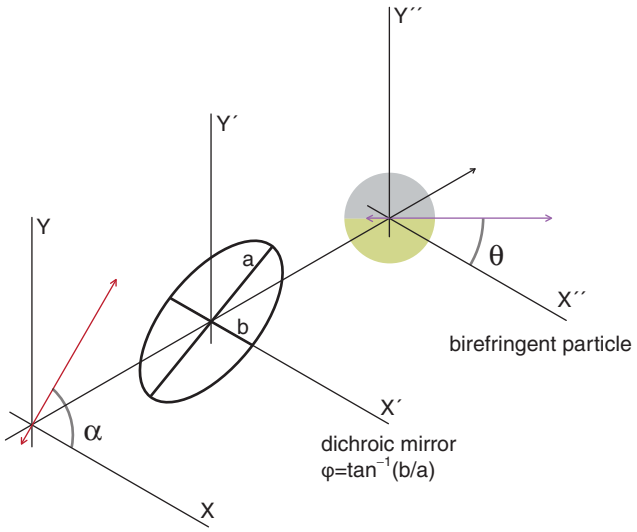

Figure 2.5: Coordinate system describing the propagation of light.
The light passes a polarizer and a half wave plate is prepared in a polarization basis tilted at and angle α with respect to the x-axis. Then it encounters a dichroic mirror which adds a phase to the y-component of the light thereby making it elliptical. Eventually, the light encounters the birefringent microsphere tilted at an angle of ϑ with respect to the x axis. Thereafter the light is reflected from the microsphere and the path retraced. Eventually the component of light appearing the polarization tilted at α with respect to the y-axis at the half wave plate is selected.

efficients for linearly polarized light. To calibrate the rotational signal for the case of linear polarization, we first calibrated the parameters for the translation and force measurements[142]. In this manner, the lateral displacement sensitivity, trap stiffness, and, importantly, the microsphere's translational drag coefficient is measured. From the latter, we calculate the microsphere radius, which we use as an input for the rotational calibration. We record a power spectrum of the rotational Brownian motion (Figure 3.10) and determine the angle sensitivity and maximum torque, which is related to the torsional stiffness of the trap, as described in[131] using the known microsphere radius and, thus, the known rotational drag coefficient. Time traces were recorded with 40 kHz with an alias-free analog-to-digital converter. Traces were smoothed with a running median filter with a bandwidth of 200 Hz. The force-clamp was operated with an update rate of 500 Hz. In the torsion balance mode, we could resolve angular steps as low as 0.05 degree (0.9 mrad) at a bandwidth of 100 Hz.

Overall, we analyzed the motion of 243 different single rK 430 molecules 240 different microtubules, on 40 different days. 51 out of 243 events showed motility, with 43 showing rotation. The $N = 21$ angular steps were obtained from 6 different microspheres.

To understand the exact mode of interaction of elliptically polarized light with a birefringent microspheres we calculated how the back. we first start with defining the coordinate system (Figure 2.5), where

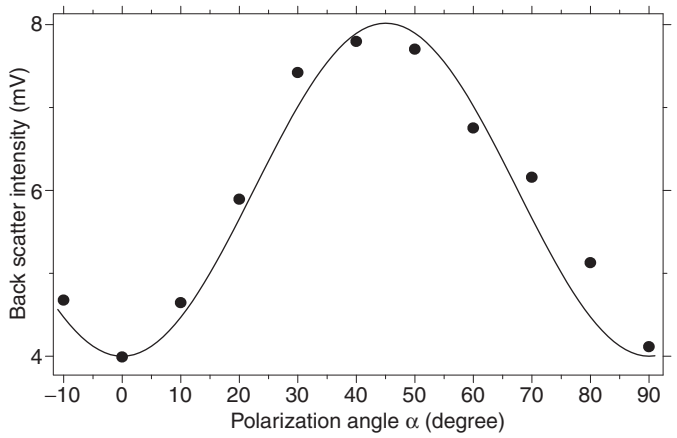

Figure 2.6: Backscattered intensity as function of α for $\alpha = \vartheta$
The measured intensity at the back-scattered QPD for rotation detection varies as the $\lambda/2$ plate rotates the α from $0^{\circ}$to 90°, with a maxima at $\alpha = 45^{\circ}$

we establish three planes of interest, the $\lambda/2$ plane which controls the polarization angle α of the incident light, the dichroic mirror which reflects the light into the objective with an added phase $\phi = \tan^{-1}(b/a)$ and the sample plane, where the laser beam orients the birefringent particle with an angle ϑ.

The polarization of light is governed by the half wave plate and tilted at an angle α from the x-axis (Figure 2.5). The backscattered intensity varies with a change in α (Figure 2.6). The rotation of polarization is observed as a change in intensity due to the polarizing beam splitter cube before the backscattered detection QPD. The projections of the polarization vector along the x and the y directions are

$$E_x = E_o \cos(\alpha) \tag{2.1}$$

$$E_y = E_o \sin(\alpha) \tag{2.2}$$

The component of the polarization along the y axis picks up a retardance due to the dichroic and hence the equations become

$$E_1 = E_o \cos(\alpha) \tag{2.3}$$

$$E_2 = E_o \sin(\alpha) e^{i\square} \tag{2.4}$$

which can be expressed in terms of transfer matrices

$$T = T_{Dich}(-\phi)T_R(\alpha) \tag{2.5}$$

where

$$T_R(\vartheta) = \begin{bmatrix} cos(\vartheta) & -sin(\vartheta) \\ sin(\vartheta) & cos(\vartheta) \end{bmatrix}$$

and

$$T_{Dich}(\phi) = \begin{bmatrix} 1 & 0 \\ 0 & e^{i\square} \end{bmatrix}$$

If the birefringent particle is inclined at an angle of ϑ with respect to the x axis and r_e and r_o be the reflection coefficients along the extraordinary and the ordinary directions respectively, then the effective components of the electric field that the light has after being reflected from the particle and passing the dichroic on the reverse path is given as

$$T_{Refl}(\phi) = \begin{bmatrix} r_1 & 0 \\ 0 & -r_2 \end{bmatrix}$$

$$T = T_R(\vartheta)T_{Refl}()T_R(-\vartheta)T_{Dich}(-\phi)T_R(\alpha) \tag{2.6}$$

Now this field has to be projected back into the component of polarization along the x axis, in which direction, the polarizer is oriented. That component of polarization is given as

$$T = T_R(-\alpha)T_{Dich}(\phi)T_R(\vartheta)T_{Refl}()T_R(-\vartheta)T_{Dich}(-\phi)T_R(\alpha) \tag{2.7}$$

The final electric field is then

$$E_b = TE_i \tag{2.8}$$

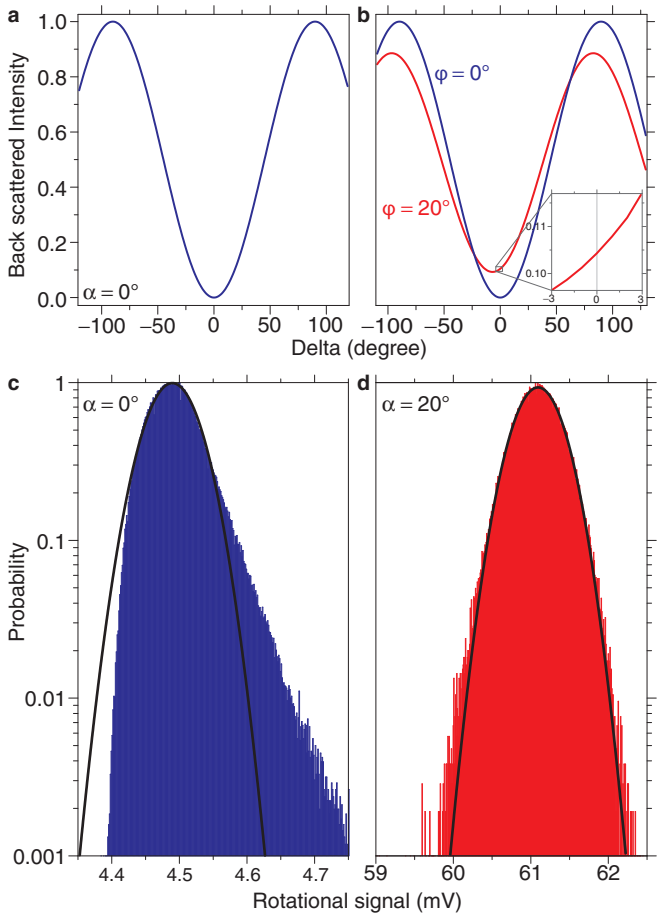

Figure 2.7: Backscattered signal for two different values of α (a) The backscattered signal as function of $\Delta = \vartheta - \alpha$ for $\alpha = 0$. (b) The backscattered signal as function of Δ for $\alpha = 20$ degrees for two different values $\phi = 0$ and 20 degrees of dichroic retardance. (c) Histogram of backscattered signal for $\alpha = 0$ and $\phi = 20$ degrees. The histogram is non-Gaussian. (d) Histogram of backscattered signal for $\alpha = 20$ degrees and $\phi = 20$ degrees. The histogram is Gaussian.

where,

$$E_i = \begin{bmatrix} E_o \\ 0 \end{bmatrix}$$

Using the refractive indices $n_o = 1.51$ and $n_e = 1.6$, the reflection coefficients are $r_e = 9.2$ percent and $r_o = 7.7$ percent. The value of birefringence is small enough compared to the refractive indices that the r_e and r_o can be assumed to be the same within a 10 percent accuracy. Using this assumption, the electric field,

$$E_b = \frac{r_o}{2}\sin(2\alpha) - \frac{r_e}{2}\sin(2\alpha)\cos(2\vartheta) + \mathcal{A}\sin(2\vartheta) \tag{2.9}$$

where,

$$\mathcal{A} = \left[(r_o + r_e)e^{-i\square}\sin^2(\alpha) + (r_o - r_e)e^{i\square}\cos^2(\alpha)\right] \tag{2.10}$$

For a particular value of α, small deviations of the microsphere orientation from the laser polarization direction are $\Delta = \phi - \alpha$ resulting in,

$$E_b = \frac{r_2}{2}\sin(2\alpha) - \frac{r_1}{4}\left[\sin(2(\alpha + \vartheta)) - \sin(2\Delta)\right] + \mathcal{A}\left[\sin(2\alpha) + \cos(2\alpha)\sin(2\Delta)\right] \tag{2.11}$$

The rotation signal voltage is proportional to the light intensity $I_b = E_b^2$ and given by

$$V = \beta_\Delta I_b = \beta_\Delta E_b^2 \tag{2.12}$$

Where β_Δ is the angular sensitivity. In the limit that Δ is small, the voltage can be written as

$$V = \beta I_b = D + C\Delta \tag{2.13}$$

Then, taking the derivative of V with respect to Δ, we get

$$\frac{\partial V}{\partial \Delta} = C = \frac{1}{\beta\Delta} \tag{2.14}$$

For a Lorentzian response of the spectrum of noise of the rotational motion detected by the photodiode, we have

$$S(f) = \frac{S_o^2 \cdot f_c^2}{f^2 + f_c^2} \tag{2.15}$$

The plateau value S_o is related to C in the following fashion, with γ_{rot} being the drag coefficient

$$S_o^2 = \frac{k_B T}{(C)^2 \gamma_{rot} \pi^2} \tag{2.16}$$

It must be noted (Figure 2.7 b and Equation 2.11) that at the polarization angle where $\alpha = 0$ the QPD response to rotation in either of the direction would be positive, thus losing any information on the directionality of the angle of rotation. For a parabolic, instead of linear, response, the calibration of

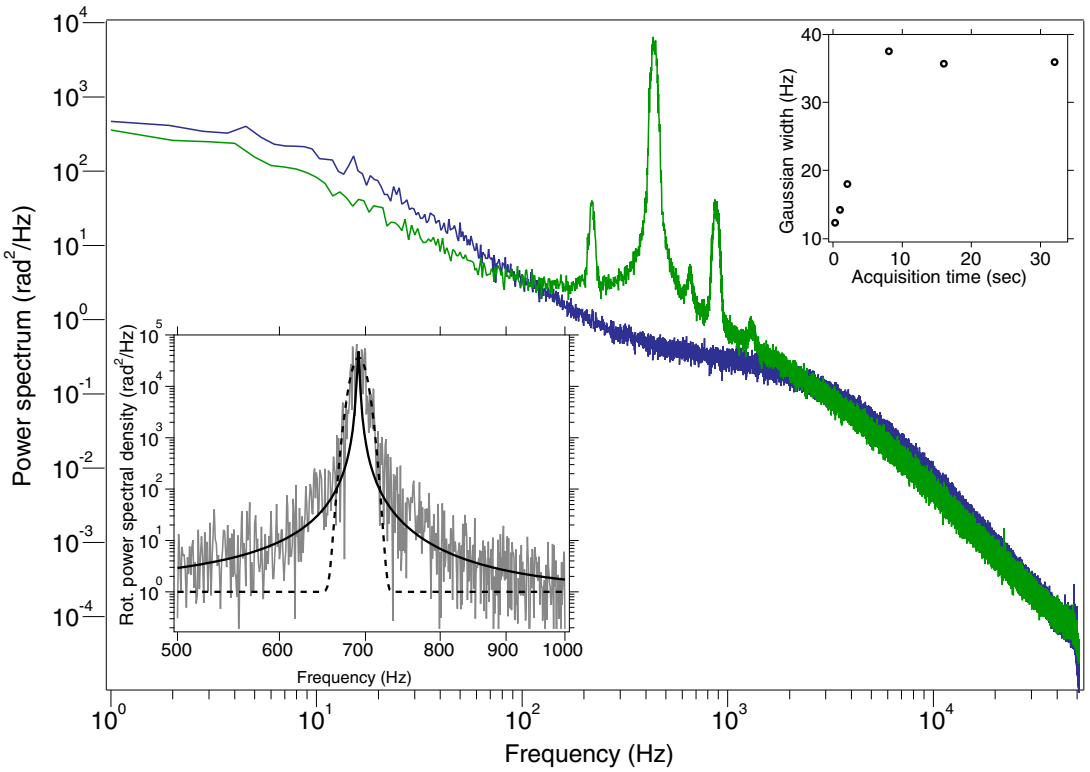

Figure 2.8: Rotation spectra of a birefringent microsphere and the corresponding 'jitter´ peak analysis.
This figure indicates the rotation of the birefringent microsphere (green) under circularly polarized light with 120 mW power. The shape of the line is convolution of a Gaussian and a Lorentzian, with the top part fitting well to a Gaussian while the tails fitting well to a Lorentzian. The center frequency is 690 Hz. The width of the fitted Gaussian is 20 Hz while that of the fitted Lorentzian is 1.4 Hz. The Gaussian can be explained by the Eq. 2.17. The upper inset shows the time that the Gaussian line width takes to saturate to a constant value. The blue curve indicates the power spectral density of the same microsphere trapped with the linearly polarized light.

the magnitude of the angle would be difficult. We circumvent this problem using $\alpha \neq 0$ by adding a small retardance angle $\phi \neq 0$. In this manner, we obtain a linear response, which can be calibrated via the power spectral density of the angular fluctuations. This is particularly useful when measuring small angles.

2.4 Rotation of birefringent microspheres induced by circularly and elliptically polarized light

When the birefringent microspheres are trapped with a circularly polarized laser beam, the transfer of spin angular momentum of light onto the microsphere causes them to rotate along the direction of propagation of the laser beam (Figure 2.8). The rotation speed depended on the the microsphere size, birefringence and the intensity of incident light. This rotation is observed as a peak in the power spectral

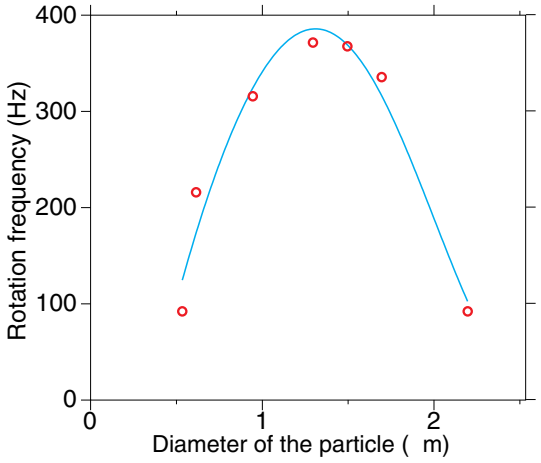

Figure 2.9: Effect of microsphere size on the rotation frequency.
Rotation rate of the microsphere as a function of microsphere size at 140 mW laser power. At microsphere sizes less than 800 nm, the birefringence reduces significantly thereby making the rotation rate slower. When the size of the microsphere becomes larger than 1.5 μm , the drag keeps on increasing. Thus the rotation rate decreases again. The maximum rotation speed is seen at about 1,2 μm diameter.

density and the peak position is proportional to the rotation frequency of the microsphere. At about 250 Hz, the translational oscillation peak and around 700 Hz, harmonics of rotation peaks, are visible (Figure 2.8).

The shape of the line is a convolution of a Gaussian and a Lorentzian. The top part fits well to a Gaussian while the tails fit well to a Lorentzian. The center frequency is 690 Hz. The width of the fitted Gaussian is 20 Hz while that of the fitted Lorentzian is 1.4 Hz (inset Figure 2.8). We can understand this convolution of a Lorentzian and a Gaussian fit by recalling that the governing equation is the Eq. 2.17. Such signals are also called to have a Voigt profile. A Voigt profile is a convolution of the Lorentzian signal from the sample and the Gaussian response function from the microsphere. Here it may be noted that Lorentzian line shapes are very common in atomic spectroscopy describing (non-relativistic) resonance behavior[22,87], while the Gaussian line shapes are also prevalent in systems involving pressure broadening[169] etc.

2.4.1 Rotation frequency varies with the size of birefringent microsphere

The rotation rate of the microspheres was highest for microspheres with about 1 to 1.5 μm diameter(Figure 2.9). We have obtained our highest rotation rate at 1.2 μm diameter (Figure 2.10). This behavior can be understood by recalling that during the formation of liquid crystal microspheres like RM257, there is a competition between the anchoring energy and the orientation energy[116]. The orientation energy is in-

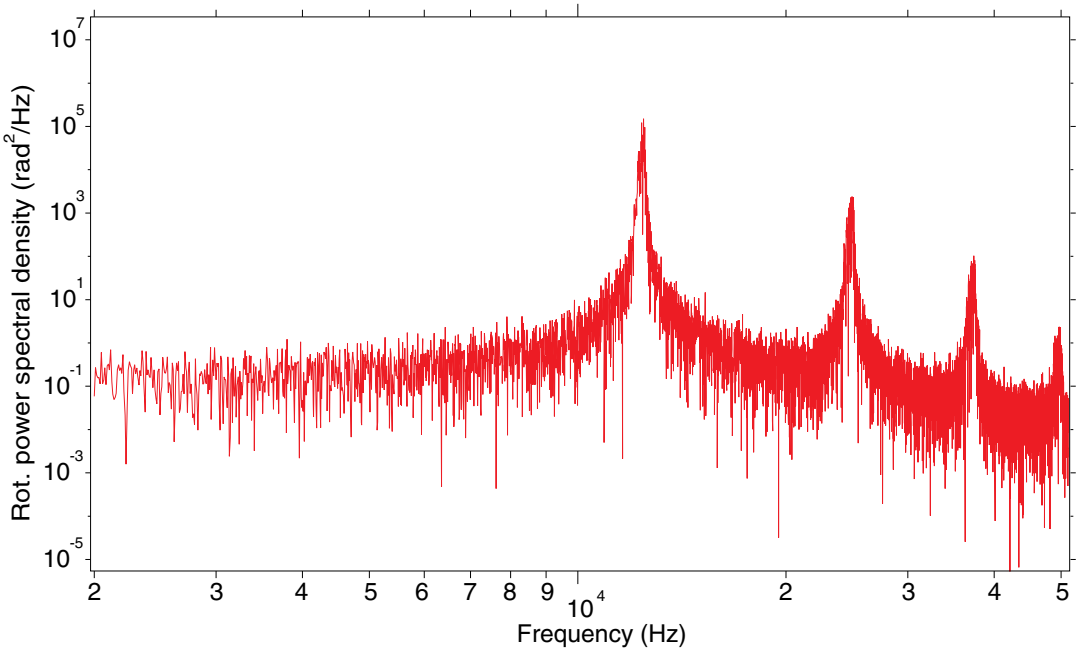

Figure 2.10: High speed rotation of birefringent microsphere under circularly polarized trapping laser.
Power spectrum of the rotational motion of an RM257 microsphere of 1.2 μm diameter when applied with a circularly polarized light with 1.2 W of power at the sample plane. Higher harmonics are visible because the angular momentum of the light is not completely transferred to the microsphere leading to a non-sinusoidal modulation of the power spectrum.

dicated by the splay Frank constant (K) which is about 10^{-11} N while the anchoring energy of RM257 (W_o) is 1.886×10^{-5} J/m^2 Thus, the critical diameter is given by K/W_o = 600 nm. When the size is smaller than this diameter, the structure prefers to remain in the radial configuration which has a birefringence of zero. However, when the size of the microsphere is larger than this diameter, the preferred structure is the bipolar one which has a net birefringence.

The rate of rotation of a 1.2 μm microsphere exceeded 7000 Hz at a trapping laser power of 1.2 W as shown in Fig. 2.10. To the best of my knowledge the fastest rotation rate reported has been a transient rate of about 3500 Hz in gold microspheres of about 400 nm diameter which have been trapped in 2-dimensions with an 830 nm wavelength laser beam[98]. Our rotation is a continuous steady one for a microsphere trapped in 3-dimensions and corresponds to a Reynolds number of about 0.08, Re= $\varrho D^2\omega/\eta$, where ϱ is the density of water, ω the angular velocity of the microsphere, d the diameter and η the viscosity of water. This is the highest Reynolds number recorded for microspheres trapped in optical tweezers.

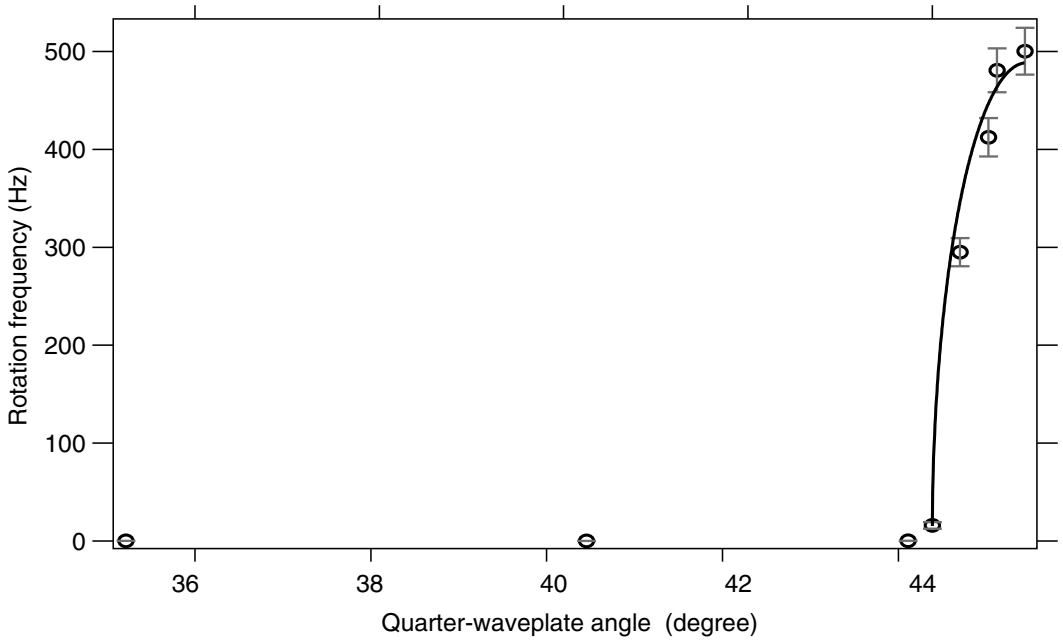

Figure 2.11: Rotation rate of an RM257 microsphere as a function of ellipticity.
A 550 nm RM257 microsphere is trapped in optical tweezers and the polarization is changed from perfectly circular polarization to elliptical polarization. The rotation frequency of microsphere drops steeply as as a function of ellipticity. The birefringence for this microsphere was estimated to be 0.006.

2.4.2 Transfer of torque of elliptically polarized light onto a birefringent particle

The rotation frequency of microsphere drops steeply as as a function of ellipticity (Figure 2.11). The torque transferred on a birefringent particle due to elliptically polarized light can be better understood with the following equations

$$\gamma \frac{d\vartheta(t)}{dt} = \tau + (2k_B T\gamma)^{1/2}\zeta \quad (t) \tag{2.17}$$

Here, γ_{rot} is the rotational drag coefficient, ϑ is the angular coordinate of the microsphere, $\zeta \quad (t)$ is the noise due to Brownian motion, k_B is the Boltzmann constant, T the temperature of the system, τ the torque due to the light and t is the time. For a given value of laser power, the torque is given as

$$\tau = -\frac{SP}{\omega c}\sin(kd(n_o - n_e))\cos(2\phi)\sin(2\vartheta) + \frac{SP}{\omega c}(1 - \cos(kd(n_o - n_e))\sin(2\phi) \tag{2.18}$$

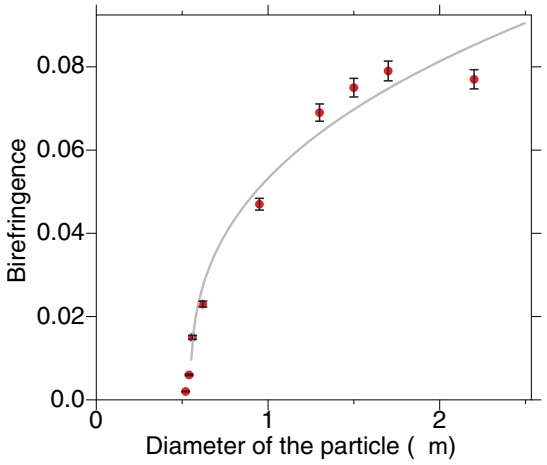

Figure 2.12: Effect of microsphere size on birefringence.
The birefringence for microspheres of about 1 μm diameter is fairly high thereafter, it starts to reduce and become 0 at about 500 nm.

where the light power is

$$P = \frac{\varepsilon E_o^2 c}{2} \tag{2.19}$$

Here, ε is the permittivity of the medium, ω the frequency of light, E_o^2 is the intensity of light, k the wavenumber, d the thickness of the material, $(n_o - n_e)$ is the birefringence of the material, $tan(\phi)$ the ellipticity of light and ϑ the angle between the ordinary axis of birefringence and the direction of polarization for a linearly polarized laser beam. S is the scattering cross-section of the microsphere. The torque is independent of time for a constant laser power and an ellipticity of 1. Thus, the rate of rotation is equal to a Gaussian distributed random noise added to a constant. We also find that the width of Gaussian is small at short time scales but tends to saturate for data acquisition of more than 10 s (upper inset Figure 2.8).

2.4.3 Rotation rate varies with changing incident polarization

The ellipticity of light can be varied to change the rotation rate for a particular microsphere as shown in Figure 2.11 for a 550 nm diameter microsphere. The birefringence of the microsphere can be accurately estimated from the value of the ellipticity at which rotation rate becomes zero. A similar analysis was performed by Juodkazis et al.[76], where the birefringence of the microspheres with different sizes were assumed constant.

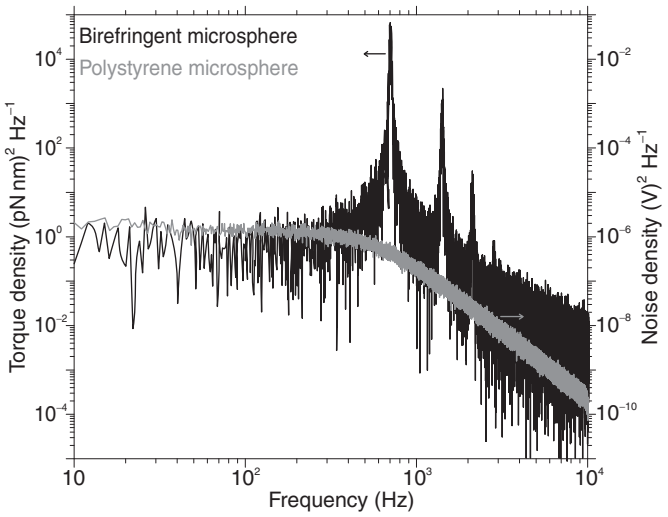

Figure 2.13: Rotation of a birefringent microsphere in circularly polarized light.
The rotational power spectral density shows a peak at 700 Hz corresponding to a microsphere rotation frequency of 350 Hz. The microsphere had a diameter of 900 nm was trapped with 12 mW laser power. A 600 nm-diameter polystyrene microsphere trapped under the same conditions did not show any rotational peak. Here, the Lorentzian is due to the axial movement of the microsphere which is proportional to the back-scattered light intensity.

The following expression can be used to calculate the rotation rate as a function of ellipticity[50]

$$f(d,\phi) = P\sqrt{A}/(2\pi\omega\gamma_{rot}), \tag{2.20}$$

where,

$$A = [1-\cos(kd(n_o - n_e))]^2 \sin^2(2\phi) - \sin^2(kd(n_o - n_e))\cos^2(2\phi) \tag{2.21}$$

We have measured the birefringence of RM257 microspheres as a function of microsphere size (Figure 2.12). The birefringence for microspheres of about 1 μm diameter is fairly high thereafter, it starts to reduce and become 0 at about 500 nm. The birefringence is smaller than the measurement resolution for microspheres smaller than 500 nm. It can be explained by an energy minimization scheme which shows that such particles tend to prefer a radial structure below 500 nm while being in a bipolar configuration above it. If a different material is used with a higher value of anchoring energy than RM257, it can retain significant values of birefringence even for smaller particles. For microspheres with no optical anisotropy the circular polarized light has no effect and no net rotations are observed (Figure 2.13).

This is a second order phase transition dependent on microsphere size. Hence, we assume that the functional form of the birefringence, which is the order parameter here, should depend upon the diam-

eter d of the microsphere as

$$(n_o - n_e) = P \times (\frac{d-a}{b})^c \tag{2.22}$$

Here, a, b, c and P are fit parameters. A fit of the form Eq. 2.22 to the data is shown in Fig. 2.9.

2.5 Conclusions

To conclude, we have trapped RM257 microspheres of sizes below 2 μm in optical tweezers and recorded their response to linearly, elliptically and circularly polarized light. We estimated the birefringence of such microspheres by changing the ellipticity of the trapping light and found that the birefringence changed from more than 0.08 at 1 μm to less than 0.006 at 500 nm. This change in birefringence can be explained by a change in the preferred molecular orientational structure of the microsphere from bipolar to radial at around 500 nm diameter. The bulk birefringence of RM257 is large and about 0.18, compared to quartz which has a birefringence of 0.009. Further, the rotation rate in circularly polarized light was highest for 1.2 μm microspheres at more than 7000 Hz in water with a Reynolds number of 0.02. This is the highest rotation rate recorded, in an aqueous medium. The ability to trap these birefringent microspheres and calibrate rotation provides for an important tool to understand the rotation of biological molecules which can be coupled to these spheres. The calibration of angular changes was performed with crossed polarized extinction imaging of visible light on a CCD camera, while a higher resolution of angular measurement was achieved with modified optical tweezers.

In the beginning there was nothing, which exploded.

Terry Pratchett

3

Rotation detection of translating Kinesin-1

Molecular motors bring about active transport in an extremely chaotic and dynamic cellular environment. This motion is governed by many regulatory proteins, ATP supply, and minerals, among other factors[162]. A simpler approach to understand the motor motion and its ramifications is to understand the individual components in the pathway. Molecular motors like kinesin are by now fairly well understood[162] and, yet, some mechanical properties are still unclear. This chapter details the importance of molecular motors and their mechanical properties. We applied the methods described in the previous chapters to molecular motors to determine their rotational behavior. I specifically focused on the question of rotational motion of kinesin while stepping and, the implication of this motion on the mechanism of kinesin hand-over-hand stepping.

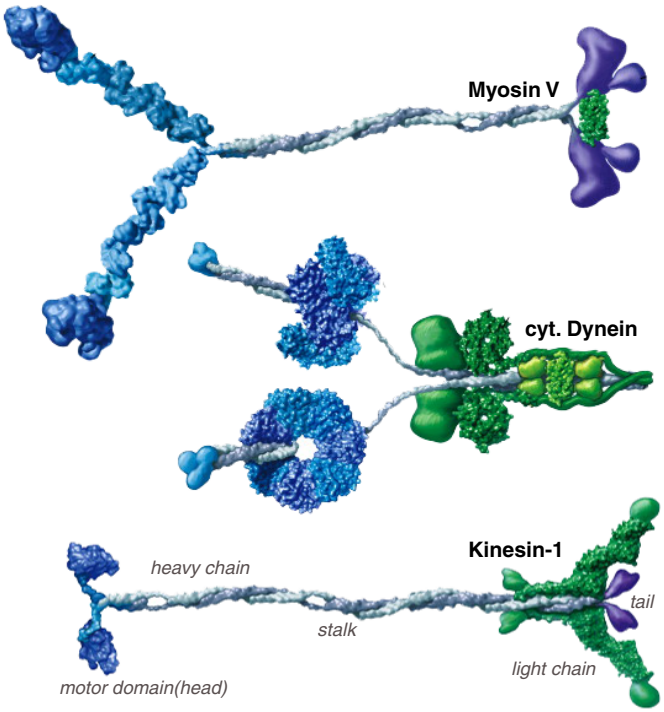

Figure 3.1: The three classes of molecular motors which employ cytoskeletal tracks for motion.
The motors represented in this figure employ tracks as actin or microtubules to perform work inside living cells. Myosin V is an actin dependent protein, while kinesin and dynein translate on microtubules. The motor domains (ATP hydrolysis) are displayed in blue, mechanical transducers in light blue, and tail domains implicated in cargo attachment are shown in purple.The motor domain of dynein (blue/purple) comprises of the AAA+ domains. Tightly associated motor subunits (light chains) are shown in green. This figure is originally shown by Vale [163] in his article on 'Molecular motor toolbox'.

3.1 Microtubular transport of Molecular Motors

Microtubules are dynamic self assembling filaments which act as tracks for molecular motors. An individual microtubule is composed of pseudo-helical substructures or protofilaments, with one turn of the helix containing 13 (11–16) approximately 8.2 nm long tubulin α and β heterodimers, each from a different protofilament. The protofilaments themselves align in a slightly skewed parallel manner to form a protofilament sheet which curves to the final hollow rigid and polar tube form of microtubules. A microtubule is $\approx$25 nm in diameter and can be several micrometer long. Depending on the orientation of the tubulin sub-units and their subsequent polymerization and depolymerization rates, the microtubule ends are classified as 'plus' ends or 'minus' ends[1].

Molecular motors, like most kinesin travel towards the plus-end of microtubules, while dyneins move towards the minus-end, because the motor heads bind to the microtubule in only one orientation. ATP binding gives each step its direction through a process known as neck linker zippering[138]. At a cellular

level it frequently translates to kinesin bringing cargo from the center of the cell to the periphery, also called 'anterograde' transport and vice-versa for dynein, 'retrograde transport'. It is known that organelle transport in cells is accomplished by multiple motor proteins[56,61,83,90,136], and mechanical and chemical regulation plays a significant role in deciding direction and speeds. Understanding the mechanics of single proteins leads to a better understanding of cellular cargo transport. Microtubules are themselves extremely dynamic and provide directionality and structure to cellular transport[1]. The microtubule networks attract a host of regulatory proteins and these tracks are assumed to be extremely crowded. Studying the stepping behavior of molecular motors allows us to understand how this microtubular transport is regulated despite a possible crowded and chaotic environment[68].

3.1.1 Stepping behavior of kinesin and torque

The molecular motor kinesin is a homodimer comprised of two, motor or ATP hydrolyzing domains (heads)[60] and microtubule binding domains each. The two domain types are connected by a so-called coiled-coil stalk or dimerization domain. A kinesin step is about 8nm and the motion is generally parallel to the protofilament[158]. Micro-mechanical recordings with optical tweezers of single kinesin molecules indicate that one motor can exert a force of about 5 pN. In the current model, the motion of the kinesin is a hand-over-hand mechanism with each head occupying, alternatively, the lead position in the direction of motion. This hand-over-hand mechanism can occur in two possible ways, the symmetric hand-over-hand mechanism, where each head moves in the same direction while proceeding further or the asymmetric hand-over-hand mechanism where the "left" head proceeds left and the "right" one to the right in the direction of motion[8,46,59,66,71,175]. The asymmetric hand over hand experiments are predominantly performed at low ATP concentrations and the asymmetric nature of motion was attributed to the load perpendicular to microtubule axis. Previous work suggests that the the two heads of kinesin move in a coordinated manner, undergoing a rotary motion for every stepping cycle[5,69]. Some experiments by Gutiérrez-Medina et al.[59] observe only occasional stalk reversals at low ATP conditions, while, recent work on intermediate states during stepping indicates continuous rotations[73,113], however, direct evidence for such rotational motion is still lacking.

I hypothesized that, a birefringent microsphere attached to a motile kinesin, observed with a polarization microscope and a rotation detecting optical trap would be a sensitive probe to measure the magnitude of rotation (if any) of the kinesin and directionality of rotation at every step. A kinesin stepping

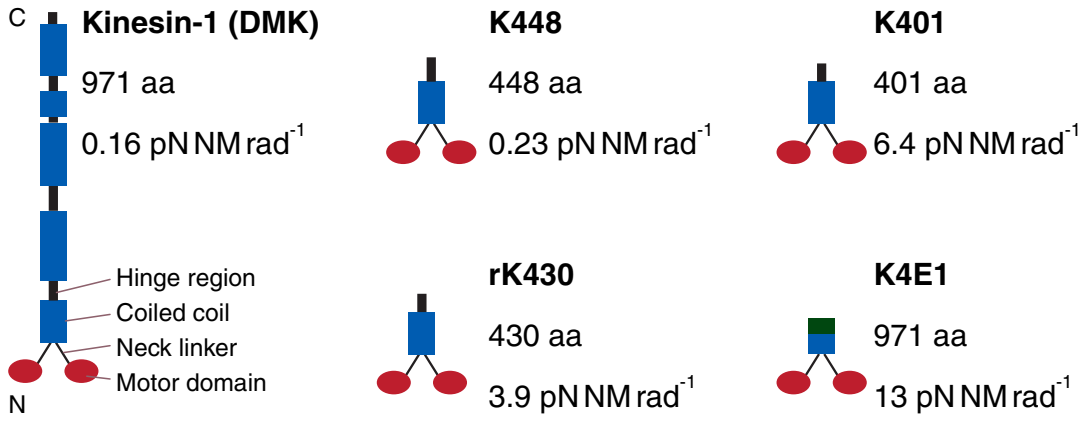

Figure 3.2: A comparison of torsional stiffness of full length kinesin-1 with respect to its truncated counterparts. Full length kinesin-1[72] is comprised of an N-terminal motor domain, a coiled coil stalk and a C-terminal tail domain. The motor domain connects to the stalk through an unstructured neck-linker. The coiled coil in itself is interspersed with the so-called hinge region. Previous reports suggest that the hinge domain and the neck linker impart flexibility to the kinesin. In this figure, we see the torsional stiffness of a full length Kinesin-1 compared to the truncated variants[58] from the same family.

with an asymmetric hand-over-hand mechanism is expected to alternate the rotation direction of a birefringent microsphere at every step with a zero net rotation of over a stretch of multiple steps. While a similar motor stepping symmetrically would show a net rotation over many steps with the magnitude of rotation being decided by the torsional stiffness of the molecule and that of the optical trap.

In this thesis, we used high-resolution optical tweezers combined with a sensitive optical micro-protractor and torsion balance employing highly birefringent, liquid crystalline probes to directly and simultaneously measure the translocation, rotation, and generation of force and torque of single kinesin-1 motors. Surprisingly, we find that motors translocating along microtubules at saturating ATP concentrations rotate unidirectionally producing significant torques on the probes. Per step, the results are consistent with the predicted 180° rotation of the motor stalk implying that the motor's gait follows a combination of a rotary symmetric and asymmetric hand-over-hand mechanism. This method is largely applicable to study rotational motion of molecular machines and our findings implicate a significant role of rotary motion in cargo transport and other motor activities such as microtubule bundling during mitosis.

To understand the rotary stepping of kinesin, we first need to understand the torsional stiffness of the molecule undergoing this motion. The next section describes our method of finding the torsional stiffness and gives a brief comparison to previous studies.

3.2 Torsional stiffness of kinesins

If kinesin is assumed to be a torsionally rigid molecule, the corresponding hand-over-hand motion over microtubules would result in a complete transfer of torque to the cargo, which would be observed as 180°cargo rotation. Biological molecules are compliant. The two kinesin-1 motor heads are linked by a coiled-coil stalk known to be interspersed with flexible elements that are capable of relieving or storing torque. These flexible elements: the so-called "hinge" domains, and the neck linker or the NL domains, connect the motor heads to the stalk, and are known to undergo nucleotide-dependent, order-to-disorder transitions[38,59,69,72,138]. The rigidity of kinesin could play a key role in the performance of various functions of kinesins like, multiple motor motility, overcoming road blocks, processivity and force efficiency[59].

3.2.1 Truncated constructs are torsionally stiffer

In 1993, Hunt & Howard[72] showed that full length kinesins are flexible molecules. They determined the torsional stiffness of full length kinesin measured with a gliding-type assay to be $0.165 \pm 0.02\, pN\, nm\, rad^{-1}$. Figure 3.2 shows that the shorter kinesins are torsionally stiffer than the full length ones. These kinesins are genetically truncated at the stalk, at different lengths from the motor domain. Despite their obvious flexibility, it is understood that kinesins are stiff enough to transfer torque to the cargo. Gutiérrez-Medina et al.[58] showed that at low ATP conditions the kinesin K401 (torsional stiffness, $6.4 \pm 0.4\, pN\, nm\, rad^{-1}$) shows occasional stalk reversal with a probability of $\approx 2\%$.

These experiments were performed with probes larger than a micrometer in diameter and an extremely low ATP so as to reduce the motor speed enough to observe rotations. Furthermore, these experiments were measured using cameras and fluorescence microscopy which could be too slow to observe instantaneous rotations which relax over larger time scales or too insensitive to measure extremely small torque transfers.

I tried to solve these problems using smaller microspheres with a lower drag and optical tweezers for high temporal and angular resolution as discussed in the previous chapters. In addition, we used truncated kinesin-1 construct, rK430 which we expected had a sufficiently high torsional stiffness to transfer torque onto cargo.

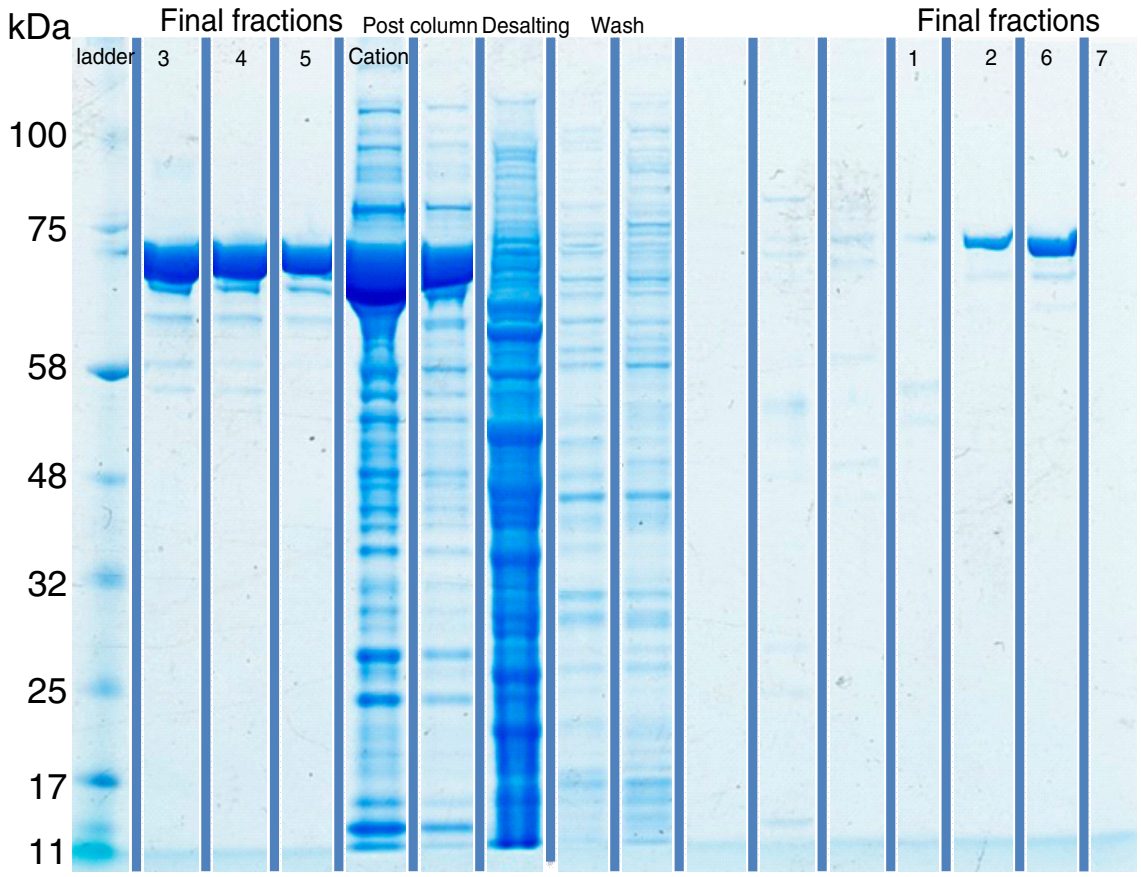

Figure 3.3: Coomasie stained gel of purification of rk430. Coomasie stained denaturing gel of rK430 at different stages of purification. The fractions 2-6 were pooled and used for the final assay.

3.2.2 Expression and purification of truncated kinesin, rK430

The rK430 kinesin is a truncated version of rat kinesin-1 (kinesin heavy chain isoform 5C from *Rattus norvegicus*) with a C-terminal GFP, and H6 histidine tag. The protein is expressed from a bacterial plasmid PET-17b with an ampicillin selection marker. The cloned plasmid was originally provided to us by the Howard laboratory, then at the Max Planck institute for Molecular Cell Biology and Genetics, Dresden. The protocol employed for expression and purification is a combination of a protocol from Naghmeh Azadfar (ZMBP, Tübingen) and Marko Storch (MPI-CBG, Dresden).

Briefly, the cloned-plasmid is transformed into Bl21 (DE3) pRARE E.coli competent-cells using heat shock. The bacteria are grown as a small culture in Lysogeny Broth (LB) and plated onto agar plates with ampicillin. The bacteria which grow on this plate are resistant to ampicillin and are so selected for further growth. The bacteria are grown further in 700 ml warm AMP-LB medium till the medium achieves a optical density of 0.8. The bacteria are then induced using IPTG and allowed to grow for 12 more hours.

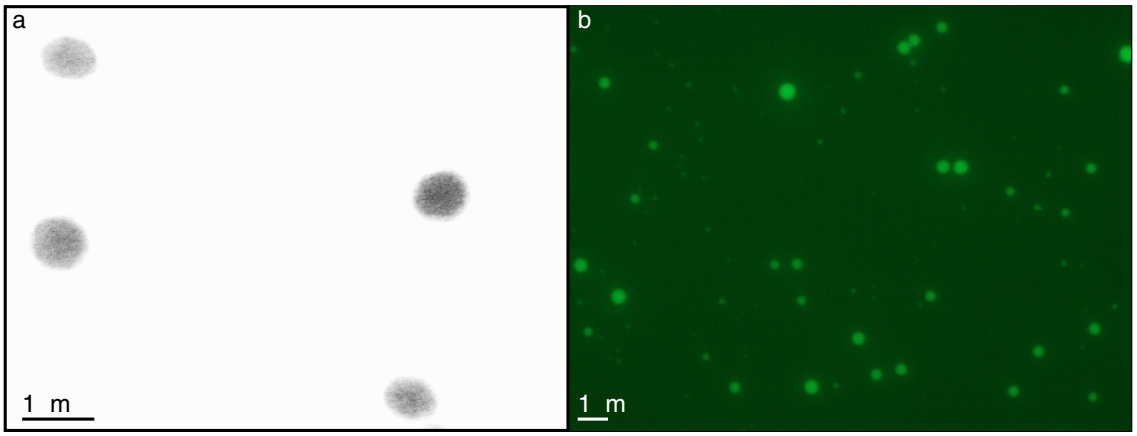

Figure 3.4: Electron micro-graph, TEM of birefringent microspheres and fluorescence imaging of GFP labeled kinesin coupled to birefringent microspheres. a) Transmission electron microscopy (TEM) images of birefringent microspheres with a diameter of 720±40 nm (N = 17). **b)** Fluorescence microscopy image of motor-coupled microspheres using a high motor concentration shows that GFP-labeled motors are bound to microspheres.

The next step is lysing the bacteria to extract kinesin from them. The bacteria are concentrated as a pellet by centrifugation, the pellet is suspended in lysis buffer and sonicated with a tip sonicator in a cold room for 60s (6 x 10s pulses with 20s intervals). The lysate is further centrifuged to separate proteins from the cellular debris. The supernatant post centrifugation is passed through a 1 ml HisTRAP (GE healthcare, 17-5247-01) at aflow rate of 1 ml/min. The protein is eluted using 300 mM Imidazole in elution buffer. Samples are collected at every stage of the expression and purification and stored on ice to be run on a SDS-PAGE gel as shown in Figure 3.3. This protocol was performed in collaboration with Nagmeh Azadfar.

The expressed rK430 was characterized for purification efficiency on a PAGE-Gel (Figure 3.3) and for normal motility using a routine TIRF motility (stepping) assay (Subsection 3.3.2). To carry birefringent microspheres over microtubules, requires a robust coupling protocol of motors to microspheres.

3.2.3 Antibody coupling of kinesin to birefringent microspheres

The coupling of rK430 to a birefringent microsphere is undertaken in two steps, the first being, an N-hydroxysuccinimide (NHS) mediated reaction of anti-GFP antibody on the birefringent microsphere surface followed with the passive binding of the C-terminal GFP of rK430 to the antibody. The protocol for synthesis of birefringent microspheres is described in detail in Appendix A.2.3, along with the subsequent acrylate coupling to NHS and PEG.

To couple the anti-GFP antibody (Protein facility, MPI-CBG, Dresden), we used a final antibody

concentration of 35 µg /ml. The microspheres were incubated with the antibody for a minimum of 45 minutes on ice. Microspheres tend to cluster over longer time and sonication for 45 seconds both, before and after the addition of antibodies is recommended. The sphericity of the microspheres is not lost during the coupling protocol and is verified using a TEM as shown in Figure 3.4.

Microspheres coupled with saturating concentration of kinesins rK430, are seen as fluorescent spheres under an inverted epi-fluorescent microscope (Figure 3.4). Microspheres were coated with kinesin rK430 along with a PEG brush which prevents motor protein denaturation[15] and microsphere coagulation. Further assays are performed at single-molecule conditions, to study the mechanics of the individual protein.

3.3 Characterization of rK430 and the experimental hypothesis

A kinesin moving on a microtubule follows a stepping rate dependent on the ATP concentration in the motility buffer surrounding it. We hypothesize that depending on the mode of translation it would undertake sequential 180°rotations for every 8 -nm step. A kinesin motor follows a stepping rate of about 50-100 steps s^{-1}[79] at 1 mM ATP. The microsphere attached, being a significantly larger object compared to the motor has a large rotational drag and torsional stiffness thus, the transferred torque only amounts for small percent of the actual rotation at the step. This percentage is determined by the torsional stiffness of the motor. The torque generated by the motor is balanced by the optical torque like in a torsion balance.

3.3.1 Experimental protocol for single molecule rK430 experiment

Method: Microtubule polymerization

Microtubules are prepared by incubating a tubulin dimer solution with 1 µl GTP, 1 µl $MgCl_2$ and 1 µl DMSO. The solution is thoroughly mixed and incubated at 37 °C in a hot air oven for 30 min. Five minutes prior to the termination of microtubule incubation, 990 µl BRB80 is warmed up to 30 °C and mixed with 10 µl taxol. 1 µl of microtubules are transferred to 100 µl of BRB80-taxol solution and kept at 37 °C .

Method: Flow-cell and motility assay

The motility assay is performed in a flow-cell made of two glass cover-slips separated by a fixed distance, using parallel aligned parafilm strips. The cover-slips are easy-cleaned and silanized (Appendix B.1.1) to increase hydrophobicity. To this flow-cell, 20 µl , 60 μg/ml anti-tubulin antibody (Sigma-Aldrich, Germany) is added and incubated for 15-20 minutes. The anti-tubulin antibody sticks to the hydrophobic surface, subsequently binding to microtubules, producing a surface coated with microtubules. The antibody is then washed with BRB80 and replaced with a 20 µl , 1 % by weight, hydrophilic non-ionic co-polymer surfactant, F127 (Sigma-Aldrich, Germany). F127 is incubated for further 15 minutes and washed thrice with 20×3 µl BRB80. To this flow-cell, the diluted microtubule solution is added and incubated for 15 minutes.

The motility assay requires the preparation of motility buffer, which is a solution of 200 µl BRB80-taxol with 4 µl Casein, 2 µl nucleotide solution (ATP, AMP-PNP), 2 µl D-Glucose, 2 µl Glucose oxidase, 2 µl Catalase and 2 µl DTT. The antibody-coupled microspheres in Subsection 3.2.3 are incubated with the appropriate concentration (10000x, for single molecule conditions) rK430 solution for 8 minutes at room temperature. The GFP on the C-terminal of rK430 forms a stable bond with the anti-GFP antibody. These microspheres are then diluted 50x in motility buffer and flowed through the microtubule coated-flow-cell.

The kinesin molecules attached to the microspheres are then attached to an individual microtubule via optical tweezers, to perform the assays mentioned in the following sub-sections.

Motor functionality under single-molecule conditions

To confirm that motors were functional after coupling, we placed motor-coupled microspheres onto surface-immobilized microtubules using the optical tweezers. After turning off the trap, we tracked the microsphere motion using LED-DIC[19]. To ensure single-molecule condition only about 1 out of 4 microspheres showed motility[18]. At a temperature of 29.2 °C [107], we measured a microsphere speed of 0.85 ± 0.11 µm /s ($N = 19$, all errors are s.e.m. unless stated otherwise) with an average run length of 3.5 ± 0.3 µm ($N = 19$) consistent with the motor speed and run length of 0.95 ± 0.07 µm /s and 2.5 ± 0.3 µm ($N = 24$), respectively, measured by single-molecule fluorescence microscopy without microspheres and literature values[18,70]. The agreement confirmed the functionality of the motor when

attached to a microsphere

3.3.2 Stepping velocity as a control for normal functionality

rK430 the truncated construct has been reported to be a stably expressing, functional construct of Kinesin-1 by many researchers in the field of single molecule kinesin motility[37,177]. It has been shown by Kawaguchi & Ishiwata[79] that the stepping rate of kinesin increases with temperature but the force remains constant.

In our study, kinesin rK430 motors are tested for their speed under single molecule conditions[18] using the TIRF microscope and found to have a speed of $0.95 \pm 0.07\,\mu m$, N=24, with an average run length of $2.5 \pm 0.3\,\mu m$ at 29.2 °C. The higher speeds can be attributed to the high temperature at which the measurement are performed. The experiment when repeated with single molecules of rK430 bound to birefringent microspheres with the attached kinesin molecules were taken and motility performed under single molecule conditions. The corresponding speed was obtained to be 0.85 ± 0.11 μm /sec, N=19. The speeds were concluded to be significant with a t-test, t = 3.44 and degrees of freedom = 30 between the freely moving kinesin speed data from TIRF microscopy and that with the microsphere attached to the kinesin. The corresponding two-sided p value is 99.5 percent. After establishing the functionality of kinesin we measured the torsional stiffness of the truncated construct.

3.3.3 Measuring torsional stiffness to check feasibility of torque transfer

To test whether both the motor-head–microtubule and, in particular, the motor-stalk–microsphere linkage are rotationally constrained and can sustain torque, we place motor-coupled microspheres under single-molecule conditions on microtubules using a linearly polarized laser trap (inset Figure 3.5a). In this experiment, we use the non-hydrolyzable ATP analogue adenylyl β,γ-imidotriphosphate (AMP-PNP). When AMP-PNP is bound to motors, they are thought to be in a two-heads-bound state mimicking the predominant motor conformation at high ATP concentrations. In contrast, at low ATP concentrations, kinesin is preferentially bound by one motor head not being able to sustain torque[117]. To observe the angular orientation of the microsphere, we removed the Nomarski prisms of our custom-built differential interference contrast (DIC) microscope, which we use to visualize single microtubules[19]. The removal converts the setup to a polarizing microscope, in which the polarization direction of the visible illumination is rotated 45 °relative to the trapping laser polarization. Thus, when viewed under crossed polarizers, trapped microspheres have maximum brightness. Subsequently, we rotated the laser polar-

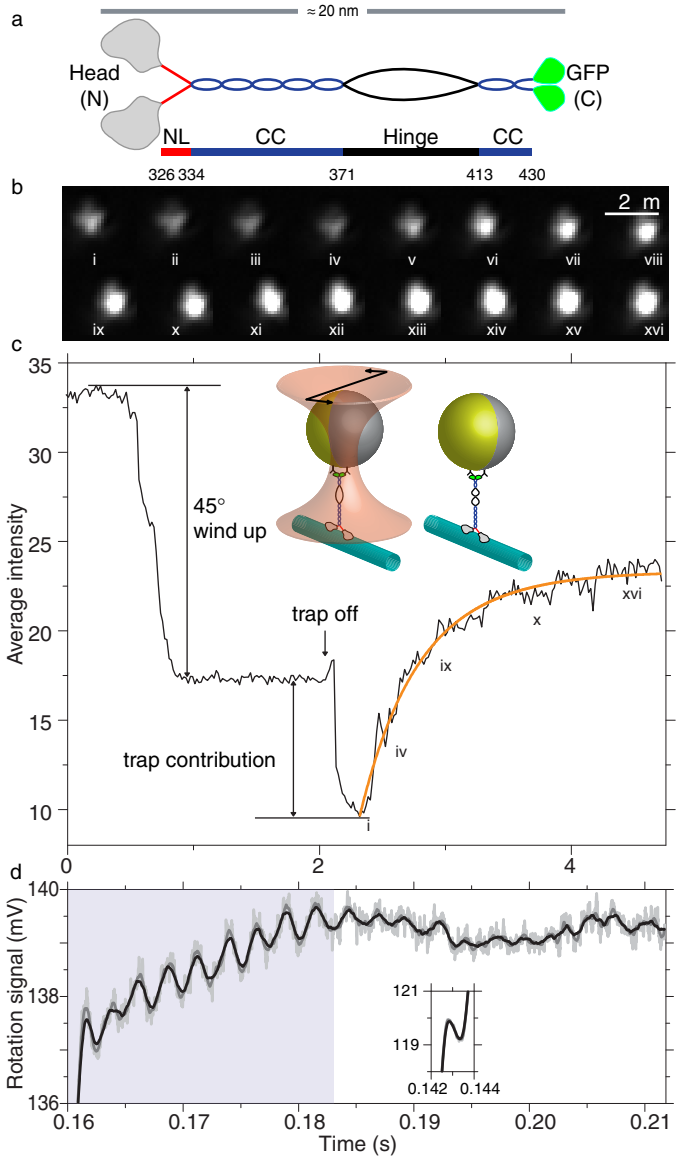

Figure 3.5: Kinesin structure and twisting of a motor coupled to a birefringent microsphere.
a) The rat kinesin-1 construct has two N-terminal motor heads, a neck linker (NL, red), a hinge domain (black), two coiled-coil domains (CC, blue) truncated after amino acid 430, and two, C-terminal GFP fluorophores (green). **b)** Image sequence of a rotating, motor-attached birefringent microsphere with radius $R = 0.65 \pm 0.04$ µm viewed under crossed-polarizers in AMP-PNP (time between frames: 136 ms). **c)** Microsphere image intensity vs. time (black line). The relaxation was fitted to $I \propto \sin^2(\frac{1}{2}[1 - \exp(-(t - t_o)/t_{rot})])$ with an offset t_o and $t_{rot} = 0.98 \pm 0.05$ s (orange line). Inset: Schematic of the twisting experiment not drawn to scale. **d**, Back-scattered laser intensity as a function of time. 10 periods are shown including one on the rise (inset).

ization by 45 °to the extinction position and thereby twisted the motor. After the trap was turned off, the microsphere brightness, quantified by an average intensity over a region of interest around the microsphere, increased again (Figure 3.5 a). This increase is consistent with a rotation back to the initial microsphere orientation. Note that we did not use an infrared filter in front of the camera that we could detect when the laser was turned off. A control measurement confirmed the expected image-intensity

dependence on the rotation angle (Figure 2.3). For the twisted kinesin, the rotation back to the initial state was well described by an exponential (orange line in Figure 3.5c) with a relaxation time constant $t_{\mathrm{rot}} = \gamma_{rot}/\kappa_{\mathrm{rot}}^{\mathrm{motor}}$, where $\gamma_{rot} = 8\pi\eta R^3\lambda$ is the rotational drag coefficient with $\lambda \approx 1.12$ accounting for the surface proximity[23] assuming a distance of 50 nm. Using the known viscosity η and microsphere radius R, we determined the torsional stiffness $\kappa_{\mathrm{rot}}^{\mathrm{motor}} = \gamma_{rot}/t_{\mathrm{rot}}$ of the motor to be 4.0 ± 0.5 pN nm rad^{-1} ($N = 9$) consistent with the reported values[38,59].

Figure 3.5a is a snapshot of birefringent microsphere as the attached kinesin relaxes from an angle of 45° labeled "1" to an angle of 0° labeled "16". The intensity of the microsphere increases 1 through 16, as expected for a birefringent particle rotating from extinction to maximum transmission for the said angles. Figure 3.5 b is the graph of transmitted microsphere intensity versus the time of relaxation. The initial ≈ 2 seconds shows the microsphere being rotated by 45° from equilibrium. The jump, labeled "trap contribution", was the effect of the laser intensity on the detection diode. At the point "trap off" the microsphere was set free from the trap and relaxed from point 1 through 16 as described before. The relaxation rate along with the drag of the medium gave us the torsional stiffness of this rK430 molecule, which was 3.9 ± 0.5 pN nm rad^{-1} consistent with that observed by Gutiérrez-Medina et al.[59].

3.3.4 Winding up the stalk of rK430

To determine how much we could twist the motor stalk, we changed the laser to circular polarization after we turned off the trap. When we turned on the laser again, we measured on average 10.4 ± 0.5 ($N = 12$) clear oscillations in the back-scattered laser intensity—independent of the rotation direction—before the oscillation amplitude was comparable to the noise level (Figure 3.5d and Figure 3.6). The oscillations are consistent with a motor that can be twisted by at least 5 full turns.

The Figure 3.6 shows the recorded rotations of a microsphere within 0.3 seconds of switching on the circularly polarized trap. The red shaded area on the left is where we expect the motor to coil up. The microsphere rotates by 3 turns (6 periods in the rotation signal with circularly polarized light) after which no modulation of the back-scatter signal is observed. At a certain point, the rotation signal is found to suddenly jump to another level we attribute to an unspecific binding event of the microsphere (grey shaded area). A second jump at ≈ 0.2s occurs after which the microtubule rotates freely. The microsphere diameter was 800 nm and the laser power 25 mW. We tried the same measurement 6 times each in circularly polarized light in clockwise and counterclockwise direction. For clockwise rotation, we

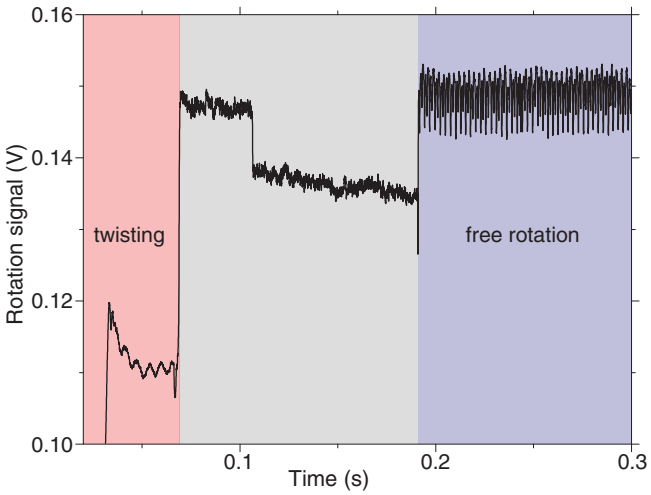

Figure 3.6: Rotation of an AMPPNP bound kinesin molecule with an attached microsphere using circularly polarized light.
The kinesin-microsphere system is initially attached to the microtubule when the trapping light with circular polarization is suddenly turned on. The rotation signal was recorded as a function of time (see text for details). The microsphere rotates by 3 turns (6 periods in the rotation signal with circularly polarized light) after which no modulation of the backscatter signal is observed. At a certain point, the rotation signal is found to suddenly jump to another level we attribute to an unspecific binding event of the microsphere (grey shaded area). A second jump at $\approx$ 0.2s occurs after which the microtubule rotates freely. The microsphere diameter was 800 nm and the laser power 25 mW. We tried the same measurement 6 times each in circularly polarized light in clockwise and counterclockwise direction. For clockwise rotation, we had 10, 12, 12, 13, 9 and 10 oscillations while for the counterclockwise rotation, we had 8, 10, 10, 11, 12 and 8 oscillations.

had 10, 12, 12, 13, 9 and 10 oscillations while for the counterclockwise rotation, we had 8, 10, 10, 11, 12 and 8 oscillations. Together, these measurements show that the birefringent microspheres are good probes to study the torsional properties of the motor and, therefore, its rotations and the possible generation of torque.

The torsional stiffness of rK430 is sufficient for transferring torque to the microspheres and also for storing torque in its structure. The next step is to test if motility with the birefringent microspheres is accompanied with the predicted rotation of the microspheres are observable.

3.4 rK430 motility and stalk rotation

3.4.1 Calibration of rotation from the intensity of transmitted visible light at known angles

The intensity of a birefringent microsphere when observed through a cross-polarized microscope varies between a maximum and extinction as the angle changes from 0° to 45°, respectively, with reference to the

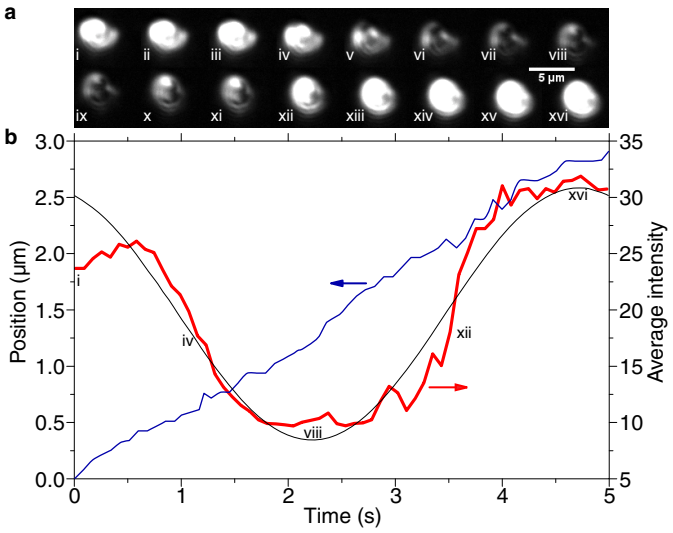

Figure 3.7: Free motility of a birefringent microsphere attached to single kinesin molecule.
a, Image sequence with 340 ms between displayed frames. The microsphere radius was 2.10 ± 0.05 µm. **b**, Microsphere position (blue thin line) and average intensity per pixel (red thick line) of the images in **a** as a function of time. A sinusoidal line (black) is drawn as a guide to the eye.

long axis of polarized light. The Figure 2.3 shows a plot of transmitted intensity of visible light through a birefringent microsphere. The microsphere is rotated from an angle of -10° to +50° using linearly polarized trapping laser. The minima observed at 0° is higher than that at ±45° due to the different index of refraction at perpendicular axes of the birefringent microsphere. A microsphere if rotated by a kinesin should show a similar intensity change with the rotation angle.

3.4.2 Video tracking of kinesin motility and rotation under crossed-polarizers

A birefringent microsphere is attached to a kinesin and allowed to step on a microtubule with a high ATP concentration of 1 mM. The motion of the microsphere is tracked with a video camera and the microscope was adjusted to cross-polarized illumination. The microsphere is left unconstrained i.e. without the optical trap and proceeds to step with previously reported speeds.

To test whether motors could generate torque during translocation, we performed a motility assay with motor-coupled microspheres powered by single motors under saturating ATP concentrations (Figure 3.7). Using the optical tweezers, we placed a microsphere on a microtubule, turned off the trap, removed the DIC prisms, and recorded on an image sequence under crossed polarizers. During the translocation, the microsphere brightness changed (Figure 3.7a). Using pattern matching, we tracked the microsphere and plotted the position and microsphere intensity, determined as above, as a function

of time (Figure 3.7b). The recorded video is then analyzed with a macro written in Fiji[145,147] to track birefringent microspheres and record their intensity. The intensity change is consistent with a constant rotation rate of the microsphere (solid line, Figure 3.7b) implying that the motor was able to generate a torque sufficient to continuously rotate the microsphere. In about 60 % of the tested microspheres, we observed more erratic and fast intensity changes consistent with the reported, occasional stalk reversals[59]. Fast changes could occur if the motor spends an extended duration in a one-head-bound state such that torque is released by a swiveling motion around the neck linker accompanied by rotational Brownian motion of the microsphere. Such changes occurred on average every 1.3 ± 0.3 s ($N = 15$) corresponding to a probability of 4 % per step, a value similar to the reported one[59].

The kinesin motility track is represented in Figure 3.7b as a blue line. The velocity of kinesin in this case was 570 nm s^{-1}. As shown in Figure 3.7a the intensity of the microsphere changes from a maximum to a minimum and back to maximum, a rotation of $\approx 90°$. The asymmetry of the maxima in this curve at time t=0 s and t=5 s, we attribute to the difference in the ordinary and the extraordinary axis of refraction of a birefringent object. In Figure 3.7, the kinesin traversed a distance of ≈ 27 μm in 5 seconds thus taking about 70 steps in one second. The video is recorded with 15 frame per second. Any information on the rotation event of a single step is completely lost. Also, the torsional relaxation rate of the microsphere was too slow, to be able to detect any discrete rotational steps. These experiments confirm that the motor can generate significant torque at saturating ATP concentrations. To achieve a higher resolution, we use optical tweezers combined with a rotation detector based on the back-scattered trapping light—an optical micro-protractor (Figure 2.2).

3.5 High resolution tracking of kinesin rotation using an optical micro-protractor

3.5.1 Motility of kinesin with a force clamp

We tested whether we could independently record both translational and rotational motion. Using a force clamp[26] and a high ATP concentration (1 mM), we observed a significant rotation signal uncorrelated to the translational signal (Figure 3.10a). In contrast, at a low ATP concentration (1 μM), we did not measure a significant rotation signal (Figure 3.10b). In the former experiment, we could not quantify the rotation signal because the motor took many steps resulting in a nonlinear rotation signal

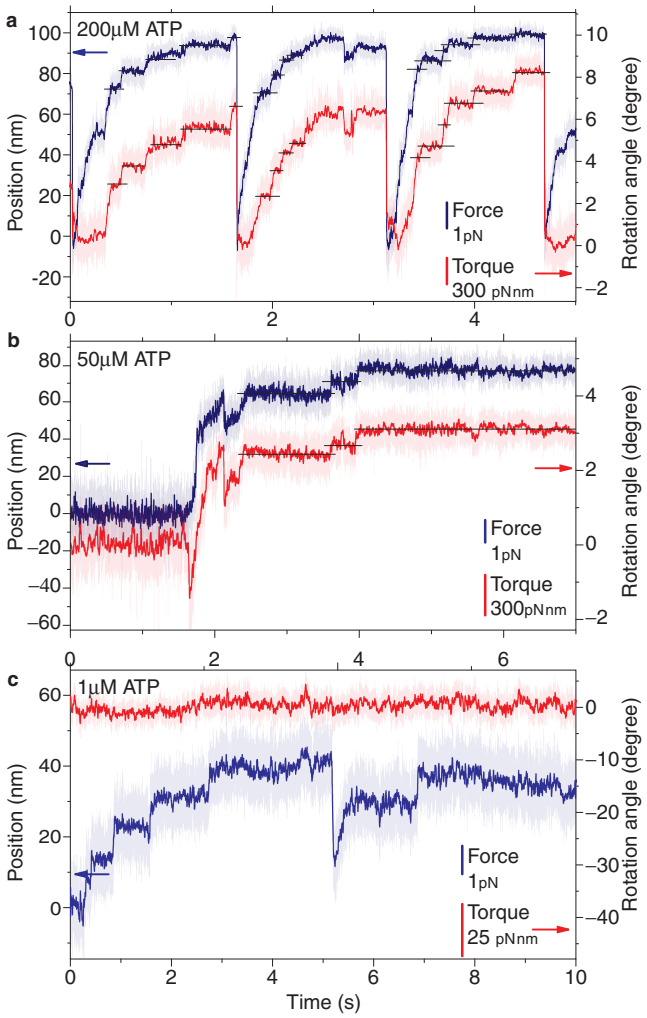

Figure 3.8: Motility of birefringent microspheres in static trap
a) A 1.02 μm diameter microsphere. The red curve indicates the displacement of the microsphere while the kinesin moves. The stall force can be computed by multiplying 0.059 pN/nm with the displacement. The black curve indicates rotation of the microparticle from the equilibrium orientation as a consequence of the motility of the kinesin. The signal in rotation due to cross talk from the translational motion has been subtracted. The rotational trap stiffness if 9560 pN nm/rad and the rotational sensitivity 410 rad/V. (b) The particle is of 0.64 μm diameter. The trap stiffness is 0.051 pN/nm, rotational trap stiffness 6883 pN nm/rad and rotational sensitivity 255 rad/V.(c) The particle is of 1.06 μm diameter. The trap stiffness is 0.05 pN/nm, rotational trap stiffness 8892 pN nm/rad and rotational sensitivity 297 rad/V.

response. Also, for large rotations, the translational displacement sensitivity depended on the rotation angle (Figure 2.4a) precluding constant force measurements. Therefore, we performed measurements using a stationary optical trap.

The static trap assay for detection of rotation is limited to recording short stretches of motility. The motor detaches as soon as the stall force is reached. Much like the recording with the video, it is interesting to observe the rotation of motor over longer times, while retaining the measurement resolution and sensitivity of the optical trap.

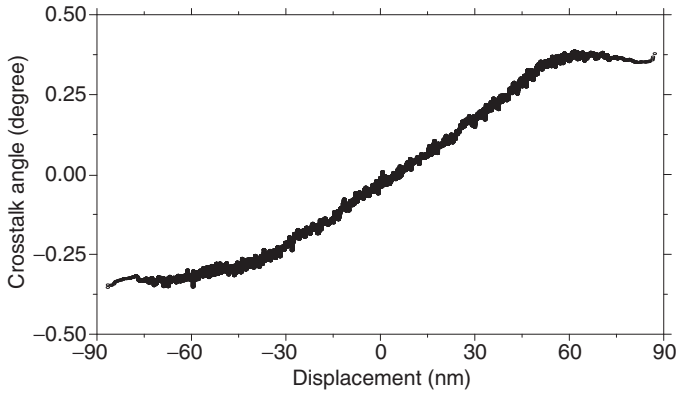

Figure 3.9: Measurement of cross-talk between the translation and rotational signal
The cross talk in the rotational signal while the birefringent microsphere attached kinesin exhibits motility after being trapped in a static trap. The corresponding cross talk in the raw signal is ≈ 0.1 percent. The diameter of the microsphere was 650 ± 28 nm.

In a force feedback or a force-clamp assay, a motile microsphere is followed by moving the stage so that a constant backward load is maintained on the motor. While this is the basis of the "force clamp" mode[148], it may be noted that the system becomes complicated due to the presence of the birefringence in the microsphere. The calibration for the translational position sensitivity in the two orthogonal directions is initially performed with the axis of birefringence defined by the axis of linear polarization. The value of the sensitivity along the two orthogonal directions were found to be different. However, as the microsphere rotates, the direction of the axis changes and hence the sensitivity also changes (Figure 2.4). This effect has not yet been considered in the "force clamp" measurement that is performed and could lead to lower clamp-force as the microsphere rotates.

3.5.2 Static trap

To quantify the torque, we calibrated the back-scattered laser intensity signal of a birefringent microsphere trapped with an elliptically polarized laser (Figure 2.4b). We ensure that the ellipticity is small enough that microspheres do not rotate spontaneously. The elliptical polarization was essential for achieving a linear angular response (Supplementary Theory). Furthermore, to remain in the linear angular response range and to avoid changes in the displacement sensitivity, we used a high torsional stiffness of the trap. In addition, we measured and corrected for a small angular cross-talk with increasing displacements (Figure 3.9). After we determined the angle sensitivity and torsional stiffness, we placed the motor-coupled microspheres on microtubules and recorded the position, force, angle and torque of the microsphere (Figure 3.8). At sufficiently high ATP concentrations, single motors simultaneously dis-

placed the birefringent microspheres from the trap center and rotated them (blue and red lines, respectively). Motors generated force up to about 5 pN and torque up to about 100 pN nm (Figure 3.8a–c). As in the force-clamp experiments (Figure 3.10b), motors did not generate any torque at low ATP concentrations (Figure 3.8d). In this case, the positional noise on the traces was larger. The absence of rotations and the higher positional noise are consistent with the motor being mostly in a one-head-bound state[117]. On close inspection, both the displacement and angular traces show discrete steps when the motor approaches its stall force. Because positional steps had a higher signal-to-noise ratio, we used an unbiased step detector[20] to determine time points at which positional steps occurred (blue and yellow shaded regions in Figure 3.8). To determine how large angular steps were, we averaged the angular trace over the dwell time of the positional steps and marked the average position and angle during a dwell with black lines. Individual angular steps concurrent with displacement steps were on average $0.27 \pm 0.03°$ ($N = 21$) large. The angular steps correspond to an increase in optical torque of $\tau_{\text{step}} = 13.6 \pm 1.2$ pN nm per step ($N = 21$). Balancing the torsion of the optical trap with that of the motor using the torsional stiffness of the motor, the angle that the motor is turning per step is $\vartheta_{\text{motor}} = \tau_{\text{step}} / \kappa_{\text{rot}}^{\text{motor}} = 195 \pm 30\,°$ (propagated SEM). This angle is consistent with the expected 180° rotation per step. Interestingly, we observed that for the translational backward step at 2.7 s that the angular step continued to increase. Only for the next forward step, the angular step decreased indicating a reversal of the motor rotation direction. Since most angular steps are in the same direction, it also implies that the motor stalk rotates unidirectional even under conditions in which up to 5 pN of hindering load are applied. Interestingly, we observed angular steps down to ATP concentration of 50 μM (Figure 3.8c). At 1 μM, we did not observe any steps any more (Figure 3.8d).

We have tried to ascertain whether the rotations prefer one sense or happen in both senses. We placed the input laser angle at 20 degrees from the x axis, when the value of $(sin^2(\vartheta))$ is halfway between 0 and 1 so as to exhibit both upward and downward signals to establish clockwise or anticlockwise motion. Then we allowed the microsphere to move on the microtubule and rotate. We find that the left-handed configuration is preferred 12 times while the right-handed rotations occurred 8 times out of 20. The corresponding error in the measurement is about 2 so as to conclude rotation in either sense with almost equal probability. Typical signals of rotations while the kinesin translates are shown in Figure 3.8.

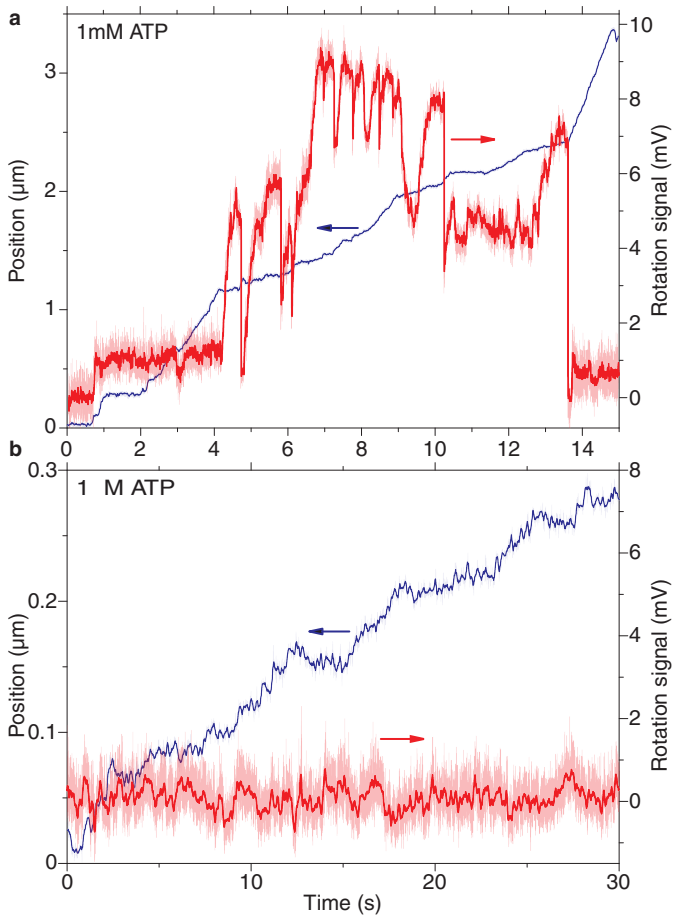

Figure 3.10: Optical trapping with force feedback to observe longer motility traces a) Motility of a 990 nm bead measured with an optical tweezers in force-clamp mode. The blue curve indicates the displacement of the microsphere while the kinesin moves. Trap follows the microsphere while keeping a constant load of 4 pN on it. The red curve indicates rotation of the microsphere from the equilibrium orientation as a consequence of the motility of the kinesin. **b)** Rotation of the microsphere at 1 μM ATP while exhibiting translational motion in a force-clamp configuration of the optical tweezers. The trap is moved in accordance with the position of the microsphere so as to provide a constant hindering load on the particle. The hindering load in this case was 2 pN. It can be seen that the microsphere moves a distance of about 1 μm in 60 sec while there is no rotational signal. This lack of rotational motion at very low ATP concentrations can be an effect observed since only one of the heads of the kinesin is supposed to be bound in the transient state leading to inefficient torque transfer to the microsphere.

3.5.3 Motility assay with force feedback

3.6 Conclusion

From the single molecule motility experiments, the kinesins seem to rotate while stepping. The mechanism of rotation suggests that such rotation is possible only when a kinesin would processively step in a symmetric hand-over-hand manner. Interestingly, the energy required for a kinesin to step must be the summation of the energy required for kinesin to rotate and to translate. Initial calculations suggest that indeed kinesin is an energy inefficient motor if rotation is not taken into account. One molecule of ATP

has much more energy than the amount kinesin requires, for translation only. Although more theory and experiments in this direction are required to comment any further on this query.

A closer inspection of relaxation characteristics, in Figure 3.6 and Figure 3.8 presents interesting features which were, during the scope of my thesis, not focused upon. In the case when kinesin heads were fixed to a microtubule and the birefringent microsphere rotated, we see that the oscillation frequency is significantly lower than when the particles are rotated freely, during this time one sees bumps in the basal oscillation amplitude which could relate to certain domains of kinesin folding or unfolding. On the other hand the ability of kinesin to store torque prods further inquiry into the structure of kinesin and its flexible domains.

The field of kinesin has still many unanswered questions and birefringent microspheres in conjugation with optical tweezers seem to be promising tools for its future.

4

Conclusion

Ashkin et al. [11] first demonstrated optical tweezers as a tool to trap dielectric particles in 1986, since, there has been little advance in the type of particles used for trapping. The polystyrene and silica microspheres used in initial experiments, are still being used in the study of forces in biological molecules. With RM257 microspheres we were able to introduce an extra degree of control of the optical trap. This is achieved by synthesizing highly birefringent microspheres so that spin angular momentum from a circularly polarized light beam can be transferred on to these spheres. An added advantage of the microspheres, which we employed in this thesis is the ability to measure small angular changes induced on these particles by an external source like molecular motors.

Birefringent microspheres find many interesting and potentially useful applications in optical traps and biology. Their high birefringence results in large torques acting to spin or align the particles, and the torque can be measured optically (Chapter 2). Moreover, it is possible to measure rotations of these

microspheres independent of the optical tweezers since the high birefringence results in a characteristic diffraction pattern, the intensity as a function of angle can be easily calibrated in a simple light microscope with crossed polarizers (Figure 2.3). The ability to measure angles and torques, finds use for these microspheres as sensors to measure the properties of the surrounding fluid, like the cytoplasm and other non-newtonian fluids. It is easy to couple my microspheres to bio-molecules, thus allowing their use as "tools" for the manipulation of microscopic polymers, like DNA, to study coiling and super-coiling properties and the associated drag due to their chemical structure. An interesting approach being recently discussed as an application for RM257 microspheres is to couple them to cellular surfaces to study the rotational component of cellular translocation or to observe local activity of membrane cytoskeleton. A simpler application would be to employ RM257 microspheres as tools for controlled rotation and alignment of cells and micro-engineered components in lab on chip devices. The high rotation rate of these microspheres in circularly polarized light when suspended in a fluid results in flow of the fluid around the particle, thus opening applications of controllable micropumps. In a recent work, rotating microspheres have enabled a control on the direction of growth of individual axons[173]. This helps to unravel axonal path-finding which is important in the development of the nervous system, nerve repair and nerve regeneration. By using the rotating particles one can create a localized microfluidic device generating shear force against the growth cone. This force can then be determined quantitatively.

RM257 microspheres exhibit a higher birefringence in their unpolymerized state compared to when the individual monomers are cross-linked. The cross linked polymers on the other hand are more robust against centrifugation and washing steps integral to many bio-coupling protocols. An obvious next step would be to make stronger unpolymerized birefringent microspheres, which can be achieved by coating them with a silica or polymer shell. We have already initiated silica coating of RM257 microspheres with successful results (Figure 1.9), with further experiments required to standardize shell thickness and surface coupling of molecules. It might be possible to further affect the effective trapping parameters by controlling the shell thickness as shown in the case of Titania microspheres by Jannasch et al.[75].

On a different note, nematic liquid crystals like RM257, exhibit 'defect regions', the morphology and the position of which depends on a delicate balance between elastic, enthalpic, and interfacial contributions to the free energy. A particle with planar degenerate anchoring by itself requires existence of surface defects, which manifest as boojums at the poles of the particle. Localization of fluorescent particles at the two termini of birefringent microspheres could prove to be an effective way to control bio-molecule lo-

calization with respect to the birefringent axis.

Birefringent microspheres independent of optical tweezers are indeed capable tools for probing large angular fluctuations in molecules and tracking cellular events. In order to achieve higher angular and temporal resolution, the use of optical tweezers is imperative. In a relatively short time, I was able to modify an existing tweezers microscope to induce and detect torque on RM257 microspheres. Our method of modification relies on the fact that the polarization of laser beam reflected from the birefringent microspheres depends on the angle of director axis with respect to the polarization angle of incident laser beam. A change in polarization is then easily converted to a change in intensity via an addition of polarization beam splitter cube before the back scattered detection diode (Figure 2.2). I believe that the angular resolution and the ease of calibration can be improved further by comparing the phase and the polarization angle between the forward scatter quadrant photo diode against the back scattered detection diode[58,131].

In the present scenario I implemented a system to rotate the polarization of incident linearly polarized light with angles as small as 1°. The same system is also capable of changing the linear polarization to circular polarization by changing the angle of quarter-wave polarization plate. It is possible to achieve these effects faster and more precise by automating the rotation of polarization plates, with controlled angles. A simple servo motor was indeed employed by me to achieve this automation, but having a liquid crystal based polarizer would probably be a more efficient tool[126] to calibrate, induce and measure microscopic torque.

Tracking individual steps of single molecular motors like kinesins and measuring small forces is ideally performed with optical tweezers, additional ease of calibrating spherical birefringent microspheres has added an extra dimension in the study of simultaneous stepping and rotation of kinesin. But how does this discovery affect the overall understanding of molecular motors, specifically kinesins? The torsional stiffness of kinesins has always been an area of interest since Howard[69] and Hunt & Howard[72] raised the question of kinesin, being 'more machine or more animal'.

Kinesin perform a cyclical action of binding, exerting force and detaching from microtubules. The lack of any organization of kinesin over microtubules means that a rigid kinesin would only have a limited degrees of freedom to search for the microtubule orient in the direction of motility and exert force. This problem would be more severe in the presence of multiple motors working together to achieve larger forces as is evidenced in living systems. Both of these problems kinesin has could be solved by being a

flexible molecule. It is known that kinesin is interspersed with non-structured domains which could be flexible. Our experiments with truncated kinesin shows that the kinesin motor is indeed flexible and can store up to 12 turns within its structure, while being stiff enough to induce torque on the birefringent cargo so as to induce rotation for every translational step undertaken. The torsional stiffness measured from the relaxation rate of a twisted kinesin, hints at a non-linear response. Gutiérrez-Medina et al.[58] have already shown that mutating or deleting certain domains of kinesin-1 could make it stiffer but a thorough understanding of the individual domains in the 'hinge' and the 'neck-linker' region can potentially yield interesting insights into the domain organization of kinesins. A twisting assay with high resolution detection might be an ideal tool to study torsional weaknesses in kinesin-micro domains. Coupled with mutations in hinge and the neck-linker region, it should be possible to create a torque map of kinesin. A further analysis of the oscillation frequency of bound kinesin would provide insights into the friction within the protein structure. It is possible that along with the energy that kinesin requires to undertake steps and induce torque, it also requires energy to overcome the impedance arising from bond stretching and dissociation.

Asbury et al.[8] back in 2003, showed that the motion of kinesin over microtubules performs a so-called 'limping', with a longer 'dwell-time' for every alternate step. This implies that there exists an asymmetry in the structure of this molecule which causes it to wait longer for one step over the other. Our experiments with high resolution angle detection would shed light into this quandary, with a possibility to comment on the symmetricity of the motion of individual heads of kinesin over the microtubule. At the first glance when looking at the rotation of the birefringent cargo in a force clamped setupFigure 3.10, it seems that the kinesin prefers to rotate in the same direction as against rotating alternatively clockwise and anti-clockwise. This hints towards a symmetric hand-over-hand mechanism, but it is very well possible that the kinesin performs a combination of symmetric and asymmetric hand-over-hand motion with the symmetricity decided by the stepping rate of the motor. The symmetric hand-over-hand mechanism of kinesin means that the cargo would always remain under constant uni-directional torque from sequential rotary steps. If the cargo has a torque applied, then the moment the motor head detaches from the microtubule, this torque should be released at a time-scale much shorter than the time it takes for the motor to undertake the subsequent step. Our data implies the kinesin heads undergo 'electrostatically guided' gliding over microtubules, and that this allows them to remain bound to the microtubule[55].

In summary, I was able to synthesize spherical birefringent microparticles with intrinsic anisotropy

for rotation detection. The sphericity of these microspheres and a control of size and birefringence has allowed us to develop a calibration protocol to resolve small angular steps, and transferred torque. Moreover, we were able to see previously unseen rotation speeds of microparticles suspended in a fluid. An understanding of the surface chemistry of RM257 microspheres has enabled me to develop a novel protocol of coupling these particles to bio-molecules like kinesin. Birefringent microspheres as cargo of truncated kinesin add another dimension to the study of motor motility over microtubule filaments. It was verified that kinesins can store and transfer torque to its cargo and individual steps of kinesin were co-related to the rotation of the birefringent microspheres.

A

Microsphere synthesis

A.1 Synthesis of birefringent microspheres

Materials

Chemicals

- Mesogen/liquid crystal precursor RM257; Merck
- Photoinitiator Darocur 1173; BASF
- Analytical ethanol
- Deionized and degassed water

Equipment

- ULTRA-VITALUX ultraviolet high-pressure lamp (13.6 W at UVA)
- IKA C-MAG-HS7, magnetic stirrer with heating plate
- Glass beakers with a volume of 250 ml and 1000 ml
- Laboratory glass bottles with screw cap (PP, blue, integral lip seal) and a volume of 250 ml or 500 ml

A.1.1 Synthesis of non-polymerized birefringent RM257 microspheres

Solution A: liquid crystal-precursor solution

1. Heat 50 ml ethanol to 55 °C in a glass beaker of 100 ml volume.
2. Add 25 mg of the mesogen RM257 to the preheated ethanol and stir the solution with a magnetic stirrer (300 rpm) while maintaining the temperature.

Solution B: Heated ethanol solution

1. Add 200 ml water to 300 ml ethanol in a glass beaker of 750 ml volume.
2. Heat the solution to 7 °C while stirring with a magnetic stirrer (300 rpm).

Reaction: Birefringent microspheres

1. Once Solution B has reached 75 °C, add Solution A in a drop-wise manner while stirring the solution with a magnetic stirrer. The stirring speed should be as high as possible without forming bubbles. The ethanol-water mixture has to be maintained above 69 °C since this is the nematic transition temperature for the mesogen RM257, above which it forms a nematic liquid crystal.
2. Let the solution evaporate at 75 °C until only 200 ml of the solution remains. The solution should turn milky by then. The rate of evaporation can be controlled by sealing the beaker with a perforated aluminum foil. An increase in the area of perforation increases the evaporation rate, thus resulting in smaller particles; and vice-versa, a decrease in the area of perforation decreases the rate of evaporation resulting in larger particles.
3. Let the solution cool down to room temperature.

4. The microspheres can be stored in a glass bottle with cap at 4 °C for several weeks with shaking once every week.

A.1.2 Synthesis of polymerized birefringent RM257 microspheres

To make polymerized microspheres, change the following steps in Section 1.2:

1. Solution A: Add 250 ,mg photo-initiator Darocur 1173 to Solution A. The concentration of the photo-initiator is 10× higher than the mesogen.

2. Reaction: Do not cool down the solution in the last step of the reaction. Instead, cover the whole beaker containing the milky microspheres solution with an aluminum foil and expose the sample to UV-light for 30 min at 75 °C while constantly stirring it (300 rpm). The distance of the lamp to the microspheres solution is 15 cm,

3. Let the solution cool down to room temperature.

4. The microspheres can be stored in a glass bottle sealed with a cap at room temperature for several months.

It must be noted that Polymerized microspheres are extremely stable and may remain suspended for months depending on the size. The microspheres can be concentrated by centrifugation.

A.1.3 Synthesis of non-polymerized birefringent microspheres embedded with photo-initiator for surface activation (activated microspheres)

To make birefringent microspheres with embedded photo-initiator, follow Subsection A.1.2 while skipping Step '2'.
Leaving out the UV-polymerization step allows for the microspheres to remain in nematic liquid crystalline state preserving the trapped photo-initiator for polymerization. The acrylate groups exposed on the microspheres surface and the acrylate groups of other non-RM257 molecules like Acrylate-PEG or Acrylate-NHS are concatenated by RM257 catalyzed polymerization (Figure 1.6).

Unpolymerized microspheres are less stable and remain suspended for 3–4 weeks depending on the microspheres size. The microspheres can be concentrated by evaporation as mentioned above. The UV-light exposure time(30 min.) and distance(15 cm) to the sample was optimized by a test series. It is possible

to couple bio-molecules to these microspheres via a silica coating of the particles. Alternatively, acrylate polymerization of exposed acrylate groups of the crystal precursor RM257 can be covalently coupled to polyethylene glycol (PEG). For example, PEG is used as linker to attach functional single molecules to surfaces[74].

Materials

Chemicals

- Activated birefringent microspheres as synthesized in A.1.3
- Acrylic acid N-hydroxysuccinimide ester(NHS-Ac), Sigma
- mPEG-Acrylate (mPEG-Ac Mn 2K), Creative PEG works
- BRB80 buffer, pH 6.8 see Appendix

Equipment

- ULTRA-VITALUX ultraviolet high-pressure l amp (13.6 W at UVA)
- 35 mm plastic petri-dish, Nunc
- 500 µl plastic tubes, eppendorf
- Ice-box/Ice

Reaction: Polymerization of acrylate groups on RM257 surface with acrylate groups of NHS-Ac and mPEG-Ac

1. Pipette out 200 µl activated birefringent microspheres in a 500 µl tube. Place the tube on ice and let it cool to 4 °C.
2. To this tube add 10 µ M 10 µl mPEG-Acrylate solution. Mix the solution by pipetting 10x. let it cool for 2 min.
3. Add to this, 1 µl , NHS-Ac solution (in DMSO). Pipette gently 10x and incubate for 2 min.
4. Pipette out the entire solution into 3 drops of ≈ 100 µl onto a pre-cooled petri-dish (on ice).

5. Place the icebox with the petri-dish under the UV lamp. Make sure that the lamp is directly above the dish. Expose to UV for 20 seconds from a distance of 15 cm.

Reaction: Coupling protein to NHS activated microspheres (NHS-Ms)

1. Collect the NHS-microspheres from the petri-dish into a 500 µl tube. Place on ice
2. While this tube is in ice, add the protein of interest and pipette gently 40 ×. Incubate for 2 hours on ice.

A.1.4 Protein coupling of polymerized birefringent microspheres

Reaction: Reaction: Polymerization of acrylate groups on polymerized RM257 surface with acrylate groups of NHS-Ac and mPEG-Ac

To couple proteins to polymerized microspheres, change the following steps in section 1.3:

1. Step 1: Replace "activated birefringent microspheres" with equal volume of "polymerized birefringent microspheres"
2. Step 1: Additionally add 20 µl , photo-initiator Darocur 1173.
3. Follow rest of the steps in section 1.3.

This protocol can be used for coupling any molecule (protein) with an exposed -amine group. For kinesin motility assays in chapter 3 we couple anti-eGFP antibody to the NHS group on activated birefringent microspheres. As mentioned before NHS is reactive to Water. The reaction rate of NHS with water is relatively slower to that of NHS with -amine at low temperatures. Hence the solution is incubated on ice through out the reaction. Excess unreacted -NHS on the microspheres can be quenched with proteins like BSA or casein.

A.2 Alternative routes to surface modification of RM257 birefringent microspheres

A.2.1 Silica coating of polymerized RM257 microspheres

Silica coating of microspheres[134] makes them robust and allows the application of standard surface modification reactions. The silica shell is produced via a conventional base-catalyzed, sol-gel reaction via the

hydrolysis and condensation of tetraethyl orthosilicate (TEOS) in ethanol according to the Stöber et al.[156] method modified by using RM257 microspheres as negatively-charged cores and using the surfactant Cetrimonium bromide (CTAB) as a template for mesopores which are formed through the self-assembly of CTAB. This protocol was first established by Suman De in our lab for silica coating of nano-diamonds and modified further to suit RM257 microspheres.

Materials

Chemicals

- Analytical ethanol, Sigma-Aldrich
- Ammonium hydroxide (NH_4OH) solution 30 %; Sigma-Aldrich
- Polymerized RM257 birefringent microspheres
- Cetrimonium bromide: $(C_{16}H_{33})N(CH_3)_3Br$ also called cetyl-trimethyl-ammonium bromide or hexadecyl trimethyl ammonium bromide often abbreviated by CTAB; Sigma-Aldrich
- Tetraethyl orthosilicate (TEOS); Sigma-Aldrich
- Ammonium nitrate solution (NH_4NO_3); 15 g/l in ethanol
- Deionized water

Equipment

- Heidolph Type 50300 magnetic mixing plate
- Laboratory glass bottles with crew cap (PP, blue, integral lip seal) and a volume of 100 ml
- TEM grids: 400 Mesh, hexagonal, Cu (G400H-Cu, Science Services) subsequently coated with Pioloform and carbon

Method

The coating method was originally based on the formation of polydisperse, mesoporous silica microspheres[57] of type MCM-41[89]. The pores with a diameter of about 3–4 nm result from worm-like micelles (with a persistence length of about 15 nm) that CTAB forms at concentrations well above its critical

micelle concentration (CMC ≈1 mM; we use about 10 mM)[28,152] in particular in the presence of negatively charged molecules. The surfactant and ethanol[102] are also crucial for a monodisperse[180] coating on negatively charged, nanometer-sized cores[82]. Ethanol (i) segregates to the micelles and swells them and (ii) slows-down the hydrolysis and condensation reaction of TEOS promoting the growth of spherical particles via a reaction-limited monomer-cluster growth, also called Eden growth, in combination with Ostwald ripening (pp. 199–201 in[143]). The shell thickness is determined by the amount of both, CTAB and TEOS[134].

Solution A: CTAB solution

1. Dissolve 80 mg CTAB in 1.32 ml deionized water and 600 µl analytic ethanol in a glass bottle.
2. Stir the solution using a magnetic stirrer (600 rpm) until it gets clear.
3. Store at 4 °C.

Solution B: Washing solution

1. Dissolve 1.5 mg ammonium nitrate (NH_4NO_3) in 100 ml analytic ethanol in a glass bottle.
2. Stir the solution using a magnetic stirrer until it gets clear.
3. The solution can be stored for several weeks at room temperature.

Reaction: Silica coating

1. Take 15 ml birefringent microspheres in a glass bottle and cool on ice.
2. Add drop-wise 25 µl of NH_4OH to the microspheres. Pipette the solution to mix uniformly. Note:NH_4OH is extremely volatile. Perform the entire reaction in a hood
3. Add 2 ml of Solution-A to the solution above in a drop-wise manner. Stir gently on ice for 30 min.
4. Add 150 µl TEOS to the bottle. With this amount, a shell thickness of 80–100 nm is expected at the end of the reaction. Note:TEOS is hygroscopic and should be stored in a moisture free environment (inert gas)

5. The solution is stirred with a magnetic stirrer (200 rpm) at room temperature for 30 minutes.The solution should be milky without any clusters or precipitates.

6. Now incubate this solution overnight at room temperature with a gentle shake every hour.

Cleaning and storage

The following cleaning procedure can be applied only to Silica coated polymerized RM257 microspheres.

1. Gently agitate the silica coated RM257 microspheres by pipetting.

2. To remove CTAB, wash the mixture 2× with the washing solution (Solution-B; use about 3–5 ml per step). Start by centrifuging the silica coated microspheres at 10,500 × rcf for 10 min. Discard the supernatant.

3. Re-suspend the pellet from the last washing step in 5 ml BRB80.

4. Store the solution at 4 °C in glass bottles.

Preparation for TEM imaging

1. Dilute 1 µl of silica coated RM257 microspheres in 9 µl EtOH (100 %)

2. Add a drop of 3 µl of this solution onto the grid.

3. Wait until the drop evaporates and then add additional 3 µl .

4. Wait until the drop evaporates.

5. Image the microspheres using a TEM.

A.2.2 Surface modification of silica coated of RM257 microspheres with APTES

Chemicals :

- Silica coated birefringent microspheres
- 2-amino propyl-triethoxy silane APTES
- Anhydrous DMF

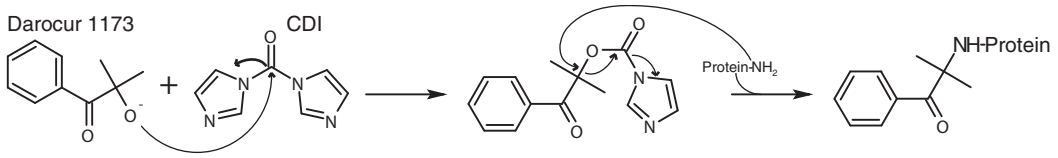

Figure A.1: Reaction mechanism of embedded photo-initiator Darocur 1173, activated with Carbonyl-diimidazole (CDI). An Alternative route of coupling proteins to birefringent microspheres employs the hydroxyl groups of embedded photo-initiator to couple amine moieties of proteins to the microspheres.

- Ultra-Sonicator
- Dialysis Tubes 100 KDa
- Sulfo-NHS-Biotin

Reaction

1. Dissolve 50mg Sulfo-NHS-LC Biotin in 270 µl anhydrous DMF
2. Add 31.8 µl APTES and shake for 1.5 hour at RT
3. Optional- Verify product with TLC
4. React 500 µl silica coated particles with 100 µl of Silanized biotin at ph 7.5, agitation for 40 h at RT
5. Dialyze in DI H_2O using dialysis tube. changes over 48 hours, Store final product in 4 °C

A.2.3 Surface modification of RM257 microspheres with carbonyl-diimidazole

N,N'-Carbodiimide (CDI) is a zero length crosslinking reagent used to couple primary amines to carboxyllic acid functional groups. CDI reacts with the hydroxyl ion (OH-) of proteins or other organic compounds, forming a reactive intermediate that is subsequently reacted with an amino group (-NH_2). This reagent can be used to couple two proteins, and is commonly used in protein immobilization to a solid support or membrane. Conveniently, CDI can be used in both aqueous and organic solvent systems.

Chemicals :

- polymerized RM257 birefringent microspheres
- Tetrahydrofuran (THF), Sigma-Aldrich
- Carbonyl-diimidazole (CDI MW 162.15), Sigma-Aldrich
- Deionized, degassed water
- Protein of interest (Anti-eGFP)

Method

Reaction

1. Start by centrifuging the polymerized RM257 microspheres at 10,500 × rcf for 10 min.
2. Discard half of the supernatant and add same volume of THF. Repeat 5×. In the last step replace the entire volume of supernatant with THF.
3. Add 50 mg/ml (0.3 M) cabonyldiimidazole CDI and incubate for 2 hours.
4. Wash the microspheres with cold water.
5. Add (fluorescent)protein 10mg/ml, incubate for 24 hrs.
6. Wash and observe for coupling (fluorescence).

The reaction assumed that Darocur 1173 was trapped in the RM257 microspheres.The presence of Darocur 1173 was checked with PCl_5. Similar reaction was conducted in the absence of THF, but only in the presence of BRB80 buffer. The aqueous scheme of reaction was the only way to modify non-polymerized birefringent microspheres using CDI.

B

Silanization of cover-slip

B.1 Hydrophobic silanized coverslips for flowcells

(Protocol standardized by Tobias Jachowski)

During 'silanization' the hydrophilic surface of a coverslip glass will be coupled to a hydrophobic layer of FDTS (Perfluorodecyltrichlorosilane). A hydrophobic surface is important if you want to coat the surface of the coverslip with antibodies – eg. for experiments that need an antibody coating on the surface of the coverslip in order to immobilize distinct proteins of your sample onto the surface (like sticking microtubules via α-tubulin onto a surface). Antibodies [AB] can be easily immobilized onto hydrophobic surfaces – they adsorb via hydrophobic interactions. AB coatings on hydrophobic surfaces are more stable than on hydrophilic surfaces, that's why a hydrophobic surface is crucial. The advantages of silanization are: 1) The level of hydrophicity of the surface can be adjusted by different FDTS incubation

times. 2) The FDTS is covalently bound to the glass surface, thus is irreversible and will not peel off. This is the big advantage compared to Teflon treatment, as the Teflon layer is less 'robust' and tends to peel off the glass surface. Additionally, one can pretreat a glass surface with FDTS prior to spin coating with Teflon, to stabilize the Teflon layer and get a very hydrophobic surface. Storage: The silanized coverslips can be stored in a closed container for long-term usage.

B.1.1 Protocol

Ingredients

- use fresh easy-cleaned coverslips (* each cleaning step should be performed for 15min during the easy-clean protocol)
- 1 x microscope slide
- 70% EtOH
- H_2O (deionized Millipore H_2O for all steps !!)
- ≈250 ml 1 M HCL in Millipore H_2O
- 100 µl FDTS
- Sonicator with heating function
- Desiccator, vacuum pump, N2-supply

Part 1

1. clean a microscope slide with 70% EtOH (rub with clean lint-free tissue), H_2O, dry with N_2
2. Put the clean coverslip into the desiccator (*bottom part of the desiccator)
3. put easy-cleaned coverslips in 1 M HCl
   (use 'easy-clean glass-container' here)
4. sonicate 99 min, 75 °C (→ warm up time 39 min → 60 min @ 75 °C) (* careful when taking the container with hot acid out of sonicator!)

5. 3 x washes in H_2O
6. dry coverslips with N_2, thoroughly
7. dry the glass container with N_2 to later store the silanized slides

Part 2: Silanization procedure

1. Place dry coverslips into the desiccator
   (* don't cover the hole in the ground plate for pipetting the FDTS)
2. Apply vacuum on desiccator, 10 min to remove remnant H_2O molecules
   (* stop vacuum: close blue valve clockwise on top of the desiccator to keep vacuum in desiccator, close red/white valve counterclockwise at the vacuum tube, remove vacuum tube from the desiccator's top inlet)
3. Fill the desiccator with N_2
   (* no ambient air! Connect N2 outlet tip to the desiccator's top inlet, switch on N2 with slow flow, carefully open counterclockwise the desiccator's blue valve, fill up with N2 until lid of desiccator floats on top, close blue valve clockwise, disconnect N_2)
4. Open desiccator and pipette 0.1ml FDTS onto the coverslip in the bottom of the desiccator through the hole in the ground plate
   (* after using FDTS, fill the FDTS bottle up with N2 before closing it !!)
5. Apply vacuum on desiccator (20 mbar), 35 min
   (** optimum time varies – Tobi found out that 25 – 40 min is the best compromise between stable adsorption of IgG and low extend of unwanted complete denaturation of IgG)

Part 3: Test the hydrophobicity of the coverslip

1. Take one silanized coverslip and place a drop of 0.02 ml of H2O onto the coverslip, observe the water droplet for its surface curvature.
2. The coverslip has a sufficient hydrophobicity when the water drop is 'well-curved', meaning when the angle between the lateral surface of the water drop and the glass surface is $> 90°$.

3. Hydrophobicity is not sufficient, when the water droplet 'flattens out' on the glass surface and when the described angle is < 90°. In this case, repeat the silanization / last protocol step with incubation times of 5 – 10 min, until the coverslips show the right hydrophobicity.

C

Compounds and recipes

C.1 Chemicals for motility assay

C.1.1 Britton-Robinson buffer, BRB80

Ingredients

- piperazine-N,N′-bis(2-ethanesulfonic acid) (PIPES MW 302.37) - 80mM, Sigma
- Ethylene glycol tetraacetic acid (EGTA MW 380.35) - 1 mM, Sigma
- Magnesium Cloride ($MgCl_2$ 203.3), Merck
- Potassium hydroxide (KOH MW 56.11) - 100mM, Merck

Method

1. Prepare a solution of 4.83g PIPES, 76mg EGTA and 40.66mg $MgCl_2$ in 140 ml water.
2. While stirring the solution add KOH until the buffer solution is clear.
3. Adjust pH to 6.9 with KOH.
4. Transfer to volumetric flask and fill up to the appropriate volume.
5. Filter through Millipore "Stericup" 0.22 µm .
6. Aliquot 10 ml and store at -20 °C .

C.1.2 NHS-Ac Stock solution (30 mM)

Ingredients

- Acrylic acid N-hydroxysuccinimide ester (NHS-Ac MW 169.13) - 30 mM, Sigma
- Dimethyl Sulfoxide (DMSO MW 78.13), Sigma

Method

1. Add 5.1mg NHS-Ac to 1 ml DMSO. Pipette or shake till completely dissolved.
2. Make 10 µl aliquots and store at -20 °C .
   Note: NHS is extremely sensitive to moisture. Make sure to flush inert gas (e.g. N_2, Argon) into the stock vial and storage vials.

C.1.3 NHS-PEG-Ac Stock solution (30 mM)

Ingredients

- Acrylic acid, Poly ethylene glycol, N-hydroxysuccinimide ester (NHS-Ac MW 3.4k) - 30 mM, Sigma
- Dimethyl Sulfoxide (DMSO MW 78.13), Sigma

Method

1. Add 102mg NHS-PEG-Ac to 1 ml DMSO. Pipette or shake till completely dissolved.
2. Make 10 µl aliquots and store at -20 °C.

   Note: NHS is extremely sensitive to moisture. Make sure to flush inert gas (e.g. N_2, Argon) into the stock vial and storage vials.

C.1.4 mPEG-Ac stock solution (150 mM)

Ingredients

- Poly(ethylene glycol) methyl ether acrylate (mPEG-Ac Mn 2k) - 150mM, Sigma
- BRB80, see C.1.1.

Method

1. Add 300mg mPEG-Ac to 1 ml BRB80. Shake till dissolved
2. Make 10 µl aliquots and store at -20 °C

C.1.5 Magnesium Cloride (MgCl2)

Ingredients

- Magnesium Cloride ($MgCl_2$ MW 203.3)- 100 mM Merck

Method

1. Add 203mg D-Glucose to 10ml dd H_2O. Stir till dissolved.
2. Make 10 µl aliquots, flash freeze and store at -20 °C.

C.1.6 Adenosine tri-phosphate (ATP)

Ingredients

- Adenosine Triphosphate, disodium salt (ATP MW 605.2)-100 mM, Roche
- Magnesium Cloride ($MgCl_2$ MW 203.3)- 100 mM Merck

Method

1. Add 605.2mg ATP to 700 ml 100 mM $MgCl_2$(in water) . Stir till dissolved.
2. Measure in UV spec, adjust to desired concentration.
3. Make 10 µl aliquots, flash freeze and store at -20 °C .

UV spectroscopy

1. Dilute 1:3000 in double distilled water (dd H_2O). Once diluted check pH.
2. Put 1 ml into 1 cm cuvette, blank against dd H_2O.
3. Measure absorbance at 260 nm.
    - Extinction coefficient $\varepsilon = 1.54 \times 10^{-3}$ [L mol^{-1} cm^{-1}]

C.1.7 Adenylyl-imidodiphosphate (AMP-PNP)

Ingredients

- Adenylyl-imidodiphosphate (AMP-PNP MW 529.9)-100 mM, Sigma-Aldrich
- Magnesium Cloride ($MgCl_2$ MW 203.3)- 100 mM Merck

Method

1. Add 529.9mg AMP-PNP to 700 ml 100 mM $MgCl_2$(in water). Stir till dissolved.
2. Measure in UV spec, adjust to desired concentration.
3. Make 10 µl aliquots, flash freeze and store at -20 °C .

UV spectroscopy

1. Dilute 1:3000 in phosphate buffer(PBS).
2. Put 1 ml into 1 cm cuvette, blank against (dd H_2O).
3. Measure absorbance at 259 nm.

- Extinction coefficient ε = 1.54 x 10^{-3} [L mol^{-1} cm^{-1}]
- Lambda max = 259nm (O.IM phosphate buffer, pH 7.0)
- E^{mM} (259nm) = 15.4 (O.IM phosphate buffer, pH 7.0)
- Ratios: A250nn/A260nm = 0.80
- A280nn/ A260nm = 0.15

C.1.8 Casein

Ingredients

- Casein from bovine milk, Sigma-Aldrich
- BRB80
- Filter 0.45 µm , Millipore

Method

1. Add 1g Casein to 35 ml BRB80. Stir in a cold room till dissolved (over night).
2. Place the thick viscous fluid standing up in a 4°refrigerator for 12 hours.
3. Decant the supernatant and centrifuge in a precooled centrifuge at 8500 rpm.
4. Discard the pellet and filter supernatant through 0.45 µm filter.
5. Measure in UV spec, adjust to desired concentration.
6. Make 20 µl aliquots, flash freeze and store at -20 °C .

UV spectroscopy

1. Dilute 1:20 in dd H_2O.
2. Put 1 ml into 1 cm cuvette, blank against (dd H_2O).
3. Measure absorbance at 280 nm.
    - Extinction coefficient ε = 0.67 [L mol^{-1} cm^{-1}]

C.1.9 Catalase

Ingredients

- Catalase (240 kDa)-2mg/ml, Sigma-Aldrich
- Magnesium Cloride ($MgCl_2$ MW 203.3)- 100 mM Merck

Method

1. Add 4mg Catalase to 2 ml BRB80. Stir till dissolved.
2. Measure in UV spec, adjust to desired concentration.
3. Make 5 µl aliquots, flash freeze and store at -20 °C

UV spectroscopy

1. Dilute 1:10 in BRB80.
2. Put 1 ml into 1 cm cuvette, blank against BRB80.
3. Measure absorbance at 276 nm and 406 nm.
    - A276nm (1%, 1cm) = 12.9 Extinction coefficient ε = 31.4 x 10^4[L mol^{-1} cm^{-1}]
    - A406nm (1%, 1cm) = 6.9 Extinction coefficient ε= 16.6 x 10^4[L mol^{-1} cm^{-1}]

C.1.10 Dithio-DL-threitol (DTT)

Ingredients

- Dithio-DL-threitol (DTT MW 154.25), Sigma-Aldrich

Method

1. Add 154.25mg DTT to 1 ml dd H_2O. Stir till dissolved.
2. Make 5 µl aliquots, flash freeze and store at -20 °C .

C.1.11 Dimethyl·Sulfoxide (DMSO)

Ingredients

- Dimethyl·Sulfoxide (DMSO 99%), Sigma-Aldrich

Method

1. Make 10 µl aliquots, flash freeze and store at -20 °C.

C.1.12 D-Glucose, Dextrose

Ingredients

- D-Glucose, Dextrose (MW 180.16) 1M, Sigma-Aldrich

Method

1. Add 3.6g D-Glucose to 10ml dd H_2O. Stir till dissolved.
2. Make 10 µl aliquots, flash freeze and store at -20 °C.

C.1.13 Glucose Oxidase

Ingredients

- Glucose Oxidase from Aspergillus niger (160 kDa)-20mg/ml, Sigma-Aldrich
- BRB80

Method

1. Add 200mg Glucose oxidase to 10 ml BRB80. Stir till dissolved.
2. Measure in UV spec, adjust to desired concentration.
3. Make 5 µl aliquots, flash freeze and store at -20 °C

UV spectroscopy

1. Dilute 1:100 in BRB80.
2. Put 1 ml into 1 cm cuvette, blank against BRB80.
3. Measure absorbance at 276 nm and 406 nm.
    - Extinction coefficient ε = 31.1 x 10^4 [L mol^{-1} cm^{-1}]

C.1.14 Guanosine Triphosphate (GTP) disodium salt.

Ingredients

- Guanosine Triphosphate disodium salt (GTP MW 567.1)-25mM, Sigma-Aldrich

Method

1. Add 28.35mg Glucose oxidase to 2 ml dd H_2O. Stir till dissolved.
2. Measure in UV spec, adjust to desired concentration.
3. Make 5 µl aliquots, flash freeze and store at -20 °C

UV spectroscopy

1. Dilute 1:1000 in dd H_2O.
2. Put 1 ml into 1 cm cuvette, blank against BRB80.
3. Measure absorbance at 260 nm.
    - Extinction coefficient ε = 11.7 x 10^3 [L mol^{-1} cm^{-1}]

C.1.15 Paclitaxel, Taxol

Ingredients

- Paclitaxel (MW 853.93) 1mM, Sigma-Aldrich

Method

1. Add 1.7mg D-Glucose to 2ml DMSO. Stir till dissolved.

2. Make 10 µl aliquots, flash freeze and store at -20 °C.

References

[1] Akhmanova, A. & Steinmetz, M. O. (2015). Control of microtubule organization and dynamics: two ends in the limelight. *Nature Reviews Molecular Cell Biology*, 16(12), 711–726.

[2] Alberts, B., Johnson, A., Lewis, J., Raff, M., Roberts, K., & Walter, P. (2002). *Molecular Motors*. Garland Science.

[3] Allen, L., Barnett, S. M., & Padgett, M. J. (2003). *Optical angular momentum*. IOP Publishing Ltd.

[4] Allen, M. P. & L. (2000). Light with a twist in its tail. *Contemporary Physics*, 41(5), 275–285.

[5] Andrecka, J., Arroyo, J. O., Takagi, Y., de Wit, G., Fineberg, A., MacKinnon, L., Young, G., Sellers, J. R., & Kukura, P. (2015). Structural dynamics of myosin 5 during processive motion revealed by interferometric scattering microscopy. *eLife*, 2015(4), e05413.

[6] Andrienko, D. (2006). Introduction to liquid crystals. *International Max Planck Research School, Modelling of Soft Matter*, 1(September), 1–32.

[7] Asavei, T., Parkin, S., Persson, M., Vogel, R., Funk, M., Loke, V., Nieminen, T., Rubinsztein-Dunlop, H., & Heckenberg, N. (2008). Engineering Optically Driven Micromachines. *International Society for Optics and Photonics*, 7038(10.1117/12.798529), 703816–703816.

[8] Asbury, C. L., Fehr, A. N., & Block, S. M. (2003). Kinesin moves by an asymmetric hand-over-hand mechanism. *Science (New York, N.Y.)*, 302(5653), 2130–4.

[9] Ashkin, a. (1998). Forces of a single-beam gradient laser trap on a dielectric sphere in the ray optics regime. *Methods in cell biology*, 55(February), 1–27.

[10] Ashkin, a. & Dziedzic, J. M. (1987). Optical trapping and manipulation of viruses and bacteria. *Science (New York, N.Y.)*, 235(4795), 1517–1520.

[11] Ashkin, A., Dziedzic, J. M., & Yamane, T. (1987). Optical trapping and manipulation of single cells using infrared laser beams. *Nature*, 330(6150), 769–771.

[12] Batters, C. & Veigel, C. (2011). Using optical tweezers to study the fine details of myosin ATPase mechanochemical cycle. *Methods in molecular biology (Clifton, N.J.)*, 778, 97–109.

[13] Berg-Sørensen, K. & Flyvbjerg, H. (2004). Power spectrum analysis for optical tweezers. *Review of Scientific Instruments*, 75(3), 594–612.

[14] Beth, R. A. (1936). Mechanical detection and measurement of the angular momentum of light. *Physical Review*, 50(2), 115–125.

[15] Bieling, P., Telley, I. A., Piehler, J., & Surrey, T. (2008). Processive kinesins require loose mechanical coupling for efficient collective motility. *EMBO reports*, 9(11), 1121–7.

[16] Bishop, A., Nieminen, T., Heckenberg, N., & Rubinsztein-Dunlop, H. (2003). Optical application and measurement of torque on microparticles of isotropic nonabsorbing material. *Physical Review A*, 68(3), 033802.

[17] Bloch, D. B., Smith, B. R., & Ault, K. a. (1983). Cells on microspheres: a new technique for flow cytometric analysis of adherent cells. *Cytometry*, 3(6), 449–52.

[18] Block, S. M., Goldstein, L. S. B., & Schnapp, B. J. (1990). Bead movement by single kinesin molecules studied with optical tweezers. *Nature*, 348(6299), 348–352.

[19] Bormuth, V., Howard, J., & Schäffer, E. (2007). LED illumination for video-enhanced DIC imaging of single microtubules. *Journal of Microscopy*, 226(1), 1–5.

[20] Bormuth, V., Varga, V., Howard, J., & Schäffer, E. (2009). Protein friction limits diffusive and directed movements of kinesin motors on microtubules. *Science (New York, N.Y.)*, 325(5942), 870–873.

[21] Boyle, R. T. & McNamara, J. C. (2006). Association of kinesin and myosin with pigment granules in crustacean chromatophores. *Pigment cell research / sponsored by the European Society for Pigment Cell Research and the International Pigment Cell Society*, 19(1), 68–75.

[22] Breit, G. & Wigner, E. (1936). Capture of Slow Neutrons. *Physical Review*, 49, 519–531.

[23] Brenner, H. (1964). Slow viscous rotation of an axisymmetric body within a circular cylinder of finite length. *Applied Scientific Research, Section A*, 13(1), 81–120.

[24] Broer, D. J., Mol, G. N., & Challa, G. (1989). In situ photopolymerization of an oriented liquid-crystalline acrylate, 2. *Makromolekulare Chemie*, 190(1), 19–30.

[25] Brouhard, G. J., Schek, H. T., & Hunt, A. J. (2003). Advanced optical tweezers for the study of cellular and molecular biomechanics. *IEEE Transactions on Biomedical Engineering*, 50(1), 121–125.

[26] Bugiel, M., Jannasch, A., & Schäffer, E. (2016). *Implementation and Tuning of an Optical Tweezers Force-Clamp Feedback System*, volume 1486 of *Methods in Molecular Biology*, book section Implementation and Tuning of an Optical Tweezers Force-Clamp Feedback System, (pp. 81–120). Humana Press.

[27] Cairns, D. R., Sibulkin, M., & Crawford, G. P. (2001). Switching dynamics of suspended mesogenic polymer microspheres. *Applied Physics Letters*, 78(18), 2643–2645.

[28] Cates, M. E. & Candau, S. J. (1999). Statics and dynamics of worm-like surfactant micelles. *Journal of Physics: Condensed Matter*, 2(33), 6869–6892.

[29] Chandrasekhar, S., Sadashiva, B. K., & Suresh, K. A. (1977). Liquid crystals of disc-like molecules. *Pramana*, 9(5), 471–480.

[30] Charlebois, B. D., Schek, H. T., & Hunt, A. J. (2010). Nanometer-resolution microtubule polymerization assays using optical tweezers and microfabricated barriers. *Methods in cell biology*, 95, 207–19.

[31] Chu, S., Bjorkholm, J. E., Ashkin, A., & Cable, A. (1986). Experimental observation of optically trapped atoms. *Physical Review Letters*, 57(3), 314–317.

[32] Coates, D. (2000). *Liquid Crystal Polymers: Synthesis, Properties and Applications*. iSmithers Rapra Publishing.

[33] Collings, P. J. (1992). *Liquid Crystals: Nature's Delicate Phase of Matter*. Collings Harper.

[34] Coppin, C. M., Pierce, D. W., Hsu, L., & Vale, R. D. (1997). The load dependence of kinesin's mechanical cycle. *Proceedings of the National Academy of Sciences of the United States of America*, 94(16), 8539–44.

[35] Craighead, H. G., Cheng, J., & Hackwood, S. (1982). New display based on electrically induced index-matching in an inhomogeneous medium. *Applied Physics Letters*, 40(1), 22–24.

[36] Crawford, G. P., Stannarius, R., & Doane, J. W. (1991). Surface-induced orientational order in the isotropic phase of a liquid-crystal material. *Physical Review A*, 44(4), 2558–2569.

[37] Crevel, I. M.-T. C., Nyitrai, M., Alonso, M. C., Weiss, S., Geeves, M. A., & Cross, R. A. (2004). What kinesin does at roadblocks: the coordination mechanism for molecular walking. *The EMBO journal*, 23(1), 23–32.

[38] Crevenna, A. H., Madathil, S., Cohen, D. N., Wagenbach, M., Fahmy, K., & Howard, J. (2008). Secondary structure and compliance of a predicted flexible domain in kinesin-1 necessary for cooperation of motors. *Biophysical journal*, 95(11), 5216–27.

[39] De Jong, W. H. & Borm, P. J. a. (2008). Drug delivery and nanoparticles:applications and hazards. *International journal of nanomedicine*, 3(2), 133–149.

[40] Degiorgio, V., Piazza, R., & Bellini, T. (1994). Static and dynamic light scattering study of fluorinated polymer colloids with a crystalline internal structure. *Advances in Colloid and Interface Science*, 48(C), 61–91.

[41] Deufel, C., Forth, S., Simmons, C. R., Dejgosha, S., & Wang, M. D. (2007). Nanofabricated quartz cylinders for angular trapping: DNA supercoiling torque detection. *Nature methods*, 4(3), 223–225.

[42] Dierking, I. (2014). A review of polymer-stabilized ferroelectric liquid crystals. *Materials*, 7(5), 3568–3587.

[43] Doane, J. W., Vaz, N. A., Wu, B. G., & Žumer, S. (1986). Field controlled light scattering from nematic microdroplets. *Applied Physics Letters*, 48(4), 269–271.

[44] Drzaic, P. S. (1986). Polymer dispersed nematic liquid crystal for large area displays and light valves. *Journal of Applied Physics*, 60(6), 2142–2148.

[45] Endow, S. A., Kull, F. J., & Liu, H. (2010). Kinesins at a glance. *Journal of Cell Science*, 123(20), 3420.

[46] Fehr, A. N., Guti??rrez-Medina, B., Asbury, C. L., & Block, S. M. (2009). On the origin of kinesin limping. *Biophysical Journal*, 97(6), 1663–1670.

[47] Forth, S., Deufel, C., Sheinin, M. Y., Daniels, B., Sethna, J. P., & Wang, M. D. (2008). Abrupt Buckling Transition Observed during the Plectoneme Formation of Individual DNA Molecules. *Physical Review Letters*, 100(14), 148301.

[48] Friedel, G. (1922). The Mesomorphic States of Matter. *Annales de Physique*, 18(273-474), 163–174.

[49] Friese, M., Enger, J., Rubinsztein-Dunlop, H., & Heckenberg, N. (1996). Optical angular-momentum transfer to trapped absorbing particles. *Physical Review A*, 54(2), 1593–1596.

[50] Friese, M. E. J., Nieminen, T. A., Heckenberg, N. R., & Rubinsztein-Dunlop, H. (1998). Optical alignment and spinning of laser-trapped microscopic particles. *Nature*, 394(October), 348–350.

[51] Fuchigami, K., Taguchi, Y., & Tanaka, M. (2007). Preparation of hemispherical hollow silica microcapsules with different affinity surface by using spherical vaterite calcium carbonate as template. *Polymers for Advanced Technologies*, 18(11), 946–952.

[52] Ge, J., Lee, H., He, L., Kim, J., Lu, Z., Kim, H., Goebl, J., Kwon, S., & Yin, Y. (2009). Magnetochromatic microspheres: Rotating photonic crystals. *Journal of the American Chemical Society*, 131(43), 15687–15694.

[53] Ghislain, L. P., Switz, N. A., & Webb, W. W. (1994). Measurement of small forces using an optical trap. *Review of Scientific Instruments*, 65(9), 2762–2768.

[54] Gilbert, S. P., Webb, M. R., Brune, M., & Johnson, K. A. (1995). Pathway of processive ATP hydrolysis by kinesin. *Nature*, 373(6516), 671–6.

[55] Grant, B. J., M. Gheorghe, D., Zheng, W., Alonso, M., Huber, G., Dlugosz, M., McCammon, J. A., & Cross, R. A. (2011). Electrostatically Biased Binding of Kinesin to Microtubules. *PLoS Biology*, 9(11), e1001207.

[56] Gross, S. P., Vershinin, M., & Shubeita, G. (2007). Cargo Transport: Two Motors Are Sometimes Better Than One. *Current Biology*, 17(12), R478–R486.

[57] Grün, M., Unger, K. K., Matsumoto, A., & Tsutsumi, K. (1999). Novel pathways for the preparation of mesoporous MCM-41 materials: control of porosity and morphology. *Microporous and Mesoporous Materials*, 27(2-3), 207–216.

[58] Gutiérrez-Medina, B., Andreasson, J. O. L., Greenleaf, W. J., LaPorta, A., & Block, S. M. (2010). An Optical Apparatus for Rotation and Trapping. *Methods in Enzymology*, 475(C), 377–404.

[59] Gutiérrez-Medina, B., Fehr, A. N., & Block, S. M. (2009). Direct measurements of kinesin torsional properties reveal flexible domains and occasional stalk reversals during stepping. *Proceedings of the National Academy of Sciences*, 106(40), 17007–17012.

[60] Hackney, D. D. (1995). Highly processive microtubule-stimulated ATP hydrolysis by dimeric kinesin head domains. *Nature*, 377(6548), 448–50.

[61] Hancock, W. O. (2008). Intracellular Transport: Kinesins Working Together. *Current Biology*, 18(16), R715–R717.

[62] Happel, J. & Brenner, H. (1983). Wall Effects on the Motion of a Single Particle. In *Mechanics of fluids and transport processes* (pp. 286–357).

[63] Harada, Y. & Asakura, T. (1996). Radiation forces on a dielectric sphere in the Rayleigh scattering regime. *Optics Communications*, 124(5-6), 529–541.

[64] He, H., Friese, M. E., Heckenberg, N. R., & Rubinsztein-Dunlop, H. (1995). Direct observation of transfer of orbital angular momentum to absorbing particles from a laser beam with a phase singularity. *Physical Review Letters*, 75(5), 826–829.

[65] Hermanson, G. T. (2013). *Bioconjugate techniques*. Elsevier LTD, Oxford.

[66] Higuchi, H., Bronner, C. E., Park, H.-W., & Endow, S. A. (2004). Rapid double 8-nm steps by a kinesin mutant. *The EMBO journal*, 23(15), 2993–9.

[67] Hirokawa, N., Noda, Y., & Okada, Y. (1998). Kinesin and dynein superfamily proteins in organelle transport and cell division. *Current opinion in cell biology*, 10(1), 60–73.

[68] Hoffmann, P. M. (2016). How molecular motors extract order from chaos (a key issues review). *Reports on progress in physics. Physical Society (Great Britain)*, 79(3), 032601.

[69] Howard, J. (1996). The movement of kinesin along microtubules. *Annual review of physiology*, 58, 703–29.

[70] Howard, J., Hudspeth, A. J., & Vale, R. D. (1989). Movement of microtubules by single kinesin molecules. *Nature*, 342(6246), 154–158.

[71] Hua, W., Chung, J., & Gelles, J. (2002). Distinguishing inchworm and hand-over-hand processive kinesin movement by neck rotation measurements. *Science*, 295(5556), 844–848.

[72] Hunt, A. J. & Howard, J. (1993). Kinesin swivels to permit microtubule movement in any direction. *Proceedings of the National Academy of Sciences*, 90(24), 11653–7.

[73] Isojima, H., Iino, R., Niitani, Y., Noji, H., & Tomishige, M. (2016). Direct observation of intermediate states during the stepping motion of kinesin-1. *Nature Chemical Biology*, 12(4), 290–297.

[74] Jannasch, A., Bugiel, M., Fantana, H., Bormuth, V., Schiemann, F., Howard, J., & Sch, E. (2015). Versatile microsphere attachment of GFP-labeled proteins with preserved functionality Microsphere preparation. *Journal of Biological Methods*, 2(4), 1–12.

[75] Jannasch, A., Demirörs, A. F., van Oostrum, P. D. J., van Blaaderen, A., & Schäffer, E. (2012). Nanonewton optical force trap employing anti-reflection coated, high-refractive-index titania microspheres. *Nature Photonics*, 6(7), 469–473.

[76] Juodkazis, S., Matsuo, S., Murazawa, N., Hasegawa, I., & Misawa, H. (2003). High-efficiency optical transfer of torque to a nematic liquid crystal droplet. *Applied Physics Letters*, 82(26), 4657–4659.

[77] Juodkazis, S., Shikata, M., Takahashi, T., Matsuo, S., & Misawa, H. (1999). Size Dependence of Rotation Frequency of Individual Laser Trapped Liquid Crystal Droplets. *Japanese Journal of Applied Physics, Part 1: Regular Papers and Short Notes and Review Papers*, 38(5 PART 2), 518–520.

[78] Kaseda, K., Higuchi, H., & Hirose, K. (2003). Alternate fast and slow stepping of a heterodimeric kinesin molecule. *Nat. Cell Biol.*, 5(12), 1079–1082.

[79] Kawaguchi, K. & Ishiwata, S. (2000). Temperature dependence of force, velocity, and processivity of single kinesin molecules. *Biochemical and biophysical research communications*, 272(3), 895–9.

[80] Kepler, J. (2000). *Optics : Paralipomena to Witelo & optical part of astronomy / Johannes Kepler ; translated by William H. Donahue.* Green Lion Press,.

[81] Kim, D. S. & Lee, C. K. (2002). Surface modification of precipitated calcium carbonate using aqueous fluosilicic acid. *Applied Surface Science*, 202(1-2), 15–23.

[82] Kim, J. H., Yoon, S. B., Kim, J. Y., Chae, Y. B., & Yu, J. S. (2008). Synthesis of monodisperse silica spheres with solid core and mesoporous shell: Morphological control of mesopores. *Colloids and Surfaces A: Physicochemical and Engineering Aspects*, 313-314, 77–81.

[83] Klumpp, S. & Lipowsky, R. (2005). Cooperative cargo transport by several molecular motors. *Proceedings of the National Academy of Sciences of the United States of America*, 102(48), 17284–9.

[84] Knoener, G. G., Parkin, S. J. W., Heckenberg, N. R., & Rubinsztein-Dunlop, H. (2005). Microrheology using dual beam optical tweezers and ultrasensitive force measurements. *International Society for Optics and Photonics*, 5736, 73–80.

[85] Kojima, H., Muto, E., Higuchi, H., & Yanagida, T. (1997). Mechanics of single kinesin molecules measured by optical trapping nanometry. *Biophysical journal*, 73(4), 2012–22.

[86] Koster, G., Cacciuto, A., Derényi, I., Frenkel, D., & Dogterom, M. (2005). Force Barriers for Membrane Tube Formation. *Physical Review Letters*, 94(6), 068101.

[87] Kovalenko, I. N., Kuznet?s?ov, N. I. N. I., & Shurenkov, V. M. V. M. (1996). *Models of random processes : a handbook for mathematicians and engineers*. CRC Press.

[88] Kozielski, F., Sack, S., Marx, A., Thormählen, M., Schönbrunn, E., Biou, V., Thompson, A., Mandelkow, E. M., & Mandelkow, E. (1997). The crystal structure of dimeric kinesin and implications for microtubule-dependent motility. *Cell*, 91(7), 985–94.

[89] Kresge, C. T., Leonowicz, M. E., Roth, W. J., Vartuli, J. C., & Beck, J. S. (1992). Ordered mesoporous molecular sieves synthesized by a liquid-crystal template mechanism. *Nature*, 359(6397), 710–712.

[90] Kunwar, A., Vershinin, M., Xu, J., & Gross, S. P. (2008). Stepping, strain gating, and an unexpected force-velocity curve for multiple-motor-based transport. *Current biology : CB*, 18(16), 1173–83.

[91] Kuo, S. C. & Sheetz, M. P. (1993). Force of single kinesin molecules measured with optical tweezers. *Science (New York, N.Y.)*, 260(5105), 232–4.

[92] La Porta, A. & Wang, M. D. (2004). Optical torque wrench: Angular trapping, rotation, and torque detection of quartz microparticles. *Physical Review Letters*, 92(19), 190801–1.

[93] Langel, W. (2006). *Condensed matter physics. Crystals, liquids, liquid crystals, and polymers*, volume 11. Springer Science & Business Media.

[94] Laschat, S. (2009). Progress in liquid crystal chemistry. *Beilstein Journal of Organic Chemistry*, 5(1), 48.

[95] Lebedew, P. (1901). Untersuchungen über die Druckkräfte des Lichtes. *Annalen der Physik*, 311(11), 433–458.

[96] Lebel, P., Basu, A., Oberstrass, F. C., Tretter, E. M., & Bryant, Z. (2014). Gold rotor bead tracking for high-speed measurements of DNA twist, torque and extension. *Nature Methods*, 11(4), 456–62.

[97] Lehmann, O. (1889). Über fließende Krystalle. *Zeitschrift für Physikalische Chemie*, 4, 462–472.

[98] Lehmuskero, A., Ogier, R., Gschneidtner, T., Johansson, P., & Käll, M. (2013). Ultrafast spinning of gold nanoparticles in water using circularly polarized light. *Nano Letters*, 13(7), 3129–3134.

[99] Li, M., McGrail, M., Serr, M., & Hays, T. S. (1994). Drosophila cytoplasmic dynein, a microtubule motor that is asymmetrically localized in the oocyte. *The Journal of cell biology*, 126(6), 1475–94.

[100] Lipfert, J., Lee, M., Ordu, O., Kerssemakers, J. W. J., & Dekker, N. H. (2014). Magnetic tweezers for the measurement of twist and torque. *Journal of visualized experiments : JoVE*, 19(87), 1–18.

[101] Liu, S., Chistol, G., Hetherington, C. L., Tafoya, S., Aathavan, K., Schnitzbauer, J., Grimes, S., Jardine, P. J., & Bustamante, C. (2014). A viral packaging motor varies its DNA rotation and step size to preserve subunit coordination as the capsid fills. *Cell*, 157(3), 702–713.

[102] Liu, S. Q., Cool, P., Collart, O., Van der Voort, P., Vansant, E. F., Lebedev, O. I., Van Tendeloo, G., & Jiang, M. H. (2003). The influence of the alcohol concentration on the structural ordering of mesoporous silica: Cosurfactant versus cosolvent. *Journal of Physical Chemistry B*, 107(38), 10405–10411.

[103] Loke, V. & Nieminen, T. (2006). Computational modeling of optical trapping of vaterite microspheres. *17th National Congress ...*, (December), 3–6.

[104] Loos, C., Syrovets, T., Musyanovych, A., Mailänder, V., Landfester, K., Nienhaus, G. U., & Simmet, T. (2014). Functionalized polystyrene nanoparticles as a platform for studying bio–nano interactions. *Beilstein Journal of Nanotechnology*, 5(Figure 1), 2403–2412.

[105] Lubensky, T. C. (2008). *Soft Condensed Matter Physics*, volume 19104.

[106] Ma, Y. Z. & Taylor, E. W. (1997). Interacting head mechanism of microtubule-kinesin ATPase. *The Journal of biological chemistry*, 272(2), 724–30.

[107] Mahamdeh, M. & Schäffer, E. (2009). Optical tweezers with millikelvin precision of temperature-controlled objectives and base-pair resolution. *Optics express*, 17(19), 17190–17199.

[108] Maier, B., Bensimon, D., & Croquette, V. (2000). Replication by a single DNA polymerase of a stretched single-stranded DNA. *Proceedings of the National Academy of Sciences of the United States of America*, 97(22), 12002–7.

[109] Mandelkow, E. & Mandelkow, E.-M. (2002). Kinesin motors and disease. *Trends in Cell Biology*, 12(12), 585–591.

[110] Martin, S., Reichert, M., Stark, H., & Gisler, T. (2006). Direct observation of hydrodynamic rotation-translation coupling between two colloidal spheres. *Physical Review Letters*, 97(24), 248301.

[111] Maxwell, J. C. (1873). *A Treatise on Electricity and Magnetism 1*, volume 1.

[112] Messitt, T. J., Gagnon, J. A., Kreiling, J. A., Pratt, C. A., Yoon, Y. J., & Mowry, K. L. (2008). Multiple kinesin motors coordinate cytoplasmic RNA transport on a subpopulation of microtubules in Xenopus oocytes. *Developmental cell*, 15(3), 426–36.

[113] Mickolajczyk, K. J., Deffenbaugh, N. C., Arroyo, J. O., Andrecka, J., Kukura, P., & Hancock, W. O. (2015). Kinetics of nucleotide-dependent structural transitions in the kinesin-1 hydrolysis cycle. *Proceedings of the National Academy of Sciences of the United States of America*, 112(52), E7186–93.

[114] Miki, H., Okada, Y., & Hirokawa, N. (2005). Analysis of the kinesin superfamily: insights into structure and function. *Trends in Cell Biology*, 15(9), 467–476.

[115] Miki, H., Setou, M., Kaneshiro, K., & Hirokawa, N. (2001). All kinesin superfamily protein, KIF, genes in mouse and human. *Proceedings of the National Academy of Sciences of the United States of America*, 98(13), 7004–11.

[116] Miller, D. S. & Abbott, N. L. (2013). Influence of droplet size, pH and ionic strength on endotoxin-triggered ordering transitions in liquid crystalline droplets. *Soft Matter*, 9(2), 374–382.

[117] Mori, T., Vale, R. D., & Tomishige, M. (2007). How kinesin waits between steps. *Nature*, 450(7170), 750–4.

[118] Murazawa, N., Juodkazis, S., Jarutis, V., Tanamura, Y., & Misawa, H. (2006). Viscosity measurement using a rotating laser-trapped microsphere of liquid crystal. *Europhysics Letters (EPL)*, 73(5), 800–805.

[119] Nakagawa, T., Tanaka, Y., Matsuoka, E., Kondo, S., Okada, Y., Noda, Y., Kanai, Y., & Hirokawa, N. (1997). Identification and classification of 16 new kinesin superfamily (KIF) proteins in mouse genome. *Proceedings of the National Academy of Sciences of the United States of America*, 94(18), 9654–9.

[120] Neuman, K. C. & Block, S. M. (2004). Optical trapping. *Review of Scientific Instruments*, 75(9), 2787.

[121] Neuman, K. C. & Nagy, A. (2008). Single-molecule force spectroscopy: optical tweezers, magnetic tweezers and atomic force microscopy. *Nature Methods*, 5(6), 491–505.

[122] Nichols, E. F. & Hull, G. F. (1901). A preliminary communication on the pressure of heat and light radiation. *Physical Review (Series I)*, 13(5), 307–320.

[123] Nieminen, T. A., Heckenberg, N. R., & Rubinsztein-dunlop, H. (2001). Optical measurement of microscopic torques. *Journal of Modern Optics*, 48(3), 405–413.

[124] Nieminen, T. A., Loke, V. L. Y., Stilgoe, A. B., Knöner, G., Brańczyk, A. M., Heckenberg, N. R., & Rubinsztein-Dunlop, H. (2007). Optical tweezers computational toolbox. *Journal of Optics A: Pure and Applied Optics*, 9(8), S196–S203.

[125] Niori, T., Sekine, T., Watanabe, J., Furukawa, T., & Takezoe, H. (1996). Distinct ferroelectric smectic liquid crystals consisting of banana shaped achiral molecules. *Journal of Materials Chemistry*, 6(7), 1231.

[126] Oldenbourg, R. (2013). Polarized light microscopy: principles and practice. *Cold Spring Harbor protocols*, 2013(11).

[127] O'Neil, A. T., MacVicar, I., Allen, L., & Padgett, M. J. (2002). Intrinsic and Extrinsic Nature of the Orbital Angular Momentum of a Light Beam. *Physical Review Letters*, 88(5), 053601.

[128] Parkin, S., Knöner, G., Nieminen, T. a., Heckenberg, N. R., & Rubinsztein-Dunlop, H. (2006). Measurement of the total optical angular momentum transfer in optical tweezers. *Optics express*, 14(15), 6963–6970.

[129] Paterson, L. (2001). Controlled Rotation of Optically Trapped Microscopic Particles. *Science*, 292(5518), 912–914.

[130] Pedaci, F., Huang, Z., van Oene, M., Barland, S., & Dekker, N. H. (2011). Excitable particles in an optical torque wrench. *Nature Physics*, 7(3), 259–264.

[131] Pedaci, F., Huang, Z., van Oene, M., & Dekker, N. H. (2012). Calibration of the optical torque wrench. *Optics Express*, 20(4), 3787.

[132] Phillips, W. D., Gould, P. L., & Lett, P. D. (1988). Cooling, stopping, and trapping atoms. *Science (New York, N.Y.)*, 239(4842), 877–883.

[133] Poynting, J. H. (1909). The Wave Motion of a Revolving Shaft, and a Suggestion as to the Angular Momentum in a Beam of Circularly Polarised Light. *Proceedings of the Royal Society A: Mathematical, Physical and Engineering Sciences*, 82(557), 560–567.

[134] Prabhakar, N., Näreoja, T., von Haartman, E., Karaman, D. S., Jiang, H., Koho, S., Dolenko, T. a., Hänninen, P. E., Vlasov, D. I., Ralchenko, V. G., Hosomi, S., Vlasov, I. I., Sahlgren, C., & Rosenholm, J. M. (2013). Core-shell designs of photoluminescent nanodiamonds with porous silica coatings for bioimaging and drug delivery II: application. *Nanoscale*, 5(9), 3713–22.

[135] Pralle, A., Prummer, M., Florin, E. L., Stelzer, E. H., & Hörber, J. K. (1999). Three-dimensional high-resolution particle tracking for optical tweezers by forward scattered light. *Microscopy research and technique*, 44(5), 378–86.

[136] Rai, A., Rai, A., Ramaiya, A., Jha, R., & Mallik, R. (2013). Molecular Adaptations Allow Dynein to Generate Large Collective Forces inside Cells. *Cell*, 152(1), 172–182.

[137] Reinitzer, F. (1888). Beiträge zur Kenntniss des Cholesterins. *Monatshefte für Chemie - Chemical Monthly*, 9(1), 421–441.

[138] Rice, S., Lin, A. W., Safer, D., Hart, C. L., Naber, N., Carragher, B. O., Cain, S. M., Pechatnikova, E., Wilson-Kubalek, E. M., Whittaker, M., Pate, E., Cooke, R., Taylor, E. W., Milligan, R. A., & Vale, R. D. (1999). A structural change in the kinesin motor protein that drives motility. *Nature*, 402(6763), 778–784.

[139] Rodriguez-Otazo, M., Augier-Calderin, A., Galaup, J.-P., Lamère, J.-F., & Fery-Forgues, S. (2009). High rotation speed of single molecular microcrystals in an optical trap with elliptically polarized light. *Applied optics*, 48(14), 2720–30.

[140] Sandomirski, K., Martin, S., Maret, G., Stark, H., & Gisler, T. (2004). Highly birefringent colloidal particles for tracer studies. *Journal of Physics: Condensed Matter*, 16(38), S4137–S4144.

[141] Santamato, E., Sasso, A., Piccirillo, B., & Vella, A. (2002). Optical angular momentum transfer to transparent isotropic particles using laser beam carrying zero average angular momentum. *Optics express*, 10(17), 871–878.

[142] Schäffer, E., Nørrelykke, S. F., & Howard, J. (2007). Surface forces and drag coefficients of microspheres near a plane surface measured with optical tweezers. *Langmuir*, 23(7), 3654–3665.

[143] Scherer, G. W. & Brinker, C. J. (1990). *Sol-gel science: The physics and chemistry of sol-gel processing*.

[144] Schief, W. R., Clark, R. H., Crevenna, A. H., & Howard, J. (2004). Inhibition of kinesin motility by ADP and phosphate supports a hand-over-hand mechanism. *Proc. Natl. Acad. Sci. U. S. A.*, 101(5), 1183–1188.

[145] Schindelin, J., Arganda-Carreras, I., Frise, E., Kaynig, V., Longair, M., Pietzsch, T., Preibisch, S., Rueden, C., Saalfeld, S., Schmid, B., Tinevez, J.-Y., White, D. J., Hartenstein, V., Eliceiri, K., Tomancak, P., & Cardona, A. (2012). Fiji: an open-source platform for biological-image analysis. *Nature methods*, 9(7), 676–82.

[146] Schliwa, M. & Woehlke, G. (2003). Molecular motors. *Nature*, 422(6933), 759–765.

[147] Schneider, C. A., Rasband, W. S., & Eliceiri, K. W. (2012). NIH Image to ImageJ: 25 years of image analysis. *Nature Methods*, 9(7), 671–675.

[148] Schnitzer, M. J., Visscher, K., & Block, S. M. (1999). Single kinesin molecules studied with a molecular force clamp. *Nature*, 400(6740), 184–189.

[149] Schwarz, T., Petit-Pierre, G., & Dual, J. (2013). Rotation of non-spherical micro-particles by amplitude modulation of superimposed orthogonal ultrasonic modes. *The Journal of the Acoustical Society of America*, 133(3), 1260–8.

[150] Serrano, J. L., Ed. (1995). *Metallomesogens*. Wiley-VCH Verlag GmbH.

[151] Shafran, M. S. (2008). *Responsive liquid crystal polymer rods*. PhD thesis.

[152] Shikata, T., Formation, M., Hirata, H., & Solutions, C. B. (1987). Micelle formation of detergent molecules in aqueous media: viscoelastic properties of aqueous cetyltrimethylammonium bromide solutions. *Langmuir*, 4(10), 1081–1086.

[153] Simmons, R. M., Finer, J. T., Chu, S., & Spudich, J. A. (1996). Quantitative measurements of force and displacement using an optical trap. *Biophysical journal*, 70(4), 1813–22.

[154] Simpson, N. B., Dholakia, K., Allen, L., & Padgett, M. J. (1997). Mechanical equivalence of spin and orbital angular momentum of light: an optical spanner. *Optics letters*, 22(1), 52–54.

[155] Squires, T. M. & Mason, T. G. (2010). Fluid Mechanics of Microrheology. *Annual Review of Fluid Mechanics*, 42(1), 413–438.

[156] Stöber, W., Fink, A., & Bohn, E. (1968). Controlled growth of monodisperse silica spheres in the micron size range. *Journal of Colloid and Interface Science*, 26(1), 62–69.

[157] Svoboda, K. & Block, S. M. (1994). Biological applications of optical forces. *Annual Review of Biophysics and Biomolecular Structure*, 23, 247–285.

[158] Svoboda, K., Schmidt, C. F., Schnapp, B. J., & Block, S. M. (1993). Direct observation of kinesin stepping by optical trapping interferometry. *Nature*, 365(6448), 721–7.

[159] Tolić-Nørrelykke, S. F., Schäffer, E., Howard, J., Pavone, F. S., Jülicher, F., & Flyvbjerg, H. (2006). Calibration of optical tweezers with positional detection in the back focal plane. *Review of Scientific Instruments*, 77(10), 103101.

[160] Umbanhowar, P. B., Prasad, V., & Weitz, D. A. (2000). Monodisperse emulsion generation via drop break off in a coflowing stream. *Langmuir*, 16(2), 347–351.

[161] Vale, R. D. (1996). Switches, latches, and amplifiers: common themes of G proteins and molecular motors. *The Journal of cell biology*, 135(2), 291–302.

[162] Vale, R. D. (2000). The Way Things Move: Looking Under the Hood of Molecular Motor Proteins. *Science*, 288(5463), 88–95.

[163] Vale, R. D. (2003). The molecular motor toolbox for intracellular transport. *Cell*, 112(4), 467–80.

[164] Vale, R. D., Reese, T. S., & Sheetz, M. P. (1985). Identification of a novel force-generating protein, kinesin, involved in microtubule-based motility. *Cell*, 42(1), 39–50.

[165] Van de Witte, P., Brehmer, M., & Lub, J. (1999). LCD components obtained by patterning of chiral nematic polymer layers. *Journal of Materials Chemistry*, 9(9), 2087–2094.

[166] Vogel, R., Persson, M., Feng, C., Parkin, S. J., Nieminen, T. A., Wood, B., Heckenberg, N. R., & Rubinsztein-Dunlop, H. (2009). Synthesis and surface modification of birefringent vaterite microspheres. *Langmuir*, 25(19), 11672–11679.

[167] Walsh, D., Lebeau, B., & Mann, S. (1999). Morphosynthesis of calcium carbonate (vaterite) microsponges. *Advanced Materials*, 11(4), 324–328.

[168] Wang, E. C. & Wang, A. Z. (2014). Nanoparticles and their applications in cell and molecular biology. *Integrative Biology*, 6(1), 9–26.

[169] Wang, H. & Shen, J. (2012). Power spectral density of self-mixing signals from a flowing Brownian motion system. *Applied Physics B*, 106(1), 127–134.

[170] Wang, M. D., Yin, H., Landick, R., Gelles, J., & Block, S. M. (1997). Stretching DNA with optical tweezers. *Biophysical journal*, 72(3), 1335–46.

[171] Wickstead, B., Gull, K., & Richards, T. A. (2010). Patterns of kinesin evolution reveal a complex ancestral eukaryote with a multifunctional cytoskeleton. *BMC Evolutionary Biology*, 10(1), 110.

[172] Wilderbeek, J. T. (2001). Liquid crystalline driven morphology control of in-situ formed polymers. (pp. 197).

[173] Wu, T., Nieminen, T. A., Mohanty, S., Miotke, J., Meyer, R. L., Rubinsztein-Dunlop, H., & Berns, M. W. (2011). A photon-driven micromotor can direct nerve fibre growth. *Nature Photonics*, 6(1), 62–67.

[174] Wulff, K. D., Cole, D. G., & Clark, R. L. (2008). Controlled rotation of birefringent particles in an optical trap. *Applied optics*, 47(34), 6428–33.

[175] Xie, P., Dou, S. X., & Wang, P. Y. (2007). Limping of Homodimeric Kinesin Motors. *Journal of Molecular Biology*, 366(3), 976–985.

[176] Xing, J., Bai, F., Berry, R., & Oster, G. (2006). Torque-speed relationship of the bacterial flagellar motor. *Proceedings of the National Academy of Sciences of the United States of America*, 103(5), 1260–1265.

[177] Yajima, J., Alonso, M. C., Cross, R. A., & Toyoshima, Y. Y. (2002). Direct long-term observation of kinesin processivity at low load. *Current Biology*, 12(4), 301–306.

[178] Yeh, C.-F. (1994). The physicochemical properties and growth mechanism of oxide ($SiO_{2-x}F_x$) by liquid phase deposition with H_2O addition only. *Journal of The Electrochemical Society*, 141(11), 3177.

[179] Yildiz, A. & Selvin, P. R. (2005). Kinesin: walking, crawling or sliding along? *Trends in cell biology*, 15(2), 112–20.

[180] Yoon, S. B., Kim, J.-Y., Kim, J. H., Park, Y. J., Yoon, K. R., Park, S.-K., & Yu, J.-S. (2007). Synthesis of monodisperse spherical silica particles with solid core and mesoporous shell: mesopore channels perpendicular to the surface. *Journal of Materials Chemistry*, 17(18), 1758.

[181] Zhang, J., Guo, J., Li, T., & Li, X. (2010). Chemical Surface Modification of Calcium Carbonate Particles by Maleic Anhydride Grafting Polyethylene Wax. *International Journal of Green Nanotechnology: Physics and Chemistry*, 1(2), P65–P71.

[182] Zhang, P., Knowles, B. A., Goldstein, L. S. B., & Hawley, R. S. (1990). A kinesin-like protein required for distributive chromosome segregation in Drosophila. *Cell*, 62(6), 1053–1062.

[183] Zhang, X., Ma, L., & Zhang, Y. (2013). High-resolution optical tweezers for single-molecule manipulation. *The Yale journal of biology and medicine*, 86(3), 367–83.

Acknowledgments

Firstly, I would like to express my sincere gratitude to my advisor Prof. Erik Schäffer for the continuous support of my Ph.D study and related research, for his patience and motivation. His guidance helped me during my research and throughout the writing of this thesis.

My sincere thanks to Dr. Basudev Roy, for developing a calibration system to make sense of molecular motor motion. He provided me with conversations and shelter when I needed them most. Dr. Nagmeh Azadfar for expression and purification of kinesins. Dr. Kirill Sandomirski, Dr. Thomas Gisler, and Dr. Joe Howard and his lab for sharing freely, all the information and resources on birefringent microspheres, microtubules and motor proteins. Dr. Peter Kühn for sharing his polarization microscope at the geology department at Uni. Tübingen. And, my lab, never have they hesitated in lending their time when any thing science, needed fixing or understanding. I would also like to thank the financial agencies which supported my PhD namely the International Max Planck Research Society and the University of Tübingen.

My PhD was a long journey, like many of my rotation curves it fluctuated severely, the ups were always significantly more than the downs and it is all owed to the wonderful people surrounding me.

I would like to thank my parents, for being brave through the last ten years and for giving me the strength to follow my crazy ideas. Nilesh, Gaurav, Pri, Chitrapu and Arpan, for being constant reminders of the wonderful times of the past and those to come. Roop Mallik, for providing me with a firm base to launch myself into a PhD. A big thanks goes to Debo, who shared his magic of music and a place of comedy and party we called abode. Adrian, for keeping up with all my stupid conversations and the ever changing hobbies. Ruby, so we now know what certain medical facilities look like from inside. Somu, for all the adventures. Mohammed, for being the big brother, we all need and for building "Aswad" a real die-hard microscope. Anita and Martin, for providing shelter, and for buffering the culture shock with acceptance and friendship. Freddy and Nick, for all the fun in the lab and for discussing ideas which "could have been...". Varadha, for times, when only humor is not enough to get by. Prisha, food never tasted so good again. My offshore family, Elisa, Mayank, Suman, Mohammad, Ishita, Steve, Tine, Gero and Tobi. Big thanks are in order for Sukhi for keeping the fun alive. Arpad was like a father to me and I survived 2016 because of him.

As I come to the conclusion of my acknowledgments, there is one person who deserves the largest of thanks, Mansi. She taught me a lot about myself. Stood by me through great times and when not-so-much. Now that our futures converge I would like to thank her that she chose me.